2012

Quantification of Multiple Types of Uncertainty in Physics-Based Simulation

Inseok Park
Wright State University

Quantification of Multiple Types of Uncertainty in Physics-Based Simulation

A dissertation submitted in partial fulfillment of the
requirements for the degree of
Doctor of Philosophy

By

IN-SEOK PARK
B.S., Ajou University, South Korea, 2002
M.S., Ajou University, South Korea, 2004

2012
Wright State University

WRIGHT STATE UNIVERSITY
THE GRADUATE SCHOOL

September 7, 2012

I HEREBY RECOMMEND THAT THE DISSERTATION PREPARED UNDER MY SUPERVISION BY In-Seok Park ENTITLED Quantification of Multiple Types of Uncertainty in Physics-Based Simulation BE ACCEPTED IN PARTIAL FULFILLMENT OF THE REQUIREMENTS FOR THE DEGREE OF Doctor of Philosophy

_____

Ramana V. Grandhi, Ph.D.
Dissertation Director

_____

Ramana V. Grandhi, Ph.D.
Director, Ph.D. in Engineering Program

_____

Andrew Hsu, Ph.D.
Dean of Graduate School

Committee on Final Examination

_____

Ramana V. Grandhi, Ph.D., WSU

_____

Ravi Penmetsa, Ph.D., AFRL

_____

Joseph C. Slater, Ph.D., P.E., WSU

_____

Daniel T. Voss, Ph.D., WSU

_____

Alan W. Johnson, Ph.D., AFIT

ABSTRACT

Park, In-Seok. Ph.D., Department of Mechanical and Materials Engineering, Wright State University, 2012. Quantification of Multiple Types of Uncertainty in Physics-Based Simulation.

In general, more than one simulation model can be created to analyze and design engineering systems. Uncertainty is inevitably involved in selecting a single best approximating model from among a set of simulation models. Uncertainty in model selection (called model-form uncertainty in the present research) cannot be ignored, especially when the differences between the predictions by plausible models are significant. Also, each simulation model involves uncertainty in its input parameters and unknown errors in its predictions of system responses. A methodology is developed to quantify model-form uncertainty using the differences between experimental data measured from an engineering system and model predictions of the data which may involve parametric and/or predictive uncertainty under a Bayesian statistical framework. The proposed methodology is numerically demonstrated with two engineering problems.

Given that model-form uncertainty is quantified, two model combination techniques called the adjustment factor approach and model averaging are utilized to incorporate model-form uncertainty in response prediction by combining predictions by a model set. A nonlinear vibration system is used to illustrate the processes for implementing the adjustment factor approach and model averaging.

The proposed methodology is applied to quantify multiple types of uncertainty associated with the finite element simulation of a laser peening process. The adjustment factor approach is utilized to incorporate model-form uncertainty alone into the composite prediction of a residual stress field, while model averaging is utilized to incorporate parametric uncertainty and predictive uncertainty in addition to model-form uncertainty. Using the composite prediction of the residual stress field, a confidence band for the predicted residual stress field is established to indicate the reliability of the composite prediction.

Although the proposed methodology can effectively quantify model-form uncertainty given observed experimental data, it does not supply any practical framework for quantifying model-form uncertainty depending on expert evidence. Another methodology is developed to quantify both model-form and parametric uncertainty using human expertise under evidence theory, which handles imprecise human knowledge more realistically than probability theory. The process for implementing the proposed methodology is numerically demonstrated with the nonlinear vibration system problem. The laser peening process problem is addressed to examine the applicability of the proposed methodology to large-scale physics-based simulations.

TABLE OF CONTENTS

LIST OF FIGURES

LIST OF TABLES

ACKNOWLEDGEMENTS

I am deeply grateful to my advisor, Professor Ramana V. Grandhi, for his academic guidance and individual attention. His continuous suggestions and encouragement sustained me throughout research and writing of this dissertation.

I would also like to extend my thanks to the Ph.D. committee members: Dr. Ravi Penmetsa, Dr. Joseph Slater, Dr. Dan Voss, and Dr. Alan Johnson. My thank also goes to my friends, Dr. Hemanth Amarchina, Dr. Gulshan Singh, Dr. Seung-Kyum Choi, Dr. Jong-Bin Im, Dr. T J Spradlin, Dr. Matthew Reliy, and Mr. Anoop Vasu, Mr. Josh Deaton, Mr. Greg Loughnane, and Mr. Ryan Vogel whose friendship and encouragement were always with me during my Ph.D. research work. I would also like to thank Alysoun Taylor, whose corrections and suggestions on English style and grammar is really appreciated. I am also grateful to Professor Young-Suk Shin of Ajou University, who patiently taught many valuable lessons and gave me the opportunity to continue my studies in the U.S.A.

I would like to acknowledge the support from the Wright-Patterson Air Force Base under grant FA8650-04-D-3446-25 and from the Ph.D. fellowship granted by the Dayton Area Graduate Studies Institute (DAGSI).

I would like to give my special thanks to my parents and brother, Jae-Hyeong Park and Young-Sun Choi, and Hyeon-Seok Park, for their continuous support that enabled me to

complete this work. Finally, to God. Thanks for providing me all of the great family, friends, and colleagues whom you have blessed me with.

To my father and mother.

1. Introduction

1.1 Motivation and Research Objective

During the last four decades, computer simulations have played an increasingly important role in analyzing and designing engineering systems as the cost of simulation has been significantly decreased due to phenomenal increases in digital computing speed. Physics-based simulation is an efficient way to analyze an engineering system by generating a simulation model and executing it on a computer. It is widely recognized that a simulation model can be created in various manners from different viewpoints of an engineering system to be analyzed. For a system under consideration, different simulation models can be generated by making different sets of simplifying assumptions which are unavoidable in the phases of mathematically conceptualizing the system and representing the conceptualized system in computer code.

Most of modelers and analysts have been inclined to select a single simulation model thought of as correctly describing an engineering system from among a set of plausible models [1, 2] rather than take all the possibilities into consideration. However, a model selection process is made based on the hardly realistic assumption that we can certainly select a correct (or at least the best approximating) one from a set of models [3]. In most cases, it is impossible to identify a correct model among a set of possibilities due to our lack of complete knowledge about an engineering system. The lack of confidence associated with model selection brings about the uncertainty that resides in a given model set. In the present research, this uncertainty is called model-form uncertainty because a

model set comprises the models of different mathematical forms; in that regard, model-form uncertainty is clearly differentiated from parametric uncertainty. The degree of model-form uncertainty may be considerably large in problems for which the predictions by plausible simulation models are significantly different.

Also, a simulation model may involve uncertainty in its parameters and unknown prediction error. An objective of this research is to develop an effective and efficient methodology to quantify model-form uncertainty using the measured differences between experimental data and multi-model predictions that may involve parametric and/or predictive uncertainty (uncertainty in prediction error). After model-form uncertainty associated with a model set is quantified, predictions by the considered models are combined using the adjustment factor approach or model averaging as shown in Figure 1.1; by combining multi-model predictions, model-form uncertainty is propagated into a response prediction.

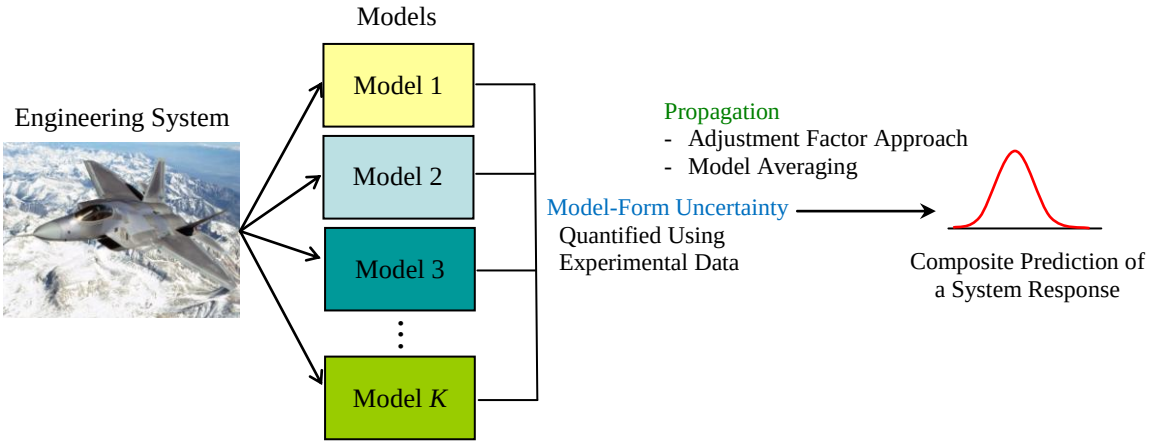

Figure 1.1 Quantification of model-form uncertainty and its propagation into response prediction

Another aim of this research is to develop a methodology to quantify both model-form and parametric uncertainty depending on expert knowledge systems. Model-form uncertainty is numerically specified using the mathematical structures of evidence theory. Then, using the disjunctive rule of combination, an attempt is made to combine predictions by a model set that involves parametric uncertainty.

1.2 Multiple Types of Uncertainty in Engineering Analysis

This Section describes three different types of uncertainty—which are involved in an engineering analysis when using a set of simulation models. Model-form uncertainty is stated in Section 1.2.1. Parametric and predictive uncertainties are discussed in the context of quantifying model-form uncertainty in Section 1.2.2.

1.2.1 Model-Form Uncertainty

According to the definition given by Apostolakis [4], "the model of the world is defined to be the mathematical model that is constructed for the physical situation of interest, such as the occurrence and impact on a system of a physical phenomenon." Here, the "world" is defined as "the object about which the person is concerned." Through the model, we can understand physical behaviors and predict the responses of physical systems. For instance, we can come up with mathematical models to explain and predict the motion of many physical objects and systems based on Newton's laws of motion. Usually, a mathematical model is represented as a map linking output variables with input variables. The relation between inputs and outputs may be expressed as $\mathbf{Y} = f(\mathbf{X})$, where $\mathbf{X}$ represents the vector of input variables, $\mathbf{Y}$ the vector of output variables, and f

the mathematical model form relating **X** to **Y**. When the input variables $\mathbf{X} = \{x_1, x_2, \ldots, x_n\}$ take their numerical values, the mapping f determines the corresponding values of output variables $\mathbf{Y} = \{y_1, y_2, \ldots, y_m\}$.

In many cases, a model is assumed to mirror a real physical situation. However, "a model is just a reduced and parsimonious representation of a physical, chemical, or biological system in a mathematical, abstract, numerical, or experimental form." [5] Generating a model is, in fact, the process of idealizing the complicated real world into a relatively simple form through making a set of assumptions. No model can completely represent a real situation or process because of the assumptions made during the modeling process. Also, if other sets of assumptions are introduced, different, incomplete models would be generated that represent the identical physical phenomenon or process in question. Apart from the simplifying assumption, models may also vary depending on the decisions made during the modeling process with regard to the modeler's preference, requirements of the model user, or economic matters. For example, a modeler can construct a variety of finite element models to analyze an engineering system by varying the element types, geometry, shape functions, mesh sizes, material behavior, expected operating loads, or boundary conditions. To summarize, different models can be constructed for a certain physical system, but none of them is a complete representation of physical behavior.

Given two or more approximating models for a physical system, the problem may occur of whether it is feasible to select the particular physical model that represents the system with the highest fidelity from the set of considered models. Generally, it is beyond our

ability to select the best approximation from a set of models. This is because we cannot measure the relative degrees of discrepancy between a physical system and a set of models approximating the system due to lack of knowledge about the system. So, uncertainty is involved in selecting the best model from a set of models. This uncertainty is called model-form uncertainty in this research. Model-form uncertainty is categorized as epistemic uncertainty [6] since it derives from our lack of knowledge.

Given experimental data, it is practical to make a guess that a certain model is best of a set of models using model selection criteria, such as the Akaike information criterion or the Bayesian information criterion [7, 8]. Model selection criteria selects a particular model that fits better into observed experimental data with a smaller number of regression parameters compared to the other models in a model set as the best model. However, the relative goodness of fit of considered models may vary depending on the sample size of experimental data. This means that a model selected as the best of a model set might not be the best if additional experimental data support another model better than the first model. Therefore, model-form uncertainty cannot be eliminated even after observing experimental data.

Model-form uncertainty is generally quantified by assigning probability to each element of a model set (e.g. $\Pr(\text{model 1}) = 0.1$, $\Pr(\text{model 2}) = 0.5$, and $\Pr(\text{model 3}) = 0.4$). Model-form uncertainty should be incorporated into the prediction of a system response, especially when two or more competing models show significant differences between

their predictions. Ignoring model-form uncertainty is problematic because it may lead to underestimating the variability of predictions or making erroneous predictions [9, 10].

1.2.2 Parametric and Predictive Uncertainty

It is well known that parametric uncertainty exists in a simulation model. Parametric uncertainty may be defined as the uncertainty residing in the input parameter set **X** of a model expressed by $\mathbf{Y} = f(\mathbf{X})$, while model-form uncertainty may be regarded as the uncertainty existing in the model form f. Parametric uncertainty occurs because of the randomness inherent in parameter(s) within a model; randomness implies a lack of predictability resulting from the fact that the events considered occur by chance. In general, the randomness in input parameter(s) is represented by probability distribution function.

Although a simulation model is used to predict responses of an engineering system, the predictions by the model involve errors because any simulation model is no more than an approximation of the real system. A prediction error of a model is regarded as an unknown variable because the prediction error is unpredictable due to its inherent randomness. The uncertainty in prediction error is often called predictive uncertainty [11]. Given observed experimental data, predictive uncertainty can be quantified by measuring the differences between the experimental data and the model outcomes of the data. In this research, unknown prediction error is critical to quantifying model-form uncertainty in that it serves as a link between a set of models and the real system described by the model set.

Parametric and predictive uncertainty are associated with each member of a model set, while model-form uncertainty resides in the considered model set as shown in Figure 1.2. The quantification of parametric and predictive uncertainty in response predictions should precede the quantification of model-form uncertainty because given observed experimental data, model predictions involving parametric and predictive uncertainty are used to quantify model-form uncertainty. As shown in Figure 1.3, model-form uncertainty is incorporated into the composite prediction of a response through the action of linearly combining multi-model predictions involving parametric and/or predictive uncertainty.

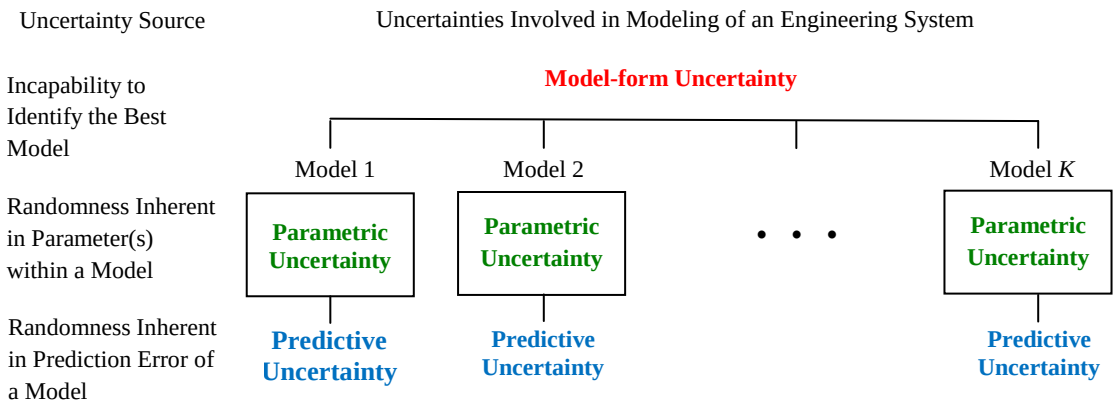

Figure 1.2 Three types of uncertainty involved in modeling an engineering system

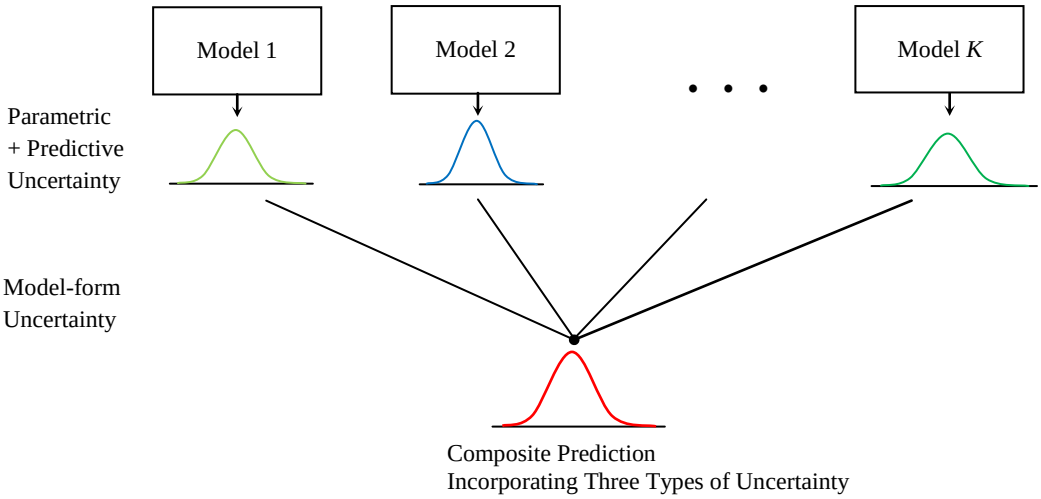

Figure 1.3 Combining multi-model predictions into a composite prediction

1.3 Literature Review on Quantification of Multiple Types of Uncertainty

1.3.1 Literature Review on Model-Form UQ

While model-form Uncertainty Quantification (UQ) is in its initial stages of consideration in the engineering field, model-form UQ has been studied extensively in statistics, economics, and environmental science over the past generation.

Given two or more statistical models available to explain the process generating observed data, it is a natural way of thinking to select the model that best explains the data from among the considered model set. In statistics, a variety of model selection criteria have been developed from different perspectives with the aim to select the best model from a plausible regression model set. Generally, a statistical model selection process is implemented with the concept that the best model balances goodness of fit with simplicity (usually measured by counting the number of regression parameters) better

than the other considered models. Akaike Information Criterion (AIC) [7] and Bayesian Information Criterion (BIC) [8] are the most famous among them. Both AIC and BIC attempt to find the model that best explains observed data with a minimum of regression parameters. AIC offers a relative measure of the information lost when an approximating model is used in place of the unknown true model [1]. BIC provides a large-sample asymptotic estimator of a transformation of the Bayesian posterior probability associated with an approximating model [12]. Choosing the better criterion depends on how fast the approximation errors of the considered models—depending on the sample size and the error variance—decrease; AIC performs better when the approximation errors of good competing models decrease slowly [13]. Other advocated criteria for model selection include Mallows' Cp [14, 15], cross-validation [16, 17], minimum description length [18] and the focused information criterion [19].

A model selection process inevitably accompanies the uncertainty not captured within the model selected from a plausible model set. Uncertainty associated with model selection (model-form uncertainty in this research) is attributed to the fact that the model selection process may well select a model other than the selected model if another set of data was generated under the same condition. It has been argued that a simple way to account for model-form uncertainty is by model averaging, or weighted average of a set of predictions obtained under different models. Model combination produces predictions that incorporate the (epistemic) variation inherent in the statistical model selection process as well as the (aleatory and/or epistemic) variation conditional on each model.

Model combination techniques from a Bayesian perspective have been intensively developed since Leamer [20] built the basic paradigm of Bayesian model averaging (BMA) in 1978. Contributions to model combination from a frequentist perspective have been fewer, but frequentist literature on model combination is growing with recent significant progress. Roughly speaking, a distinction between the two perspectives is that frequentists make inferences based only on observed data, while Bayesians make inferences based on both observed data and prior information. Primary contributions to BMA include those by Draper [9], Raftery, Madigan, and Hoeting [21], and Hoeting et al. [22]. BMA is a natural way to systematically deal with model-form uncertainty from a Bayesian point of view. BMA requires assumptions about prior distributions of unknown parameters and prior model probabilities. This requirement becomes an advantage or a disadvantage of BMA depending on whether prior opinions regarding unknown parameters and model probabilities are numerically specified in a proper way or not. A drawback of BMA is that posterior model probability can rarely be calculated in closed form for high-dimensional models. Markov Chain Monte Carlo (MCMC) numerical methods [23 - 25] have been well established as powerful numerical tools to implement practical analyses of a wide range of models that are unmanageable by purely analytic methods. Raftery [26] suggests the use of BIC approximation for BMA. Unlike the Bayesian approach for which many conflicting prior opinions regarding unknown parameters have to be numerically specified and then mixed, frequentist model combination can be implemented without any dependence on prior opinions. Buckland, Burnham and Augustin [27] proposed bootstrap model combination which applies AIC model selection criteria independently to each of the bootstrap samples. In this method,

the weight for a model is estimated by observing the proportion of bootstrap resampled data sets in which the model is identified as the best approximating model. Bootstrap model combination was modified by Augustin et al. [28] to include a variable screening step in order to identify and eliminate variables with no or a negligible effect on the outcome. Hansen [29] suggested selecting model weights by minimizing a Mallows' Cp. Cross-validation and bootstrapping have been used to linearly combine different estimators to improve accuracy by finding the best linear combination [30, 31]. Claeskens and Hjort [32] proposed specifying model weights based on the focused information criterion.

Model selection criteria such as AIC, BIC, Mallows' Cp, cross-validation and the focused information criterion which can be adapted to the task of model combination are the approaches developed with the aim of selecting the best approximating model from a plausible regression model set. Unlike the statistical regression models that fit observed experimental data, mathematical or simulation models used in the engineering field (specifically functional forms in the models) are fundamentally created based on scientific and engineering knowledge. Some of analytical models such as semi-empirical models have their functional forms derived from both theoretical knowledge and empirical data. For many engineering models, input parameters such as dimension and material property have their own physical meanings and are usually determined using empirical data on them. The numerical specification of input parameters is made independently of experimental data on system responses such as stress and displacement. Therefore, model combination based on purely statistical model selection criteria is not

applicable to engineering models that have their functional forms and input parameter values not determined by statistical regression procedures. BMA is believed to be suitable for quantifying model-form uncertainty associated with the engineering models and performing model averaging. BMA requires prior distributions of unknown parameters and prior model probabilities to be defined by the state of knowledge prior to obtaining empirical evidence. This requirement becomes an advantage or a disadvantage of BMA depending on whether expert elicitation of prior knowledge regarding unknown parameters and model probabilities is compatible with numerical specification of those quantities. The adjustment factor approach [33] was suggested as another model combination technique for engineering application. The adjustment factor approach assumes that model-form uncertainty is associated with the model identified as the best model and can be represented as a normal or log-normal distribution when being propagated into the prediction of a response.

In the engineering field, little research has been done to quantify model-form uncertainty compared to other fields such as statistics, economics, and environmental science. Alvin et al. [34] used Bayesian Model Averaging (BMA) to estimate the model-form uncertainty in frequency predictions of a bracket resulting from the use of three probabilistic simulation models—parametric uncertainty in the elastic material modulus is assumed by each simulation model. The three simulation models had different levels of simplifying assumptions in their PDE form, as well as different spatial meshes and different discrete solution variables. Model probability—the degree of belief that a model is the best of a set of models—was simply assumed to be uniform across the considered

simulation models. Zio and Apostolakis [33] used the adjustment factor approach to estimate the model-form uncertainty in the response predictions regarding the cumulative release of a radionuclide to the water table given by six different models. The six models differ by some fundamental hypotheses on the groundwater flow and transport mechnisms. Model probabilities were evaluated based on expert opinions. Zhang and Mahadevan [35] estimated the failure probabilities for butt welds of a steel bridge using two competing crack growth models (the Foreman and the Weertman crack growth models). They made a reliability analysis of fatigue life by averaging the estimated failure probabilities weighted by the probabilities of the crack models. The uncertainty in crack size measurement was quantified to evaluate the model probabilities using Bayes' theorem. Zouaoui and Wilson [36] used BMA to quantify the model-form uncertainty in the prediction of a message delay in a computer communication network. Although simulation models were used to predict a message delay, model probabilities were not assigned to the simulation models but to three different types of distributions that represent the uncertainty in an input variable (i.e. a message length). The distributions for a message length were assumed to be of exponential, normal and lognormal forms. McFarland and Bichon [37] used BMA to incorporate probability distribution model-form uncertainty into the estimation of failure probability of a bistable MEMS device. As in the work of Zouaoui and Wilson, model probabilities were assigned to the three types of distributions (normal, lognormal and Weibull) representing the uncertainty in an input variable (i.e. edge bias on beam widths).

1.3.2 Literature Review on Parametric UQ

The methodologies to handle parametric uncertainty are sorted into two categories depending on whether to address aleatory or epistemic type of uncertainty as shown in Figure 1.4.

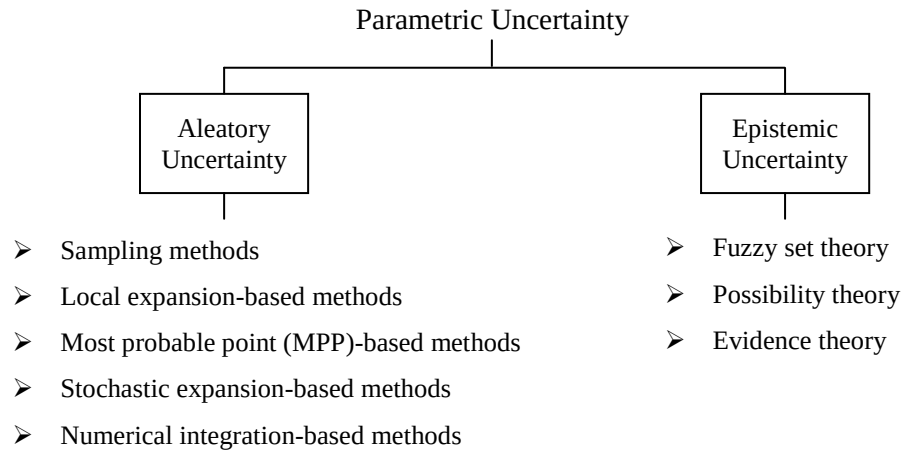

Figure 1.4 Methodologies to handle aleatory and epistemic uncertainty

① Methodologies to Handle Aleatory Uncertainty

Aleatory uncertainty indicates uncertainty due to natural variability inherent in the physical system or the environment under consideration. Generally, aleatory uncertainty is represented by a probability distribution when enough experimental data are presented to estimate the distribution. Probability distributions expressing the inherent variability in system parameters are propagated through a mathematical model or simulation process. A large number of methodologies have been developed to propagate probability distributions representing parametric uncertainty. Those methodologies are classified into five groups [38] as follows:

The first category is the sampling methods like Monte Carlo Simulation (MCS) [39, 40], importance sampling [41, 42] and Latin Hypercube Sampling (LHS) [43, 44]. Sampling

methods are characterized by the strategy that makes realizations by a simulator based on randomly generated sampling sets for random input variables to attain stochastic information about system responses. The implementation procedure of MCS consists of specification of the probability distributions representing random input variables, generation of sampling sets from the distributions, simulation of response outputs using the generated sampling sets, and calculation of probabilistic information about the responses. Importance sampling is a variance reduction technique that utilizes a sampling set generated from a biased distribution which concentrates on the important regions of an input variable. LHS is another variance reduction technique which generates a distribution of plausible collections of input variable values from a multi-dimensional distribution to reduce the number of simulation runs for higher dimensional problems. A basic advantage of sampling methods is in their direct utilization of simulated outputs to obtain probabilistic information about system responses which cannot be solved easily by known procedures. The drawback of sampling methods is that uncertainty analysis using sampling techniques would require an overwhelming number of realizations, making it virtually impossible to use the methods for large-scale engineering problems.

The second category is the local expansion-based methods like Taylor series expansion [45], perturbation method [46, 47], and the Neumann expansion method [48, 49]. The idea of the expansion methods is to estimate statistical moments of system responses with a small perturbation in random input variables. Taylor series expansion and perturbation method involve expansion of a system response as a series in terms of a small random perturbation in input variables and the subsequent solution of the series coefficients.

Taylor series expansion and perturbation method require high-order partial derivatives to maintain good accuracy. The Neumann expansion method involves finding the inverse of random matrices through Neumann series expansion of the matrices. The expansion methods require less computation and are suitable for small levels of uncertainties. The local expansion-based methods have been popularly applied to compute the first two statistical moments of system responses. The major drawback of these methods is that the methods could become computationally inefficient or inaccurate when the number or the degree of input uncertainty is higher. In addition, these methods may not be practical for large-scale engineering applications due to the requirement of high-order partial derivatives of system responses.

The third category is the most probable point (MPP)-based methods [50-52]. The first-order reliability method (FORM) and second-order reliability methods (SORM) in this category are the two popular approximation methods that estimate the probability of failure associated with a limit-state function. The distinction between the two methods depends on the utilization of a first-order or a second-order Taylor series expansion to approximate a limit-state function at the MPP. Rotationally symmetric safety index is introduced through the Hasofer and Lind (HL) transformation for both the methods. If the approximation of a limit-state function at the MPP is accurate, the MPP-based methods can produce satisfactory results. In addition, these methods can calculate the relative effect of each input variable (sensitivity factor) on the probability of failure at no additional computational cost. However, the FORM and the SORM may result in large errors when the limit-state function is highly nonlinear. Moreover, these methods require

the calculation of the first-order or second-order derivatives of system responses which is extremely computer intensive for a multi-physics simulation with a large number of random variables.

The fourth category is the stochastic expansion-based methods. The spectral stochastic finite element method (SSFEM) [53] and the stochastic response surface method (SRSM) [54, 55] can be classified into this group. In 1990, Ghanem and Spanos [53] proposed SSFEM in which FEM is extended to tackle uncertain systems governed by stochastic partial differential equations. SSFEM is an approach well suited for analysis involving random fields; in this method, the Karhunen–Loève (KL) expansion is effectively used to represent random fields. The basic idea of SSFEM is to represent a system response by a linear combination of orthogonal polynomials of standard random variables. SRSM also uses orthogonal polynomials to represent stochastic system responses, but does not require any modification of the FE codes already built unlike SSFEM. Due to the non-intrusive formulation procedures, SRSM supplies a practical approach for stochastic analysis of large-scale engineering problems which have already been analyzed in the deterministic domain using established and verified FE codes. The stochastic expansion-based methods can provide information on higher order statistics of the stochastic system behaviors even for large levels of input uncertainty involved. However, these methods may be poor for problems involving high nonlinearity and discontinuity in which potential divergence in higher order moments may be observed.

The last category is the numerical integration-based methods. Multi-dimensional numerical integration methods are characterized by use of moment-based quadrature rules to numerically integrate a multidimensional distribution of a system response [56]. Response function is evaluated at a set of well-designed sampling points, often called quadrature points, for the numerical integration. A newly developed method in this category is the so-called dimension reduction (DR) method [57, 58]. The DR method approximates a multi-dimensional integration of a system response by multiple one-dimensional integrations based on an additive decomposition of a response function. An additive decomposition of a multi-dimensional response function makes this method substantially simpler and more efficient than conventional multi-dimensional integration methods. However, the DR method may produce a relatively large error for the second-order or higher moments of responses of a system involving large random variation and/or high nonlinearity. The numerical integration-based methods do not require the calculation of any derivatives of responses, and yet can predict response moments accurately. The downside of the moment-based methods is the numerical efficiency. The moment-based methods tend to become inefficient as the number of random variables becomes large.

② Methodologies to Handle Epistemic Uncertainty

Epistemic uncertainty indicates uncertainty due to the lack of knowledge or information regarding the modeling of a physical system. Mathematical representation of epistemic uncertainty is much more challenging than representation of aleatory uncertainty. The methodologies developed to handle epistemic uncertainty are described as follows:

Fuzzy set theory [59-61] was developed by Zadeh as a brilliant generalization of the classical notion of a set. Fuzzy sets are sets whose elements have the grades of membership described by the so-called membership function valued in the real unit interval [0, 1]. Fuzzy set theory has been used to handle the uncertainty arising from impreciseness, ambiguity or vagueness in limited data base. An advantage of fuzzy set theory is that it supplies inference models that can deal with the imprecision inherently present in human knowledge with the membership function characterized by the gradual transition from membership to non-membership. However, it is difficult to provide optimal membership functions for the physical system being analyzed because membership functions are designed by experts with partial knowledge of the given system. Another disadvantage of fuzzy set theory is that there are many ways of interpreting fuzzy rules and combining the outputs of several fuzzy rules.

Possibility theory [62-64] first introduced by Zadeh and further developed by Dubois and Prade is viewed as an extension of fuzzy set theory. Possibility theory was proposed as an approach to model flexible restrictions on the values that a variable may take defined by membership functions of fuzzy sets. Possibility theory can faithfully represent states of partial ignorance by the use of possibility distribution which describes the strength of belief that a particular event can be expected. Possibility and necessity measures defined by a possibility distribution are used to represent an agent's confidence about how likely related events are to occur. Possibility theory has the advantages and disadvantages identical to those of fuzzy set theory mentioned above since the latter provides a natural basis for the former.

Dempster initiated the evidence theory (or the Dempster-Shafer theory) [65-67] by developing the theory of upper and lower probabilities, and Shafer provided a systematic explanation of belief functions to model imprecise human knowledge. The evidence theory is a promising theory that can handle uncertainty deriving from imprecise information in expert systems with ease. As opposed to Bayesian statistics where uncertain information must be represented by exactly specified additive probabilities, the evidence theory can assign numerical measures of uncertainty to overlapping sets and subsets of propositions as well as individual propositions. Basically, evidence is represented by basic belief mass which is assigned to a proposition to express the proportion of total belief supporting the proposition. From the basic belief assignment, belief and plausibility functions are defined to represent the lower and upper probability bounds of relevant propositions under consideration. The aggregation of independent pieces of evidence is carried out through a procedure called the Dempster's rule of combination. An advantage of the evidence theory is that the functions and combination rule of the theory appropriately represent evidence supplied by expert knowledge system and its aggregation. Another benefit of this theory is avoidance of the Bayesian restriction that assignment of belief to a proposition implies assignment of the remaining belief to its negation. However, when a significant conflict arises between two pieces of evidence, the Dempster's rule of combination gives a counterintuitive outcome. Also, there is an obstacle in the application of the evidence theory that the amount of computational efforts required for the combination of evidences increases exponentially with the number of probable events considered.

1.3.3 Literature Review on Predictive UQ

A traditional way to describe the probabilistic relationship between experimental and model outcomes is through modeling experimental data as the sum of the model predictions of the data plus unknown prediction errors [68-70]. In general, an unknown prediction error is represented by a probability distribution. The probability distribution of a prediction error is unknown and can be estimated based on the measured differences between possibly quite limited experimental data and the model predictions of the data. Unknown prediction errors are usually assumed to be normally distributed with zero mean and a constant variance. It is often stated that all variation in observed experimental data that cannot be explained by the considered model is included in the random error term. The statistical theory associated with unknown prediction error is well-understood and allows for constructing different types of easily interpretable statistical intervals for predictions. However, the assumption that unknown errors are only associated with model predictions does not accommodate any framework to discern between the sources attributed to prediction errors.

To differentiate between the sources causing a prediction error, Kennedy and O'Hagan [71] first introduced a model discrepancy term, which quantifies the systematic discrepancy between the true system response and model prediction, in addition to an experimental error term (similar to a random error term in regression model). The model that they propose is expressed by $z_i = \zeta(x_i) + e_i = \rho\eta(x_i, \theta) + \delta(x_i) + e_i$; z denotes the observed data, $\zeta(\cdot)$ the true system response, $\eta(\cdot,\cdot)$ the model output, e_i the experimental error for the ith observed data z_i, ρ an unknown regression parameter (an adjustment

parameter), and $\delta(\cdot)$ a model discrepancy term. The model discrepancy term $\delta(\cdot)$ empirically describes model inadequacy due to the incompleteness in the science or engineering used to construct a model, imperfect numerical implementation and any inaccurate input parameters. Bayesian statistical methodology can be utilized to quantify the uncertainty in the model discrepancy term $\delta(\cdot)$ assumed to be a Gaussian process. Bayesian approach does not require large experimental data sets unlike the frequentist approach. However, when there is only a small amount of experimental data, the choice of prior distribution tends to significantly influence the results. The experimental error term e_i is usually assumed to be an independent normal variable with zero mean. Bayarri et al. [72], Higdon et al. [73], Xiong et al. [74] and Liu et al. [75] used a formulation that is same as the one used by Kennedy and O'Hagan except the regression parameter ρ omitted. The above-mentioned formulations to model unknown prediction error are widely utilized in validating a simulation model.

1.4 Outline of Chapters

Chapter 1 states the problems to be addressed in this research and introduces multiple types of uncertainty associated with an engineering analysis along with literature survey on them. A methodology is developed to evaluate model probability given experimental data in Chapter 2. The adjustment factor approach and model averaging, which are used to combine predictions of multiple models, are described and illustrated with the numerical problem of a spring-mass system in Chapter 3. In Chapter 4, the proposed methodology is applied to the physics-based simulation of a laser peening process for the three cases incorporating only model-form uncertainty into a composite prediction and

incorporating predictive uncertainty as well as model-form uncertainty, and incorporating all the three types of uncertainty. A methodology is developed to quantify both model-form and parametric uncertainty involved in a response prediction using expert evidence in Chapter 5. Summary remarks are presented in Chapter 6.

2. Quantification of Model-Form Uncertainty

While parametric uncertainty is generally represented by probability distribution which is continuous over a feasible range of input parameter(s), model-form uncertainty is represented by discrete probabilities assigned to a finite number of countable models; although infinite number of (mathematical) models could be defined over a continuous model space, the present research only deals with discrete models because creating continuously-varying computer simulation models is neither practical nor possible. A methodology is developed to make an informed estimation of model probability under a Bayesian statistical framework.

The definition of model probability is presented in Section 2.1. Bayes' theorem, which is used to update prior model probability by means of evaluated model likelihood, is described in Section 2.2. Section 2.3 presents the proposed methodology for evaluating model likelihood using the measured differences between observed experimental data and model predictions that may involve parametric uncertainty and/or predictive uncertainty. Updating prior model probability with model likelihood using Bayes' theorem is described in Section 2.4. The proposed methodology is demonstrated with multiple linear models generated to state the underlying trend in experimental data concerning cement hardening in Section 2.5.1, and different mathematical models to estimate the amount of creep that a concrete specimen experiences in Section 2.5.2.

2.1 Definition of Model Probability

Mathematically, model probability is defined as the degree of belief that a model is correct, given that the correct model is in the set of models considered. A correct model is the model that mirrors the real system under consideration and generates the same data as observed responses of the system given no measurement error being involved. It is argued that this definition is the simplest and the only definition that is mathematically acceptable [76]. However, as discussed in Section 1.2.1, there is no such thing as a correct model because a model is no more than a certain (usually mathematical) form of representation of the model developer's interpretation of the real system by means of idealization of the reality [77]. The fact that all the engineering models are just approximations of the reality shifts our focus to the task of identifying the best approximating model among a given model set. However, it is not possible to select the best model from a set of models due to lack of knowledge about the real system. What is under our control is to assign probability to each model to represent the degree of belief that each model is the best approximation among a given set of models; the best approximating model is defined as the model that predicts system responses of interest, usually unknown, more accurately than the other models in a model set. Model probability can be quantified depending on subjective information including expert opinions and updated when experimental data are observed. Bayes' theorem to update model probability given experimental data is described in the following Section.

2.2 Bayes' Theorem

In probability theory, Bayes' theorem [78, 79] presents a way to represent a conditional probability (such as the probability of a hypothesis given observed experimental data) with its inverse (in this case, the probability of that evidence given the hypothesis). Using the theorem, the posterior probability (the probability evaluated after observing experimental data) of a hypothesis can be expressed in terms of the prior probability (the probability evaluated before observing the data) of the hypothesis and the probability of the observed data given the hypothesis. The probability of observed experimental data given a hypothesis, referred to as the likelihood of a hypothesis given experimental data, is interpreted as the relative likelihood for experimental data to occur given that the hypothesis is correct. Bayes' theorem is valid for any interpretation of probability and is applicable to science and engineering.

2.2.1 Conditional Probability

Suppose that observed data D and hypothesis H are defined in a universal space U as shown in Figure 2.1.

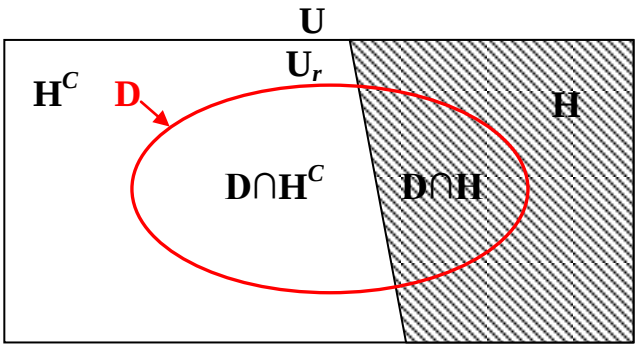

Figure 2.1 Conditional probability of a hypothesis given observed data

Observation of data D implies that the possibility of observing any data outside D is excluded from consideration. The universal space U is now reduced to the observed data space U_r= D. Since the universal space is changed, the probability of hypothesis H has to be newly defined in the reduced universal space U_r. As shown in Figure 2.1, the only part of hypothesis H that is now relevant is that of H in the reduced space U_r, or D ∩ H. Because the portion of D ∩ H compared to the reduced space U_r = D is (D ∩ H) / D, the probability of H in the reduced space is defined by

$$\Pr(H|D) = \frac{\Pr(H \cap D)}{\Pr(D)} \tag{2.1}$$

This probability is called the conditional probability of H given D as H is defined conditionally on the occurrence of D.

2.2.2 Multiplication Rule

If the positions of H and D are inversed in Eq. (2.1), Eq. (2.1) can be restated as

$$\Pr(D|H) = \frac{\Pr(H \cap D)}{\Pr(H)} \tag{2.2}$$

When the fractions in Eq. (2.2) are cleared, Eq. (2.2) turns into

$$\Pr(H \cap D) = \Pr(H) \times \Pr(D|H) \tag{2.3}$$

This is known as multiplication rule for probability. Similarly,

$$\Pr(H^C \cap D) = \Pr(H^C) \times \Pr(D|H^C) \tag{2.4}$$

2.2.3 Bayes' Theorem for a Hypothesis

Substituting Eq. (2.3) into the conditional probability of H given D shown in Eq. (2.1), the following equation is obtained:

$$\Pr(\mathrm{H}\,|\,\mathrm{D}) = \frac{\Pr(\mathrm{H}) \times \Pr(\mathrm{D}|\mathrm{H})}{\Pr(\mathrm{D})} \tag{2.5}$$

Since D ∩ H and D ∩ H^C are disjoint as shown in Figure 2.1, the following equation holds:

$$\Pr(\mathrm{D}) = \Pr(\mathrm{D} \cap \mathrm{H}) + \Pr(\mathrm{D} \cap \mathrm{H}^C) \tag{2.6}$$

Substituting Eq. (2.6) into Pr(D) in Eq. (2.5), the following equation is obtained:

$$\Pr(\mathrm{H}\,|\,\mathrm{D}) = \frac{\Pr(\mathrm{H}) \times \Pr(\mathrm{D}|\mathrm{H})}{\Pr(\mathrm{D} \cap \mathrm{H}) + \Pr(\mathrm{D} \cap \mathrm{H}^C)} \tag{2.7}$$

Now, the joint probabilities in denominator of Eq. (2.7) are substituted by the conditional probability expressions shown in Eqs. (2.3) and (2.4). This results in Bayes' theorem for a hypothesis H as shown in

$$\Pr(\mathrm{H}\,|\,\mathrm{D}) = \frac{\Pr(\mathrm{H}) \times \Pr(\mathrm{D}|\mathrm{H})}{\Pr(\mathrm{H}) \times \Pr(\mathrm{D}|\mathrm{H}) + \Pr(\mathrm{H}^C) \times \Pr(\mathrm{D}|\mathrm{H}^C)} \tag{2.8}$$

Pr(H) is the prior probability of hypothesis H, defined before observing data D. Pr(H | D) is the conditional probability of hypothesis H given observed data D, and is also called the posterior probability of H because it derives from the observed data D. Pr(D | H) (often L(D | H) used) is called the likelihood of H given D because D is considered to be fixed, and H is allowed to vary. Whereas probability allows us to predict unknown data based on known hypotheses, likelihood allows us to estimate unknown hypotheses based on known data. Bayes' theorem presents a mathematical

representation of how the conditional probability of hypothesis H given observed data D is correlated with the likelihood of H given D. In other words, given prior probability Pr(H), Eq. (2.8) gives posterior probability Pr(H | D) in terms of likelihood Pr(D | H).

2.2.4 Bayes' Theorem for a Set of Hypotheses

Suppose that a set of hypotheses constitute a universal space and the considered set of hypotheses have no common parts (collectively exhaustive and mutually exclusive). For example, as shown in Figure 2.2, a set of hypotheses $H_1, \ldots, H_K$ partition a universal space U, and they are disjoint such as:

- The union $H_1 \cup H_2 \cup \cdots \cup H_K = U$, the universe, and
- Every distinct pair of the hypotheses are disjoint, $H_i \cap H_j = \phi$ for $i = 1, \ldots, K$, $j = 1, \ldots, K$, and $i \neq j$.

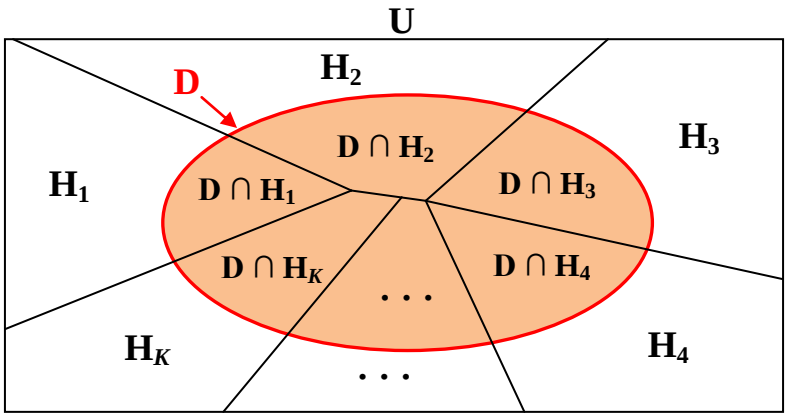

Figure 2.2 A set of hypotheses partitioning a universal space

Since a set of hypotheses $H_1, \ldots, H_K$ partition a universal space, and they are disjoint, it holds that $D = (D \cap H_1) \cup (D \cap H_2) \cup \cdots \cup (D \cap H_K)$, and $(D \cap H_i) \cap (D \cap H_j) = \phi$ for $i = 1, \ldots, K$, $j = 1, \ldots, K$, and $i \neq j$. This leads to

$$\Pr(\mathrm{D}) = \sum_{k=1}^{K} \Pr(\mathrm{D} \cap \mathrm{H}_k) \tag{2.9}$$

Eq. (2.5) can be restated for a hypothesis H_k as

$$\Pr(\mathrm{H}_k \mid \mathrm{D}) = \frac{\Pr(\mathrm{H}_k) \times \Pr(\mathrm{D} \mid \mathrm{H}_k)}{\Pr(\mathrm{D})} \tag{2.10}$$

Substituting Eq. (2.9) into the denominator in Eq. (2.10), the following equation is obtained:

$$\Pr(\mathrm{H}_k \mid \mathrm{D}) = \frac{\Pr(\mathrm{H}_k) \times \Pr(\mathrm{D} \mid \mathrm{H}_k)}{\sum_{i=1}^{K} \Pr(\mathrm{D} \cap \mathrm{H}_i)} \tag{2.11}$$

The multiplication rule shown in Eq. (2.3) gives $\Pr(\mathrm{D} \cap \mathrm{H}_k) = \Pr(\mathrm{H}_k) \times \Pr(\mathrm{D} | \mathrm{H}_k)$. Substitution of this expression into Eq. (2.11) gives Bayes' theorem for a set of hypothesis expressed by

$$\Pr(\mathrm{H}_k | \mathrm{D}) = \frac{\Pr(\mathrm{H}_k) \times \Pr(\mathrm{D} | \mathrm{H}_k)}{\sum_{i=1}^{K} \Pr(\mathrm{H}_i) \times \Pr(\mathrm{D} | \mathrm{H}_i)}, \quad k = 1, \ldots, K \tag{2.12}$$

This is a result known as Bayes' theorem published in 1763 after the death of its discoverer, Reverend Thomas Bayes. Bayes' theorem allows us to modify the initial probabilities of a set of hypotheses using observed data.

In the quantification of model probability, each hypothesis H_k in Eq. (2.12) is equivalent to each model M_k in a set of models $\mathrm{M}_1, \ldots, \mathrm{M}_K$; $\Pr(\mathrm{H}_k) = \Pr(\mathrm{M}_k)$, $\Pr(\mathrm{H}_k \mid \mathrm{D}) = \Pr(\mathrm{M}_k \mid \mathrm{D})$ and $\Pr(\mathrm{D} \mid \mathrm{H}_k) = \Pr(\mathrm{D} \mid \mathrm{M}_k)$. What these terms denote is as follows:

- $\Pr(\mathrm{M}_k)$ represents prior probability of model M_k, which measures the degree of belief in M_k before observing data D.

- $Pr(M_k \mid D)$ represents posterior probability of model M_k, which is evaluated after observing data D.
- $Pr(D \mid M_k)$ represents likelihood of model M_k given observed data D, which is used to update prior model probability $Pr(M_k)$ into posterior model probability $Pr(M_k \mid D)$.

When equal prior model probability is assumed, the only concern is the quantification of model likelihood $Pr(D \mid M_k)$.

2.2.5 Demonstration Problem

Q) A person is randomly chosen to take an AIDS test. Assume that the analytic performance of the test for HIV infection is represented by the following probabilistic description:

$$Pr(\text{Positive}| \text{ HIV}) = 0.998$$

$$Pr(\text{Positive}| \text{ HIV}^C) = 0.002$$

where HIV denotes "infected" and HIV^C denotes healthy. A survey states that 100,000 persons out of a population of 60 million are estimated to be infected with HIV. Suppose that the person proves to be HIV positive according to the analysis used for the test. What is the probability that the person is truly infected? [80]

A) It seems that one might think that the person is very likely to have been infected with HIV because the analysis used for the test shows a very good performance. However, taking the survey result into account, this intuitive thought proves to be false. Based on the result of the survey, prior probability concerning whether a person is infected is represented as follows:

$$\Pr(\text{HIV}) = 1/600$$

$$\Pr(\text{HIV}^C) = 599/600.$$

The prior probabilities above are interpreted as the probabilities of whether the person undergoing the AIDS test is infected, which are computed before the test. Using Eq. (2.8), the post probability that the person is infected is

$$\Pr(\text{HIV} \mid \text{Positive}) = \frac{\Pr(\text{HIV}) \times \Pr(\text{Positive} \mid \text{HIV})}{\Pr(\text{HIV}) \times \Pr(\text{Positive} \mid \text{HIV}) + \Pr(\text{HIV}^C) \times \Pr(\text{Positive} \mid \text{HIV}^C)}$$

$$= \frac{1/600 \times 0.998}{1/600 \times 0.998 + 599/600 \times 0.002} = 0.454$$

The calculated value (0.454) of Pr(HIV| Positive) implies that the posterior probability of a proposition (for this problem, the statement that the person taking the test is infected) might be significantly affected by the prior probability of the proposition. Prior probability of a proposition is unavoidable in the application of Bayes' theorem even if quantification of it is occasionally intricate. The influence of prior probability may become negligible when experimental evidence strongly favors a given proposition.

2.3 Evaluation of Model Likelihood

Model likelihood is defined as the relative likelihood of observing experimental data that are actually observed given that a model is correct. It may be used as a measure of the relative closeness between a real system and a set of models representing the system. Model probability is updated by means of model likelihood using Bayes' theorem. In the previous research into the quantification of model probability in the engineering field [36, 37], model likelihood was quantified using experimental data on an input parameter (not

system response). The model probabilities quantified in that way cannot supply effective measures of model-form uncertainty when making predictions of unknown system responses. This Section presents a methodology developed to evaluate model likelihood using the measured differences of experimental and model outcomes. The mathematical concept of likelihood and the maximum likelihood estimation are described in Section 2.3.1. The concept of unknown prediction error is described in Section 2.3.2. Evaluation of model likelihood is described for two cases in which parametric uncertainty is not involved and is involved in Sections 2.3.3 and 2.3.4, respectively.

2.3.1 Likelihood

① The Fundamental Concept of Likelihood

In 1922, Fisher, R. A. [81] introduced the concept of likelihood "to express the state of available information concerning the parameters of hypothetical populations." He discerned likelihood from probability because the quantitative measure of likelihood does not observe the mathematical laws of probability. The likelihood of a hypothesis H given data D is denoted by $L(\mathrm{H}\,|\,\mathrm{D})$ or $\Pr(\mathrm{D}\,|\,\mathrm{H})$. The numerical value of likelihood $L(\mathrm{H}\,|\,\mathrm{D})$ is of no importance; all that matters is the ratio of the likelihoods of two different hypotheses given the same observed data. If $\Pr(\mathrm{D}\,|\,\mathrm{H})$ is used to denote the probability of D given H, D is unknown variable and H is known variable. On the other hand, in the likelihood of H given D denoted by $L(\mathrm{H}\,|\,\mathrm{D})$ or $\Pr(\mathrm{H}\,|\,\mathrm{D})$, H is unknown and D is known variable.

Consider a binomial distribution to model the situation where a biased coin is flipped five times and the number of heads is counted. Since the coin is not fair, the probability p of

getting the head upon flipping is unknown. Suppose that the five independent trials of flipping the coin give the data of observing the head three times. The likelihood of obtaining this data D is represented as a function of unknown parameter p:

$L(p \mid \mathrm{D}) = \Pr(\mathrm{D} \mid p) = \frac{5!}{3!2!} p^3 (1-p)^2 = 10p^3(1-p)^2$. This function is called likelihood function, which expresses the probability of observed data as a function of unknown parameter(s). The likelihood function $L(p \mid \mathrm{D})$ is graphed in Figure 2.3. It is remarkable that the likelihood function is not a probability distribution function because the integral of the likelihood function over the domain of unknown parameter p is not 1. Likelihood function conveys all the relevant information that the observed data contains regarding the estimation of the unknown parameter. Likelihood function is also the basis for Bayesian statistics. The mathematical forms of likelihood function and probability distribution function are in common. The difference between the two functions is that a probability distribution function is a function of unobserved data with parameters being fixed, while a likelihood function is a function of unknown parameters with data being observed.

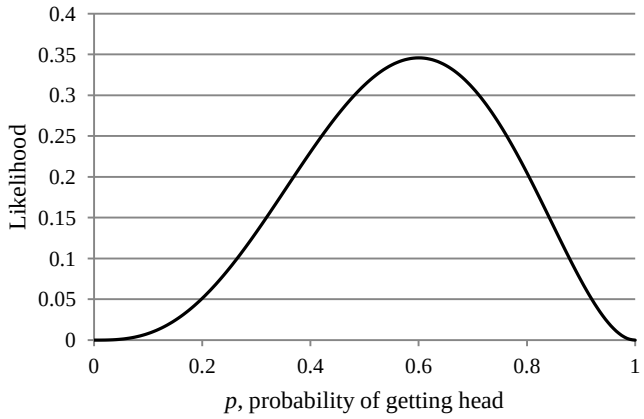

Figure 2.3 Likelihood function of unknown parameter p (the probability of getting the head of a biased coin)

The same definition of likelihood is used also in the case of handling a continuous random variable. When data is considered to be found in a continuous range, the probability of obtaining a specific data D that lies in an infinitesimal interval of length dx is $g(\mathrm{D}\,|\,\mathrm{H})dx$ (H is a fixed parameter set) as dx approaches to zero. Then, $g(\mathrm{D}\,|\,\mathrm{H})$ is the probability density function of D. However, likelihood $L(\mathrm{H}\,|\,\mathrm{D})$ can be treated in the same way as for the discrete variable case; we do not have to take the element dx into account to define likelihood $L(\mathrm{H}\,|\,\mathrm{D})$.

Let $g(x)$ denote the probability distribution function of a continuous random variable X. Supposed that $g(x)$ is a normal distribution with two parameters, mean μ and variance σ^2: $g(x) = \mathcal{N}(\mu, \sigma^2)$. $g(x\,|\,\mu, \sigma^2)$ is called a probability distribution of observable outcome X when the two parameters μ and σ^2 are fixed at specific values. For instance, if μ and σ^2 are known such as $\mu = 0$ and $\sigma^2 = 1$, the probability distribution of X is represented by $g(x\,|\,\mu = 0, \sigma^2 = 1) = \mathcal{N}(x; \mu = 0, \sigma^2 = 1)$. On the other hand, $g(x\,|\,\mu, \sigma^2)$ is called likelihood function when either or both of μ and σ^2 are regarded as being unknown, and outcome x is observed from an experiment. Consider that a sample data of X is obtained, e.g. $x = 0.1$, and μ and σ^2 are unknown. Then, the likelihood function of μ and σ^2 is represented by $L(\mu, \sigma^2 | \, x = 1) = g(x = 0.1\,|\,\mu, \sigma^2) = \mathcal{N}(x = 0.1; \mu, \sigma^2)$.

② The Maximum Likelihood Estimation (MLE)

The MLE is regarded as a method developed to provide estimates of unknown parameters in a statistical model. The idea behind the MLE is that the values of unknown parameters that are most supported by observed data are those for which the likelihoods are largest.

The maximum likelihood estimator of unknown parameter θ is the most likely value given observed data D and is defined as the point that maximizes the likelihood function of θ as shown in

$$\hat{\theta}_{mle} = \max L\left(\theta | D\right) \tag{2.13}$$

The logarithm of the likelihood function, called the log-likelihood function, is often used for the convenience of operation because the two functions have their maximum points at the same value.

Consider the coin flipping problem again. The maximum likelihood estimator of unknown probability p can be calculated by taking the derivative of the logarithm of the likelihood function with respect to p and setting it equal to zero:

$$\frac{d \ln L(p \mid D)}{dp} = \frac{d \ln\left(10 p^3 (1-p)^2\right)}{dp} = \frac{d\left(\ln 10 + \ln p^3 + \ln(1-p)^2\right)}{dp} = \frac{3}{p} - \frac{2}{1-p} = 0 .$$

Solving this linear equation yields $\hat{p}_{mle} = 0.6$, and this point corresponds to the maximum point of the curve shown in Figure 2.3.

③ Demonstration Problem

Q) A cantilever beam is subject to a tip load F as shown in Fig. 2.4. The length of the beam is $l = 1$ m, and the height and the width of the beam section are $h = 0.1$ m and $b = 0.05$ m, respectively. The young's modulus of the applied material is $E = 2\times10^5$ MPa. Tip load F is known to follow a normal distribution of standard deviation 400 N, but its mean is unknown: $F \sim \mathcal{N}(\mu,$ 400 N). Tip displacement d of the beam acted on by load F is measured from an experimental test, $d = 0.13$ cm.

Find the mean μ of tip load F.

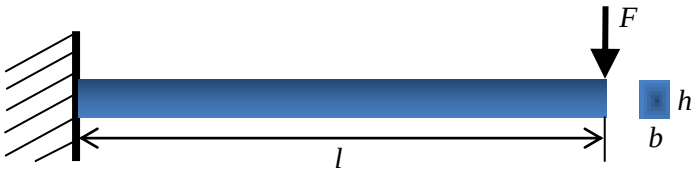

Figure 2.4 Cantilever beam subject to a tip load

A) Tip displacement d is calculated by $d = \frac{4Fl^3}{Ebh^3}$. Substituting the given values for l, E, b, and h leads to $d = 4\times10^{-7} F$. Because tip load F is considered to be a normal variable, tip displacement d is also normally distributed. According to the properties of random variable ($\mu(aX) = a\mu(X)$ and $\sigma(aX) = a\sigma(X)$, a: constant, X: random variable), the mean and standard deviation of d are $\mu_d = 4\times10^{-7}\mu_F$, and $\sigma_d = 4\times10^{-7}\times400 = 1.6\times10^{-4}$: $d \sim \mathcal{N}(4\times10^{-7}\mu_F, 1.6\times10^{-4})$.

The probability distribution function of the tip displacement d is represented by $g_D(d) = \frac{1}{\sqrt{2\pi\sigma_d^{\,2}}}\exp\left[-\frac{(d-\mu_d)^2}{2\sigma_d^{\,2}}\right] = 2.49\times10^3\times\exp\left[-1.95\times10^7\left(d-4\times10^{-7}\mu_F\right)^2\right]$. The measured tip displacement $d = 0.0013$ m is regarded as a data point sampled from $d \sim \mathcal{N}(4\times10^{-7}\mu_F, 1.6\times10^{-4})$. Likelihood function of unknown parameter μ_F is obtained by putting $d = 0.0013$ m into $g_D(d)$:

$L(\mu_F | d) = 2.49\times10^3\times\exp[-1.95\times10^7\times(0.0013 - 4\times10^{-7}\mu_F)^2]$. Taking the logarithm of $L(\mu_F | d)$ gives $\ln L(\mu_F | d) = -4.86\times10^{10}\times(0.0013 - 4\times10^{-7}\mu_F)^2$. To find the maximum

likelihood estimator of μ_F, take the derivative of log-likelihood function $\ln L(\mu_F \mid d)$ with respect to μ_F and set it to zero:

$$\frac{d \ln L\left(\mu_F \mid d\right)}{d\mu_F} = \frac{d\left\{-4.86\times10^{10}\times\left(0.0013-4\times10^{-7}\mu_F\right)^2\right\}}{d\mu_F}$$

$$= 8\times4.86\times10^{3}\times\left(0.0013-4\times10^{-7}\mu_F\right)=0.$$

Solving the equation for μ_F gives $\left(\hat{\mu}_F\right)_{mle}$=3,250 N. The calculated mean value of tip load F is the value that is most likely to have generated the observed tip displacement d = 0.13 cm.

2.3.2 Unknown Prediction Error

Consider that a set of simulation models M_1, …, M_K are available to predict system responses. Let the deterministic prediction of an unknown response y by model M_k be denoted by f_k. Because a (mathematical or simulation) model is just an approximation to a real physical system, it unavoidably involves an error in its prediction of a response. A prediction error is unknown unless the corresponding response is measured from the considered physical system.

In this research, a simple formulation [82-84] is utilized to involve an unknown error into model prediction f_k; the causes of prediction error (the difference between model prediction and experimental data) are not separately stated. The reason for not discerning between model discrepancy and experimental error is that a separate incorporation of the model discrepancy term shifts predictions by a model from the initially predicted values (although this can reduce biases involved in model predictions). Also, including an

unknown discrepancy term separately may cause the problem of degree of freedom under the circumstances there are generally quite limited amounts of experimental data available in the engineering applications. Increasing the number of unknown parameters to include the model discrepancy may lead to a reduction in the accuracy of estimation (over-fitting problem). Not separating model discrepancy and experimental error terms in mathematically specifying prediction error is thought to be desirable for addressing model form uncertainty quantification although this perspective is inappropriate for other statistical inferences such as model updating and model validation.

The formulation is represented by

$$y = f_k + \varepsilon_k, k = 1, \ldots, K \tag{2.14}$$

y is an unknown system response of interest, and f_k is the prediction of y by a deterministic model M_k. ε_k is the unknown error that encompasses both bias associated with model prediction f_k of response y and measurement error. It is implicitly supposed that the (analytical and simulation) models used in this research are verified, which means that the model prediction f_k is numerically accurate. ε_k exists even if uncertainty in model forms and parameters under consideration is perfectly quantified because we cannot take all relevant models and parameters into consideration. Uncertainty in ε_k (predictive uncertainty) is conditional on model-form and parametric uncertainty [11]. Generally, if a greater number of model forms and parameters are considered, more of uncertainty in ε_k would be changed into model-form and parametric uncertainty.

Some assumptions are made to mathematically characterize the uncertainty in prediction errors of a model. ε_k is assumed to be an independent and identically distributed (i.i.d.) normal variable with zero mean and unknown variance σ_k^2: $\varepsilon_k \sim \mathcal{N}(0, \sigma_k^2)$. The main purpose of introducing this assumption is to facilitate the development of a practical method to quantify model-form uncertainty given experimental data. Also, it is believed that the assumptions are reasonable as well as practical in many engineering applications where only limited amount of experimental data are supplied mostly due to the high cost involved. However, the assumption of zero mean and constant variance on prediction error may be impracticable if model predictions are significantly biased against experimental data due to the effect of model inaccuracy rather than due to the randomness in experimental data, and the differences between experimental data and model predictions vary to a large degree.

Because f_k is a fixed value, Eq. (2.14) can be rewritten as $y \sim \mathcal{N}(f_k, \sigma_k^2)$. Figure 2.5 shows the predictive distribution of response y by model M_k (the term "predictive distribution" is meant to be (probabilistic) model prediction in the form of probability distribution). The reason for assuming the mean of error ε_k to be zero is as follows:

1) Use of zero mean reflects the fact that each model in a model set maintains that its predictions are the most probable values. As shown in Fig. 2.5, the maximum value of normal distribution $\mathcal{N}(f_k, \sigma_k^2)$ is found at predicted value f_k by model M_k.
2) Use of ε_k with zero mean does not shift model prediction f_k. Use of non-zero mean results in shifting prediction by a model from initially predicted value. This means

that model probability is quantified depending on the shifted model prediction rather than the original model prediction f_k.

3) If the mean of an unknown error is considered as an unknown variable, the same observed data should be used to determine both unknown mean and unknown variance. Increasing the number of unknown variables usually leads to a reduction in the accuracy of estimation.

Errors are assumed to be independent in this research due to insufficient experimental data to estimate the correlation among errors. However, the covariance matrix of prediction errors with non-zero covariance and non-constant variance elements should be estimated if the prediction errors are highly correlated, the homoscedasticity assumption is seriously violated, and experimental data is enough to evaluate the covariance elements.

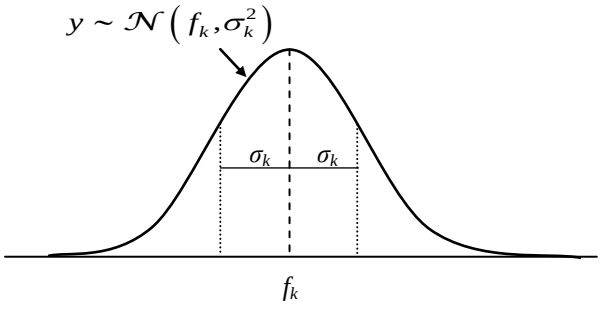

Figure 2.5 Unknown error involved in a deterministic model prediction

2.3.3 Model Likelihood for Deterministic Simulation Model

Suppose that a set of simulation models $M_1,\ldots, M_K$ are deterministic (not involving uncertainty in their input parameters). Because ε_k is assumed to be a normal variable $\mathcal{N}(0, \sigma_k^2)$, Eq. (2.14) can be restated in a probability distribution form as

$$g_Y\left(y\middle|\mathrm{M}_k\right)=\mathcal{N}\left(f_k,\sigma_k^2\right)=\frac{1}{\sqrt{2\pi\sigma_k^2}}\exp\left(-\frac{\left(y-f_k\right)^2}{2\sigma_k^2}\right),\ k=1,\ldots,K \tag{2.15}$$

$g_Y(y\,|\,\mathrm{M}_k)$ is called predictive distribution of response y under model M_k.

Consider that a sample of N independent experimental data $\mathrm{D}=\{d_1, d_2, \ldots, d_N\}$ are observed. Including an unknown error ε_k into the prediction of a single experimental data point $d_n, n=1,\ldots,N$ by model M_k can be represented by $\mathcal{N}\left(f_{k_n},\sigma_k^2\right)$ as shown in Fig. 2.6. f_{k_n} is the deterministic prediction of data d_n by model M_k. Variance σ_k^2 of the error involved in prediction f_{k_n} is the same for each data $d_n, n=1,\ldots,N$ because prediction error ε_k is assumed to be an i.i.d. random variable. Using Eq. (2.15), the likelihood function of σ_k for each model M_k given a single data d_n is expressed by

$$\Pr\left(d_n\middle|\mathrm{M}_k,\sigma_k\right)=\frac{1}{\sqrt{2\pi\sigma_k^2}}\exp\left(-\frac{\left(d_n-f_{k_n}\right)^2}{2\sigma_k^2}\right) \tag{2.16}$$

$\Pr(d_n\,|\,\mathrm{M}_k,\sigma_k)$ is mathematically equivalent to the probability density of $\mathcal{N}\left(f_{k_n},\sigma_k^2\right)$ for data d_n as shown in Fig. (2.5). $\Pr(d_n\,|\,\mathrm{M}_k,\sigma_k)$ is the likelihood function of M_k and σ_k because M_k and σ_k can vary while d_n and f_{k_n} are fixed.

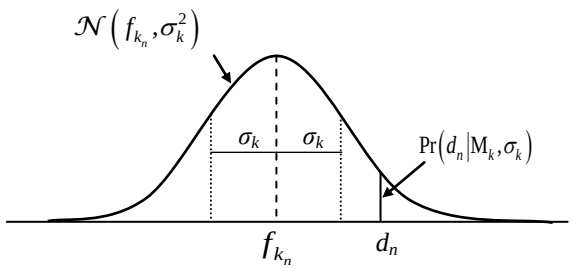

Figure 2.6 Likelihood of M_k and σ_k given a single experimental data

Because observed experimental data D = $\{d_1, d_2, \ldots, d_N\}$ are independent of one another, the likelihood of σ_k for each model M_k given data set D can be calculated by multiplying $\Pr(d_n \mid M_k, \sigma_k)$ in Eq. (2.16) over D as represented by

$$\Pr\left(D \middle| M_k, \sigma_k\right) = \prod_{n=1}^{N} \Pr\left(d_n \middle| M_k, \sigma_k\right) = \prod_{n=1}^{N} \frac{1}{\sqrt{2\pi\sigma_k^{\,2}}} \exp\left(-\frac{\left(d_n - f_{k_n}\right)^2}{2\sigma_k^{\,2}}\right) \tag{2.17}$$

It leads to

$$\Pr\left(D \middle| M_k, \sigma_k\right) = \left(\frac{1}{2\pi\sigma_k^{\,2}}\right)^{\frac{N}{2}} \exp\left(-\frac{\sum_{n=1}^{N}\left(d_n - f_{k_n}\right)^2}{2\sigma_k^{\,2}}\right) \tag{2.18}$$

Model likelihood $\Pr(D \mid M_k)$ is expressed by marginal likelihood integral

$$\Pr\left(D \middle| M_k\right) = \int \Pr\left(D \middle| M_k, \sigma_k\right) g\left(\sigma_k \middle| M_k\right) d\sigma_k \tag{2.19}$$

where $g(\sigma_k \mid M_k)$ is the prior distribution of σ_k conditional on M_k. This integral is analytically intractable, and the solution of the integral equation depends on how to specify prior distribution $g(\sigma_k \mid M_k)$. Instead of finding a direct solution of Eq. (2.19), the maximum likelihood estimation (MLE) [17] is implemented to evaluate model likelihood $\Pr(D \mid M_k)$ in an efficient way. MLE does not require specification of prior distribution $g(\sigma_k \mid M_k)$ and makes the best point estimate of σ_k.

The maximum likelihood estimator of σ_k is the value of σ_k most supported by observed data D, which maximizes likelihood function $\Pr(d_n \mid M_k, \sigma_k)$. Taking the derivative of the logarithm of Eq. (2.18) with respect to σ_k and setting it equal to zero yields

$$\frac{d}{d\sigma_k}\ln \Pr\left(\mathrm{D}\middle|\mathrm{M}_k,\sigma_k\right)=\frac{d}{d\sigma_k}\ln\left[\left(\frac{1}{2\pi{\sigma_k}^2}\right)^{\frac{N}{2}}\exp\left(-\frac{\sum_{n=1}^{N}\left(d_n-f_{k_n}\right)^2}{2{\sigma_k}^2}\right)\right]$$

$$=\frac{d}{d\sigma_k}\left[\frac{N}{2}\left(\ln 1-\ln 2\pi-2\ln\sigma_k\right)-\frac{\sum_{n=1}^{N}\left(d_n-f_{k_n}\right)^2}{2{\sigma_k}^2}\right]$$

$$=-\frac{N}{\sigma_k}+\frac{\sum_{n=1}^{N}\left(d_n-f_{k_n}\right)^2}{{\sigma_k}^3}=0$$

Solving this equation for σ_k gives

$${\sigma_k}^2=\frac{\sum_{n=1}^{N}{\varepsilon_{k_n}}^2}{N},\ \varepsilon_{k_n}=d_n-f_{k_n} \tag{2.20}$$

Measured prediction error ε_{k_n}, $n=1,\ldots,N$ is considered as a realization of an i.i.d. normal variable $\varepsilon_k \sim \mathcal{N}(0, {\sigma_k}^2)$.

By putting the determined variance ${\sigma_k}^2$ in Eq. (2.20) into the exponential term in Eq. (2.18), likelihood $\Pr(\mathrm{D}\,|\,\mathrm{M}_k)$ of each deterministic model M_k, $k=1,\ldots,K$, given a set of observed experimental data D is computed:

$$\Pr\left(\mathrm{D}\middle|\mathrm{M}_k\right)=\left(\frac{1}{2\pi{\sigma_k}^2}\right)^{N/2}\exp\left(-\frac{N}{2}\right) \tag{2.21}$$

For a very large dataset, model likelihood $\Pr(\mathrm{D}\,|\,\mathrm{M}_k)$ evaluated using MLE is fundamentally the same as it evaluated by directly solving the marginal likelihood equation Eq.(2.19). This is partly due to the fact that in large samples, prior distribution $g(\sigma_k\,|\,\mathrm{M}_k)$ has very little influence on model likelihood $\Pr(\mathrm{D}\,|\,\mathrm{M}_k)$. On the other hand, in

small samples, the influence of $g(\sigma_k \mid \mathrm{M}_k)$ can be dominant compared to the influence of observed experimental data. Model likelihood $\Pr(\mathrm{D} \mid \mathrm{M}_k)$ is not a single number but a function of prior distribution $g(\sigma_k \mid \mathrm{M}_k)$. That is, there are an infinite number of model likelihoods $\Pr(\mathrm{D} \mid \mathrm{M}_k)$ depending on prior distribution $g(\sigma_k \mid \mathrm{M}_k)$ assumed; all are mathematically true. Some prior distributions will imply a model likelihood that is exactly equal to the model likelihood calculated using the maximum likelihood method, while other prior distributions will imply a model likelihood that is far from it.

In a sense, the maximum likelihood method can be thought of as a way to calculate model likelihood $\Pr(\mathrm{D} \mid \mathrm{M}_k)$ rather than a way to obtain an approximation to $\Pr(\mathrm{D} \mid \mathrm{M}_k)$. It is believed that the usefulness of the maximum likelihood method can be judged by finding prior distributions that yield a model likelihood that matches the model likelihood calculated using the maximum likelihood method.

2.3.4 Model Likelihood for Probabilistic Simulation Model

① Estimation of Predictive Distribution by Each Model

Now consider that input parameters within model M_k consist of a set of random parameters Θ_k as well as a set of deterministic parameters X_k. Uncertainty in Θ_k is represented by a joint probability distribution $g_{\Theta_k}\left(\theta_k \mid \mathrm{M}_k\right)$ under model M_k. In this research, a set of random parameters Θ_k are considered to be independent of experimental data D. Therefore, $g_{\Theta_k}\left(\theta_k \mid \mathrm{M}_k\right)$ is not updated even after observing data D. Incorporating predictive uncertainty as well as parametric uncertainty in Θ_k into the prediction of

response y by model M_k, the predictive distribution of y under M_k given data D is represented by

$$g_Y\left(y|\mathrm{M}_k\right)=\int_{\theta_k} g_{\Theta_k}\left(\theta_k|\mathrm{M}_k\right)g_Y\left(y|\mathrm{M}_k,\theta_k,\mathrm{X}_k\right)d\theta_k \tag{2.22}$$

$$g_Y\left(y|\mathrm{M}_k,\theta_k,\mathrm{X}_k\right)=\mathcal{N}\left(f_k\left(\theta_k,\mathrm{X}_k\right),\left(\sigma_k\right)^2_{\theta_k}\right) \tag{2.23}$$

Eq. (2.22) [10] represents the marginal distribution of response y where the random variable set Θ_k is marginalized out. Due to the randomness present in a collection of variables Θ_k, the mean $f_k(\theta_k, \mathrm{X}_k)$ and variance $\left(\sigma_k\right)^2_{\theta_k}$ of $g_Y(y \mid \mathrm{M}_k, \theta_k, \mathrm{X}_k)$ are probabilistically distributed, unlike $g_Y(y \mid \mathrm{M}_k)$ in Eq. (2.15).

It is impossible to analytically solve Eq. (2.22) for most engineering problems where $f_k(\theta_k, \mathrm{X}_k)$ and $\left(\sigma_k\right)^2_{\theta_k}$ cannot be explicitly represented by probability distributions of θ_k. Using Monte Carlo integration technique [85], the integral in Eq. (2.22) can be numerically solved using data points randomly sampled from $g_{\Theta_k}\left(\theta_k|\mathrm{M}_k\right)$ as expressed by

$$g_Y\left(y|\mathrm{M}_k\right)\approx\frac{1}{L}\sum_{l=1}^{L}\mathcal{N}\left(f_k\left(\hat{\Theta}_{k_l},\mathrm{X}_k\right),\left(\sigma_k\right)^2_{\hat{\Theta}_{k_l}}\right) \tag{2.24}$$

$\hat{\Theta}_{k_l}$ is the l^{th} data point randomly sampled from $g_{\Theta_k}\left(\theta_k|\mathrm{M}_k\right)$, and L is the number of sampled data points. Given a sampled data point $\hat{\Theta}_{k_l}$ of Θ_k, $f_k\left(\hat{\Theta}_{k_l},\mathrm{X}_k\right)$ and $\left(\sigma_k\right)^2_{\hat{\Theta}_{k_l}}$ are deterministic values. Figure 2.7 shows a normal predictive distribution $\mathcal{N}\left(f_k\left(\hat{\Theta}_{k_l},\mathrm{X}_k\right),\left(\sigma_k\right)^2_{\hat{\Theta}_{k_l}}\right)$ under model M_k. The mean $f_k\left(\hat{\Theta}_{k_l},\mathrm{X}_k\right)$ is the prediction of

response y by model M_k given $\theta_k = \hat{\Theta}_{k_l}$. The variance $\left(\sigma_k\right)^2_{\hat{\Theta}_{k_l}}$ can be calculated using Eq. (2.20); f_{k_n} in Eq. (2.20) is replaced with $f_k\left(\hat{\Theta}_{k_l}, \mathrm{X}_{k_n}\right)$ which denotes the prediction of a sampled data point d_n by model M_k given $\theta_k = \hat{\Theta}_{k_l}$.

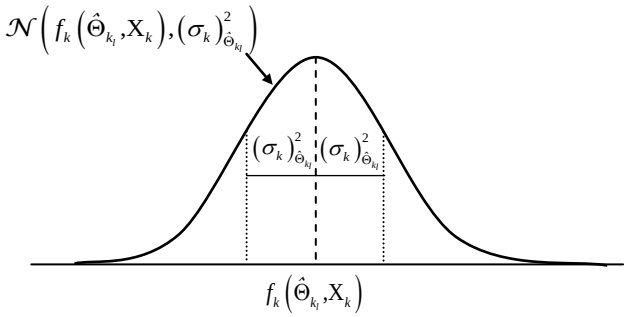

Figure 2.7 Unknown error involved in a probabilistic model prediction given a parameter set being fixed

② Quantification of Model Likelihood

The likelihood of model M_k given experimental data D is represented by [10]

$$\Pr\left(\mathrm{D}\middle|\mathrm{M}_k\right) = \int_{\theta_k} g_{\Theta_k}\left(\theta_k\middle|\mathrm{M}_k\right) g_{\Theta_k}\left(\mathrm{D}\middle|\mathrm{M}_k, \theta_k, \mathrm{X}_k\right) d\theta_k \tag{2.25}$$

Let $f_k\left(\theta_k, \mathrm{X}_{k_1}\right), \ldots, f_k\left(\theta_k, \mathrm{X}_{k_N}\right)$ denote the predictions of experimental data $\mathrm{D} = \{d_1, \ldots, d_N\}$ by model M_k. Given the assumption that experimental data D are independent of one another, $g_{\Theta_k}\left(\mathrm{D}\middle|\mathrm{M}_k, \theta_k, \mathrm{X}_k\right)$ is represented by

$$g_{\Theta_k}\left(\mathrm{D}\middle|\mathrm{M}_k, \theta_k, \mathrm{X}_k\right) = \prod_{n=1}^{N} g_{\Theta_k}\left(d_n\middle|\mathrm{M}_k, \theta_k, \mathrm{X}_{k_n}\right) = \prod_{n=1}^{N} \mathcal{N}\left(d_n; f_k\left(\theta_k, \mathrm{X}_{k_n}\right), \left(\sigma_k\right)^2_{\theta_k}\right) \tag{2.26}$$

$\mathcal{N}\left(d_n; f_k\left(\theta_k, \mathrm{X}_{k_n}\right), \left(\sigma_k\right)^2_{\theta_k}\right)$ is the probability density of $\mathcal{N}\left(f_k\left(\theta_k, \mathrm{X}_{k_n}\right), \left(\sigma_k\right)^2_{\theta_k}\right)$ for a single experimental data point d_n. To analytically calculate the integral in Eq. (2.25),

$\mathcal{N}\left(d_n; f_k\left(\theta_k, \mathrm{X}_{k_n}\right), \left(\sigma_k\right)^2_{\theta_k}\right)$ should be represented by a function (likelihood function) of θ_k. However, the explicit expression of $\mathcal{N}\left(d_n; f_k\left(\theta_k, \mathrm{X}_{k_n}\right), \left(\sigma_k\right)^2_{\theta_k}\right)$ is usually not acquired because $f_k\left(\theta_k, \mathrm{X}_{k_n}\right)$ and $\left(\sigma_k\right)^2_{\theta_k}$ cannot be explicitly represented for most of engineering problems as mentioned.

Monte Carlo integration technique is utilized to obtain a numerical solution of Eq. (2.25) depending on data points $\hat{\Theta}_{k_l}$, $l = 1, \ldots, L$, randomly sampled from $g_{\Theta_k}\left(\theta_k \middle| \mathrm{M}_k\right)$. Given $\theta_k = \hat{\Theta}_{k_l}$, $\mathcal{N}\left(d_n; f_k\left(\theta_k, \mathrm{X}_{k_n}\right), \left(\sigma_k\right)^2_{\theta_k}\right)$ in Eq. (2.26) becomes

$$\mathcal{N}\left(d_n; f_k\left(\hat{\Theta}_{k_l}, \mathrm{X}_{k_n}\right), \left(\sigma_k\right)^2_{\hat{\Theta}_{k_l}}\right) = \frac{1}{\sqrt{2\pi\left(\sigma_k\right)^2_{\hat{\Theta}_{k_l}}}} \exp\left(-\frac{\left\{d_n - f_k\left(\hat{\Theta}_{k_l}, \mathrm{X}_{k_n}\right)\right\}^2}{2\left(\sigma_k\right)^2_{\hat{\Theta}_{k_l}}}\right)$$ as shown in Fig.2.7. As a consequence, given $\theta_k = \hat{\Theta}_{k_l}$, $g_{\Theta_k}\left(\mathrm{D} \middle| \mathrm{M}_k, \theta_k, \mathrm{X}_k\right)$ in Eq. (2.26) is represented by

$$g_{\Theta_k}\left(\mathrm{D} \middle| \mathrm{M}_k, \hat{\Theta}_{k_l}, \mathrm{X}_k\right) = \prod_{n=1}^{N} \frac{1}{\sqrt{2\pi\left(\sigma_k\right)^2_{\hat{\Theta}_{k_l}}}} \exp\left(-\frac{\left\{d_n - f_k\left(\hat{\Theta}_{k_l}, \mathrm{X}_{k_n}\right)\right\}^2}{2\left(\sigma_k\right)^2_{\hat{\Theta}_{k_l}}}\right) \tag{2.27}$$

Because $\left(\sigma_k\right)^2_{\hat{\Theta}_{k_l}} = \dfrac{\sum_{n=1}^{N}\left\{d_n - f_k\left(\hat{\Theta}_{k_l}, \mathrm{X}_{k_n}\right)\right\}^2}{N}$ by Eq. (2.20), Eq. (2.27) is simplified into

$$g_{\Theta_k}\left(\mathrm{D} \middle| \mathrm{M}_k, \hat{\Theta}_{k_l}, \mathrm{X}_k\right) = \left(\frac{1}{2\pi\left(\sigma_k\right)^2_{\hat{\Theta}_{k_l}}}\right)^{N/2} \exp\left(-\frac{N}{2}\right) \tag{2.28}$$

When $g_{\Theta_k}\left(\mathrm{D}\middle|\mathrm{M}_k,\hat{\Theta}_{k_1},\mathrm{X}_k\right),...,g_{\Theta_k}\left(\mathrm{D}\middle|\mathrm{M}_k,\hat{\Theta}_{k_L},\mathrm{X}_k\right)$ are calculated, the integral in Eq. (2.25) is approximated by

$$\Pr\left(\mathrm{D}\middle|\mathrm{M}_k\right)\approx\frac{1}{L}\sum_{l=1}^{L}\left(\frac{1}{2\pi\left(\sigma_k\right)^2_{\hat{\Theta}_{kl}}}\right)^{N/2}\exp\left(-\frac{N}{2}\right) \tag{2.29}$$

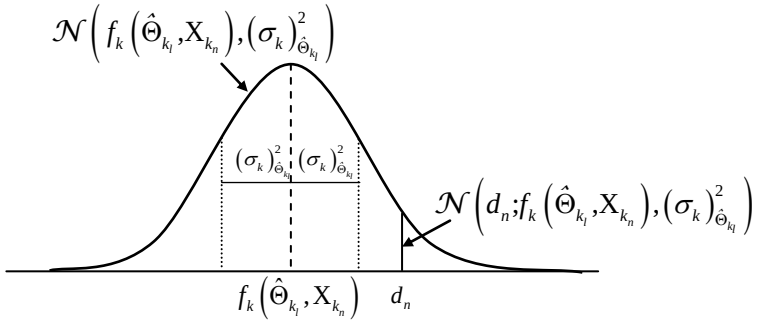

Figure 2.8 Likelihood of a probabilistic model given a single experimental data

2.4 Update of Model Probability Using Bayes' Theorem

Given that model likelihood is evaluated using observed experimental data, prior model probability can be updated into posterior probability using Bayes' theorem as shown in Figure 2.9. Bayes' theorem used to update prior model probability by means of evaluated model likelihood is represented by

$$\Pr\left(\mathrm{M}_k\middle|\mathrm{D}\right)=\frac{\Pr\left(\mathrm{M}_k\right)\times\Pr\left(\mathrm{D}\middle|\mathrm{M}_k\right)}{\sum_{i=1}^{K}\Pr\left(\mathrm{M}_i\right)\times\Pr\left(\mathrm{D}\middle|\mathrm{M}_i\right)}\ ,\ k=1,...,K \tag{2.30}$$

The denominator in Eq. (2.30) serves as a normalizing constant so that the sum of all the posterior model probabilities is one.

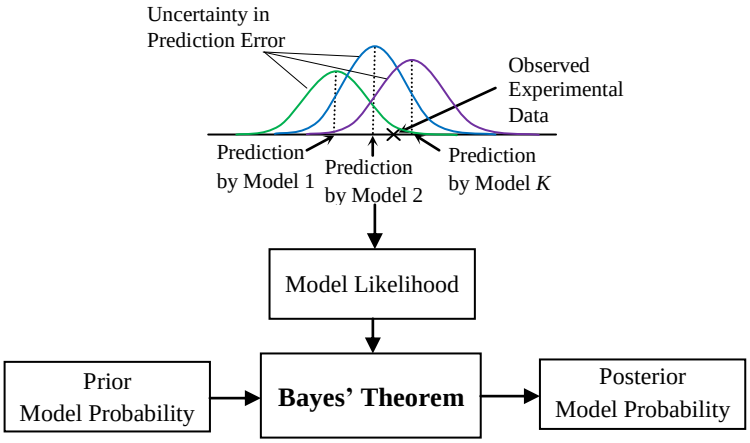

Figure 2.9 Bayes' theorem to update prior model probability

Prior model probability $\Pr(M_k)$ can be specified depending on prior knowledge (such as accumulated database and/or expert opinions) about the credibility of a model set. However, the quantification of prior model probability using a corpus of knowledge is arbitrary in nature because logically rigorous relations do not exist between knowledge about the credibility of a model set and prior model probability. Generally, a uniform prior probability is given to each model to avoid the difficulty of numerically specifying prior knowledge [22]. Uniform model probability means that the degree of belief that a model is best of a model set is equally distributed over the considered models. When uniform prior model probability is assumed, each posterior probability is just the ratio of likelihood of each model to the sum of the likelihoods of all the models as expressed by

$$\Pr\left(M_k|D\right)=\frac{\Pr\left(D|M_k\right)}{\sum_{i=1}^{K}\Pr\left(D|M_i\right)},\ k=1,...,K \tag{2.31}$$

2.5 Demonstration Problems for the Proposed Methodology

The proposed methodology is demonstrated with two engineering problems; a cement hardening problem in Section 2.5.1 and a concrete creep problem in Section 2.5.2.

2.5.1 Cement Hardening Problem

The experimental data [86] shown in Table 2.1 relate to an engineering application concerned with the effect of cement compositions on heat evolved during the hardening of Portland cement. The data have a sample size of 13 and consists of 4 explanatory variables and a response variable. The response variable *y*, total calories given off during the hardening per gram of cement after 180 days, is a function of four explanatory variables (percentage composition of each of four ingredients in samples of cement), x_1: *tricalcium aluminate*, x_2: *tricalcium silicate*, x_3: *tetracalcium alumino ferrite*, *and* x_4: *dicalcium silicate*. This problem aims to demonstrate the proposed methodology with multiple linear models which represent the relationship between the four explanatory variables and the response variable.

Suppose that four multiple linear models are generated to make the predictions of unknown response variable *y* given additional values of an explanatory variable set X = {x_1, x_2, x_3 and x_4} other than the values shown in Table 2.1:

$$M_1: y_1 = 52.6 + 1.468\, x_1 + 0.662\, x_2$$

$$M_2: y_2 = 71.6 + 1.452\, x_1 + 0.416\, x_2 - 0.236\, x_4$$

$$M_3: y_3 = 62.4 + 1.551\, x_1 + 0.510\, x_2 + 0.102\, x_3 - 0.144\, x_4$$

$$M_4: y_4 = 48.1936 + 1.6959\, x_1 + 0.6569\, x_2 + 0.25\, x_3.$$

Table 2.1 Cement hardening data: four explanatory variables (in percent by weight) [x_1: *tricalcium aluminate*, x_2: *tricalcium silicate*, x_3: *tetracalcium alumino ferrite*, *and* x_4: *dicalcium silicate*], are used to predict the response variable, *y*: calories of heat evolved per gram of cement after 180 days of hardening [86].

x_1	x_2	x_3	x_4	y
7	26	6	60	78.5
1	29	15	52	74.3
11	56	8	20	104.3
11	31	8	47	87.6
7	52	6	33	95.9
11	55	9	22	109.2
3	71	17	6	102.7
1	31	22	44	72.5
2	54	18	22	93.1
21	47	4	26	115.9
1	40	23	34	83.8
11	66	9	12	113.3
10	68	8	12	109.4

Even if for this problem, the values of parameter sets in the four linear models are determined by fitting the models to the observed data set of X and *y* values in Table 2.1, it is supposed that the parameter values are already given before observing the data. The reason for introducing this assumption is that the proposed methodology is developed to address the engineering problems for which mathematical or simulation models are created not depending on observed experimental data, but using scientific and engineering knowledge. The procedures for evaluating probability of each model given the observed data are as follows:

Step 1) Incorporating unknown errors ε_1, ε_2, ε_3, and ε_4 assumed to be normal variables with zero means and unknown variances into the predictions of response *y* by the considered models, the predictive distributions of *y* under the four models are

$$g\,(y \mid \mathrm{M}_1, \mathrm{D}) = 52.6 + 1.468\,x_1 + 0.662\,x_2 + \varepsilon_1,\ \varepsilon_1 \sim \mathcal{N}(0, \sigma_1^2)$$

$$g\,(y \mid \mathrm{M}_2, \mathrm{D}) = 71.6 + 1.452\,x_1 + 0.416\,x_2 - 0.236\,x_4 + \varepsilon_2,\ \varepsilon_2 \sim \mathcal{N}(0, \sigma_2^2)$$

$g\,(y\,|\mathrm{M}_3, \mathrm{D}) = 62.4 + 1.551\,x_1 + 0.510\,x_2 + 0.102\,x_3 - 0.144\,x_4 + \varepsilon_3,\ \varepsilon_3 \sim \mathcal{N}(0, \sigma_3^2)$

$g\,(y\,|\mathrm{M}_4, \mathrm{D}) = 48.2 + 1.6959\,x_1 + 0.657\,x_2 + 0.250\,x_3 + \varepsilon_4,\ \varepsilon_4 \sim \mathcal{N}(0, \sigma_4^2)$

Using Eq. (2.20), σ_1, σ_2, σ_3 and σ_4 are calculated to be

$$\sigma_1 = \sqrt{\sum_{n=1}^{13} \varepsilon_{1_n}{}^2 \Big/ 13} = \sqrt{57.91/13} = 2.111 \text{ (cal)}$$

$$\sigma_2 = \sqrt{\sum_{n=1}^{13} \varepsilon_{2_n}{}^2 \Big/ 13} = \sqrt{47.99/13} = 1.921 \text{ (cal)}$$

$$\sigma_3 = \sqrt{\sum_{n=1}^{13} \varepsilon_{3_n}{}^2 \Big/ 13} = \sqrt{47.87/13} = 1.919 \text{ (cal)}$$

$$\sigma_4 = \sqrt{\sum_{n=1}^{13} \varepsilon_{4_n}{}^2 \Big/ 13} = \sqrt{48.11/13} = 1.924 \text{ (cal)}$$

Step 2) The likelihood of a model given the observed experimental data is evaluated by multiplying likelihood of each experimental data given prediction of each data by the model. Using Eq. (2.21), the likelihoods of the considered four models are calculated to be

$$\Pr\left(\mathrm{D}\middle|\mathrm{M}_1\right) = \left(\frac{1}{2\pi\sigma_1^2}\right)^{13/2} \exp\left(-\frac{13}{2}\right) = \left(\frac{1}{2\pi\times(2.111)^2}\right)^{13/2} \exp\left(-\frac{13}{2}\right) = 8.264 \times 10^{-6}$$

$$\Pr\left(\mathrm{D}\middle|\mathrm{M}_2\right) = \left(\frac{1}{2\pi\sigma_2^2}\right)^{13/2} \exp\left(-\frac{13}{2}\right) = \left(\frac{1}{2\pi\times(1.921)^2}\right)^{13/2} \exp\left(-\frac{13}{2}\right) = 9.972 \times 10^{-6}$$

$$\Pr\left(\mathrm{D}\middle|\mathrm{M}_3\right) = \left(\frac{1}{2\pi\sigma_3^2}\right)^{13/2} \exp\left(-\frac{13}{2}\right) = \left(\frac{1}{2\pi\times(1.919)^2}\right)^{13/2} \exp\left(-\frac{13}{2}\right) = 9.947 \times 10^{-6}$$

$$\Pr\left(\mathrm{D}\middle|\mathrm{M}_4\right) = \left(\frac{1}{2\pi\sigma_4^2}\right)^{13/2} \exp\left(-\frac{13}{2}\right) = \left(\frac{1}{2\pi\times(1.924)^2}\right)^{13/2} \exp\left(-\frac{13}{2}\right) = 9.998 \times 10^{-6}$$

Step 3) Because the model likelihoods are computed, the prior probabilities of the considered models can be updated into the posterior model probabilities using Bayes' theorem. For this problem, the prior model probabilities are assumed to be uniform. Using Eq. (2.31), the posterior model probabilities are calculated to be

$$\Pr\left(\mathrm{M}_1|\mathrm{D}\right)=\frac{\Pr\left(\mathrm{D}|\mathrm{M}_1\right)}{\sum_{i=1}^{4}\Pr\left(\mathrm{D}|\mathrm{M}_i\right)}=\frac{8.264\times10^{-6}}{3.818\times10^{-5}}=0.216$$

$$\Pr\left(\mathrm{M}_2|\mathrm{D}\right)=\frac{\Pr\left(\mathrm{D}|\mathrm{M}_2\right)}{\sum_{i=1}^{4}\Pr\left(\mathrm{D}|\mathrm{M}_i\right)}=\frac{9.972\times10^{-6}}{3.818\times10^{-5}}=0.261$$

$$\Pr\left(\mathrm{M}_3|\mathrm{D}\right)=\frac{\Pr\left(\mathrm{D}|\mathrm{M}_3\right)}{\sum_{i=1}^{4}\Pr\left(\mathrm{D}|\mathrm{M}_i\right)}=\frac{9.947\times10^{-6}}{3.818\times10^{-5}}=0.261$$

$$\Pr\left(\mathrm{M}_4|\mathrm{D}\right)=\frac{\Pr\left(\mathrm{D}|\mathrm{M}_4\right)}{\sum_{i=1}^{4}\Pr\left(\mathrm{D}|\mathrm{M}_i\right)}=\frac{9.998\times10^{-6}}{3.818\times10^{-5}}=0.262$$

Posterior probability of each model is the ratio of likelihood for each model to the sum of the likelihoods of all the considered models. As the calculated values of posterior model probabilities indicate, the considered four models are all likely to be the best model. This means that a high degree of model-form uncertainty is involved in predictions of unknown responses.

2.5.2 Concrete Creep Problem

Creep is defined as the slow deformation a solid material undergoes under the influence of sustained stresses generated by external loads over an extended period of time. The creep deformation experienced by concrete may be three or four times as large as the

initial elastic deformation occurred by externally applied loads. It is widely accepted that creep deformation is largely attributed to shearing forces acting on material particles which cause them to slip against each other. Water within concrete has a large influence on the amount of the slip occurring between the particles of concrete through the action of weakening attractive forces binding those particles.

Creep in concrete is not fully understood because it involves many factors that influence the total amount of creep a specimen experiences. The factors considerably influencing the concrete creep are as following:

1) Aggregate – volume and mechanical properties

Because the aggregate within a concrete mixture serves to restrain creep from occurring, the magnitude of creep largely depends on the quantity and properties of the aggregate added into the mixture. When the stiffness of the chosen aggregate is higher, the amount of creep is reduced.

2) Cement types and content

The content and type of cement paste is also of large concern because creep mostly occurs in the hydrated cement paste that surrounds the aggregate. The higher the content of cement becomes, the higher the amount of creep. The type of cement affects the strength of the concrete mixture at the time of loading. When rapid-hardening cements are used, the stiffness of the concrete matrix is increased at the time of loading and thus, the concrete is more resistant to creep.

3) Water-cement (w/c) ratio

The water-cement (*w/c*) ratio is directly related to the concrete strength. As the *w/c* ratio increases, the amount of creep tends to increase. Lower water content results in higher concrete strength and fewer pores in the mature cement, which leads to a decrease in the amount of creep. When the *w*/*c* ratio is higher, the concrete contains more extra water after hydration, which results in higher amount of creep.

4) Member size

It has been indicated that creep deformation decreases with an increase in the size of a concrete specimen. Models for creep prediction consider the size effects in terms of volume to surface ratio or effective thickness. The effect of member size on creep is highly related to mobility of moisture in the concrete mixture.

5) Curing condition

Curing conditions have a substantial effect on the maturity of concrete, which is concerned with increase in concrete strength. As a concrete specimen is cured for a longer duration of time, the concrete strength becomes higher. Low pressure steam curing reduces creep.

6) Temperature and relative humidity

Ambient conditions such as temperature and relative humidity are also sources that influence creep. Although higher temperature results in higher creep, the temperature effect on creep comes to a maximum in the vicinity of 71 °C and thereafter decreases

with further rise in temperature. Lower relative humidity increases the amount of creep because more moisture within a concrete specimen is diffused from the specimen to the ambient.

7) Age at loading

Another factor that influences creep is the age when loads are externally applied to a concrete specimen. Because the concrete strength increases in process of time, the amount of creep is decreased as the age at loading is older.

8) Stress intensity

It is generally agreed upon that the amount of creep is approximately proportional to the applied stress. However, this proportionality is valid only up to 0.2 to 0.5 of the ultimate strength.

① Mathematical Models to Predict Creep in Concrete

Several mathematical models have been suggested to estimate the amount of creep in concrete. Most of the creep-prediction models developed were empirically derived based on the outcomes of experiments carried out on concrete specimens. In this problem, four empirical models recommended by different committees are used to predict the amount of creep that a concrete specimen experiences under a particular environment. The four creep-prediction models are the equations contained in the ACI 209 (1997) [87], the AASHTO (2007) [88], the CEB-FIP (1990) [89] and the JSCE (1996) [90] design codes. The four creep-prediction models are detailed below.

1) The ACI 209 creep-prediction model [87]

The creep-prediction model recommended by ACI Committee 209 uses an ultimate creep coefficient that may be corrected to account for a variety of factors influencing the magnitude of creep in concrete. Also, a time-dependent function is introduced to express the growth in creep over time. The ultimate creep coefficient is defined as the ratio of ultimate creep strain to initial elastic strain occurred by the application of external load and is expressed by

$$v_u = 2.35\left(\gamma_{la} \times \gamma_{\lambda} \times \gamma_{vs} \times \gamma_{\psi} \times \gamma_s \times \gamma_a\right) \tag{2.32}$$

where v_u: ultimate creep coefficient

γ_{la}: loading age correction factor;

$\gamma_{la} = 1.25 t_{la}^{-0.118}$ (for non-accelerated-cured concrete)

where t_{la}: loading age (days)

γ_{λ}: relative humidity correction factor;

$\gamma_{\lambda} = 1.27 - 0.0067 \times RH$ (for RH > 40%)

where RH: relative humidity (%)

γ_{vs}: volume-to-surface area ratio correction factor;

$\gamma_{vs} = (2/3)\left[1 + 1.13\exp\left(-0.0213 \times (v/s)\right)\right]$

where v/s: volume-to-surface area ratio (mm)

γ_{ψ}: fine aggregate percentage correction factor;

$\gamma_{\psi} = 0.88 + 0.0024\psi$

where ψ: ratio of fine to total aggregate by weight (%)

γ_s: slump correction factor;

$\gamma_s = 0.82 + 0.00264s$

where s: observed slump (mm)

γ_a: air content correction factor;

$\gamma_a = 0.46 + 0.09a \geq 1.0$

where a: air content (%)

Creep coefficient for a time of interest is determined by multiplying the ultimate creep coefficient by the parameter introduced to account for the concrete age as expressed by

$$v_u(t) = v_u \times \frac{t^{0.6}}{10 + t^{0.6}} \tag{2.33}$$

where t is the length of time after loading (days).

Creep in concrete at a specific time is calculated by multiplying the creep coefficient for that time by the elastic strain resulting from externally applied loads as shown in

$$predicted\ creep(t) = v_u(t) \times (elastic\ strain\ resulting\ form\ loading) \tag{2.34}$$

2) The AASHTO creep-prediction model [88]

The AASHTO (2007) creep-prediction model uses an ultimate creep coefficient like the ACI 209 creep-prediction model. The AASHTO creep-prediction model accounts for various influencing factors: the volume-to-surface area ratio, the relative humidity, the concrete strength and the development of strength with time.

Creep coefficient for each time step is determined by Eq. (2.35) along with several factors to reflect the mixture properties and the environmental conditions:

$$\psi(t,t_i) = 1.9 \times k_s \times k_{hc} \times k_f \times k_{td} \times t_i^{-0.118} \quad (2.35)$$

where k_s: factor accounting for the effect of the volume-to-surface area ratio;

$$k_s = 1.45 - 0.0051(v/s) \geq 1.0$$

k_{hc}: relative humidity factor;

$$k_{hc} = 1.56 - 0.008H$$

where H: relative humidity (%)

k_f: concrete strength factor;

$$k_f = \frac{35}{7 + f'_{ci}}$$

where f'_{ci}: compressive strength of concrete at 28 days (MPa)

k_{td}: time development factor;

$$k_{td} = \frac{t}{61 - 0.58 f'_{ci} + t}$$

t: age of concrete (days) between time of loading and time being considered for analysis of creep effects

t_i: age of concrete when load is initially applied for accelerated curing (days), minus 6 days for moist-curing.

Given the creep coefficient calculated for each time step of interest, it is multiplied by the elastic strain occurred by applied loads to get the prediction of creep as shown in

$$\textit{predicted creep}(t,t_i) = \psi(t,t_i) \times (\textit{elastic strain resulting form loading}) \quad (2.36)$$

3) The CEB-FIP creep-prediction model [89]

The mathematical model for creep prediction contained in the European design code, CEB-FIP Model Code 1990, takes into account the cement type and curing temperature that the ACI 209 creep-prediction model does not account for. Creep coefficient for each time step is determined considering the fresh and hardened properties of a concrete mixture and environmental conditions as represented by

$$\Phi(t,t_0) = \Phi_0 \times \beta_c(t - t_0) \tag{2.37}$$

where $\Phi(t,t_0)$: creep coefficient

Φ_0: notational creep coefficient

$\beta_c(t - t_0)$: coefficient describing the growth in creep with time after loading

t: age of concrete at the moment considered (days)

t_0: age of concrete at time of loading (days)

The notational creep coefficient Φ_0 is determined based on the concrete strength and relative humidity by

$$\Phi_0 = \Phi_{RH} \times \beta(f_{cm}) \times \beta(t_0) \tag{2.38}$$

where $\Phi_{RH} = 1 + \dfrac{1 - RH/RH_0}{0.46\left(h/h_0\right)^{1/3}}$

$$\beta\left(f_{cm}\right) = \frac{5.3}{\left(f_{cm}/f_{cm0}\right)^{0.5}}$$

$$\beta\left(t_0\right) = \frac{1}{0.1 + \left(t_0/t_1\right)^{0.2}}$$

where h: $2A_c/u$ (mm)

f_{cm}: mean compressive strength of concrete at 28 days (MPa)

f_{cm0}: 10 MPa

RH: relative humidity of the ambient environment (%)

RH_0: 100 %

A_c: cross-sectional area (mm^2)

u: perimeter of the member in contact with the atmosphere (mm)

h_0: 100 mm

t_1: 1 day

The growth in creep over time is expressed by

$$\beta_c(t-t_0)=\left[\frac{(t-t_0)/t_1}{\beta_H+(t-t_0)/t_1}\right]^{0.3} \tag{2.39}$$

where $\beta_H=150\left[1+\left(1.2\frac{RH}{RH_0}\right)^{18}\right]\frac{h}{h_0}+250\le 1500$

Predicted creep at each time step is obtained by multiplying the creep coefficient calculated above by the elastic strain occurred by applied loads as shown in

$$predicted\ creep(t,t_0)=\Phi(t,t_0)\times(elastic\ strain\ resulting\ form\ loading) \tag{2.40}$$

4) The JSCE creep-prediction model [90]

The creep-prediction model adopted in the JSCE Specification 1996 accounts for the unit cement and water contents, the water-cement ratio, the relative humidity, the volume-to-surface area ratio and the environmental temperature.

Creep strain under unit stress $\varepsilon'_{cc}(t, t', t_0)/\sigma'_{cp}$ for normal strength concrete having a compressive strength of up to 55 MPa is estimated for each time step by

$$\varepsilon'_{cc}(t,t',t_0)/\sigma'_{cp} = \left[1-\exp\left(-0.09\left(t-t'\right)^{0.6}\right)\right]\times\varepsilon'_{cr} \tag{2.41}$$

where $\varepsilon'_{cr} = \varepsilon'_{bc} + \varepsilon'_{dc}$

$$\varepsilon'_{bc} = 15\left(C+W\right)^{2.0}\left(W/C\right)^{2.4}\left(\log_e t'\right)^{-0.67}$$

$$\varepsilon'_{dc} = 4500\left(C+W\right)^{1.4}\left(W/C\right)^{4.2}\left(\log_e\left(V/S/10\right)\right)^{-2.2}\left(1-RH/100\right)^{0.36}t_0^{-0.30}$$

where C: unit cement content (kg/m^3)

W: unit water content (kg/m)

W/C: water-to-cement ratio

RH: relative humidity (%)

V: volume (mm^3)

S: surface area in contact with outside air (mm^2)

V/S: volume-to-surface area ratio (mm)

t_0, t' and t: age (days) of concrete at the beginning of drying, at the beginning of loading, and during loading, respectively; these factors should be corrected by

for t_0, t' and $t = \sum_{i=1}^{n}\Delta t_i \exp\left[13.65-\frac{4000}{273+T\left(\Delta t_i\right)/T_0}\right]$

where Δt_i: number of days when the temperature is T(°C)

T_0: 1 °C

Although the four mathematical models above can be used to predict the creep behavior of a concrete specimen, those models may contain considerable errors. This is because the effects of concrete ingredients and environmental conditions on creep

behavior are too complicated to be fully understood, and a limited amount of creep-test results were used when deriving those empirical creep-prediction models. Also, it is hardly possible to select an appropriate mathematical model that can explain the creep behaviors of a concrete mixture under a particular environment better than the other models because we cannot completely figure out the true behaviors of creep in concrete. The proposed methodology discussed in this Chapter accounts for unknown error involved in prediction by each creep-prediction model, and quantify the degree of belief that each creep-prediction model is best of the considered models using the measured differences between experimental outcomes and model predictions.

② Creep Test and Model Predictions

A creep test was carried out on a concrete specimen under a specific environment [91], and the four mathematical models are used to predict the amount of the creep occurring in the specimen. The specimen on which a creep test was performed was a concrete cylinder with the diameter of 152.4 mm and the height of 304.8 mm. The applied load placed on the concrete specimen was controlled to be sustained at the target load of 457,722 *kgf* for the full duration of testing. The dimensions, the mixture, the mechanical properties of the concrete specimen, and the conditions of the creep test are listed below:

- Volume of the specimen: $5.56\times10^{6}\,\mathrm{mm}^3$
- Surface of the specimen: $182{,}415\,\mathrm{mm}^2$
- Volume-to-surface ratio: 30.48
- Cross-sectional area: $182.41\,\mathrm{mm}^2$
- Perimeter of the specimen in contact with the atmosphere: 478.78 mm

- Unit cement content: 379.7 kg/m^3
- Unit water content: 160.2 kg/m^3
- Water-to-cement ratio: 0.42
- Ratio of fine to total aggregate: 0.362
- Slump flow: 184.2 mm
- Air content: 3.5 %
- Compressive strength at time of loading: 62.7 MPa
- Elastic modulus of the specimen at time of loading: 37,208.3 MPa
- Temperature: 22.8 °C
- Relative humidity: 50.0 %
- Age of concrete at time of loading: 28 day

Table 2.2 shows the creep strains measured from the creep test at several concrete ages [91]. The creep predictions by the four mathematical models are expressed with the creep strain functions obtained by putting the numerical values above into the respective models as following:

$$\text{ACI 209 model}: \; y_{cAIC} = 1{,}297 \times 10^{-6} \times \frac{t^{0.6}}{10 + t^{0.6}}$$

$$\text{AASHTO model}: \; y_{cAASHTO} = 671 \times 10^{-6} \times \frac{t}{24.7 + t}$$

$$\text{CEB-FIP model}: \; y_{cCEB} = 1{,}527 \times 10^{-6} \times \left(\frac{t}{t + 307.16} \right)^{0.3}$$

$$\text{JSCE model}: \; y_{cJSCE} = 1{,}039 \times 10^{-6} \times \left[1 - \exp\left\{ -0.09 \left(1.14 \left(t + 28 \right) - 31.8 \right)^{0.6} \right\} \right]$$

where *t* is age of concrete (days), defined as age of concrete between time of loading and each time of interest.

The predictions of creep strains expressed by the time-dependent functions above are plotted in Fig. 2.10 along with the measured creep strains. The predicted creep strain values by the four models are shown for each age of the specimen at which creeps were measured from the test in Table 2.2.

Table 2.2 Measured creep strains of the tested concreted specimen and predicted creep strains by the four models over an extended period of time

Age of concrete after loading	Measured creep strain ($\times 10^{-6}$)	Predicted creep strain ($\times 10^{-6}$)			
		ACI 209 model	AASHTO model	CEB-FIP model	JSCE model
1 day	175	118	26	274	102
7 days	367	315	148	488	281
14 days	431	425	243	597	394
21 days	490	497	308	669	473
28 days	537	551	357	725	534
90 days	711	776	527	978	795
180 days	802	899	590	113	923
270 days	875	962	615	1216	976
360 days	951	1003	628	1269	1002

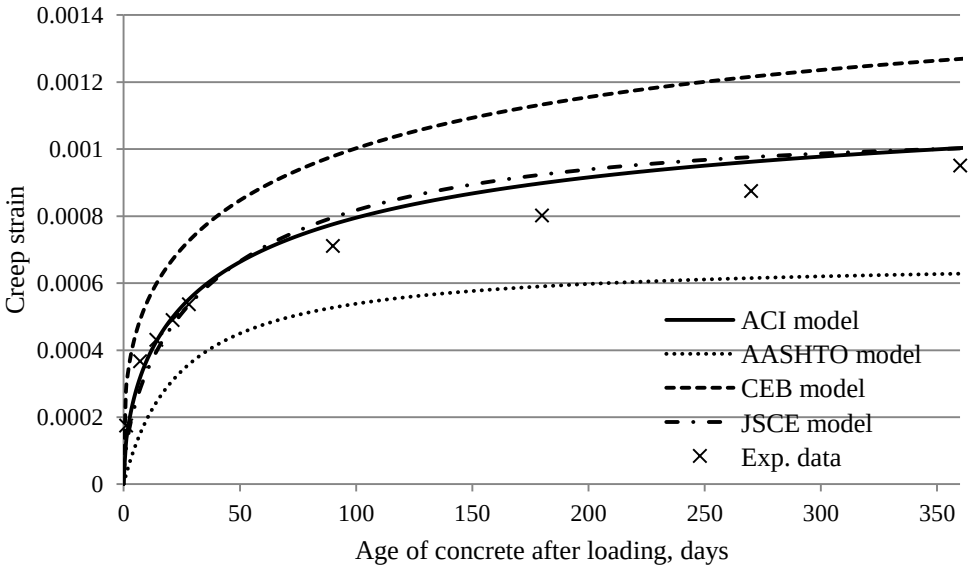

Figure 2.10 Time-dependent predictions of creep strain by the four mathematical models along with measured creep strains

The procedures for computing the posterior probabilities of the four creep-prediction models given the measured creep strains are as follows:

Step 1) Unknown errors ε_1, ε_2, ε_3 and ε_4, assumed to be normal variables with zero means and unknown variances are incorporated into the predictions of creep strains by the considered models. Predictive distribution of creep strain at each time step estimated by each model is represented by

$$\Pr\left(y\left|\mathrm{M}_{ACI},\mathrm{D}\right.\right)=1{,}297\times10^{-6}\times\frac{t^{0.6}}{10+t^{0.6}}+\varepsilon_1,\ \ \varepsilon_1\sim\mathcal{N}\left(0,\sigma_1^2\right)$$

$$\Pr\left(y\left|\mathrm{M}_{AASHTO},\mathrm{D}\right.\right)=671\times10^{-6}\times\frac{t}{24.7+t}+\varepsilon_2,\ \varepsilon_2\sim\mathcal{N}\left(0,\sigma_2^2\right)$$

$$\Pr\left(y\left|\mathrm{M}_{CEB},\mathrm{D}\right.\right)\ =1{,}527\times10^{-6}\times\left(\frac{t}{t+307.16}\right)^{0.3}+\varepsilon_3,\ \varepsilon_3\sim\mathcal{N}\left(0,\sigma_3^2\right)$$

$$\Pr\left(y\left|\mathrm{M}_{JSCE},\mathrm{D}\right.\right)\ =1{,}039\times10^{-6}\times\left[1-\exp\left\{-0.09\left(1.14\left(t+28\right)-31.8\right)^{0.6}\right\}\right]+\varepsilon_4,\varepsilon_4\sim\mathcal{N}\left(0,\sigma_4^2\right)$$

where M_{ACI}, M_{AASHTO}, M_{CEB}, M_{JSCE} denotes the ACI 209, the AASHTO, the CEB-FIP and the JSCE creep-prediction models, respectively. D denotes the measured creep strains. σ_1, σ_2, σ_3 and σ_4 are the standard deviations of ε_1, ε_2, ε_3 and ε_4. Using the differences between the measured and predicted creep strains shown in Table 2.3, the unknown standard deviation σ_1, σ_2, σ_3 and σ_4 can be estimated by Eq. (2.20). The calculated standard deviation values are

$$\sigma_1 = \sqrt{\sum_{n=1}^{9} {\varepsilon_{1_n}}^2 \Big/ 9} = \sqrt{3.008 \times 10^{-8} / 9} = 5.782 \times 10^{-5}$$

$$\sigma_2 = \sqrt{\sum_{n=1}^{9} {\varepsilon_{2_n}}^2 \Big/ 9} = \sqrt{4.222 \times 10^{-7} / 9} = 2.166 \times 10^{-4}$$

$$\sigma_3 = \sqrt{\sum_{n=1}^{9} {\varepsilon_{3_n}}^2 \Big/ 9} = \sqrt{5.173 \times 10^{-7} / 9} = 2.398 \times 10^{-4}$$

$$\sigma_4 = \sqrt{\sum_{n=1}^{9} {\varepsilon_{4_n}}^2 \Big/ 9} = \sqrt{4.895 \times 10^{-8} / 9} = 7.375 \times 10^{-5}$$

The measured experimental data are regarded to be data sets sampled from probability distributions for random variables ε_1, ε_2, ε_3 and ε_4 that represent both uncertainties involved in model discrepancy and experimental data. Although the uncertainty in the experimental data is not dealt with individually, the distances of the four models from the experimental data are treated as uncertain quantities.

Step 2) The likelihood of each model given the measured creep strains is evaluated using the calculated standard deviations σ_1, σ_2, σ_3 and σ_4 above and the number of the measured differences, 9 for this problem, by Eq. (2.21). The calculated likelihoods of the considered four models are

$$\Pr\left(\mathrm{D}\middle|\mathrm{M}_{ACI}\right)=\left(\frac{1}{2\pi{\sigma_1}^2}\right)^{9/2}\exp\left(-\frac{9}{2}\right)=\left(\frac{1}{2\pi\times\left(5.782\times10^{-5}\right)^2}\right)^{9/2}\exp\left(-\frac{9}{2}\right)=3.940\ \times\ 10^{32}$$

$$\Pr\left(\mathrm{D}\middle|\mathrm{M}_{AASHTO}\right)=\left(\frac{1}{2\pi{\sigma_2}^2}\right)^{9/2}\exp\left(-\frac{9}{2}\right)=\left(\frac{1}{2\pi\times\left(2.166\times10^{-4}\right)^2}\right)^{9/2}\exp\left(-\frac{9}{2}\right)=2.712\ \times\ 10^{27}$$

$$\Pr\left(\mathrm{D}\middle|\mathrm{M}_{CEB}\right)=\left(\frac{1}{2\pi{\sigma_3}^2}\right)^{9/2}\exp\left(-\frac{9}{2}\right)=\left(\frac{1}{2\pi\times\left(2.398\times10^{-4}\right)^2}\right)^{9/2}\exp\left(-\frac{9}{2}\right)=1.086\ \times\ 10^{27}$$

$$\Pr\left(\mathrm{D}\middle|\mathrm{M}_{JSCE}\right)=\left(\frac{1}{2\pi{\sigma_4}^2}\right)^{9/2}\exp\left(-\frac{9}{2}\right)=\left(\frac{1}{2\pi\times\left(7.375\times10^{-5}\right)^2}\right)^{9/2}\exp\left(-\frac{9}{2}\right)=4.406\ \times\ 10^{31}$$

Step 3) Given the evaluated model likelihoods, the prior probabilities of the considered models can be updated into the posterior model probabilities using Bayes' theorem. For this problem, the prior model probabilities are assumed to be uniform because any expert opinion about credibility of the considered models is not available. Using Eq. (2.31), the posterior model probabilities are calculated to be

$$\Pr\left(\mathrm{M}_{ACI}\middle|\mathrm{D}\right)=\frac{\Pr\left(\mathrm{D}\middle|\mathrm{M}_{ACI}\right)}{\sum_{i=1}^{4}\Pr\left(\mathrm{D}\middle|\mathrm{M}_i\right)}=\frac{3.940\ \times\ 10^{32}}{4.380\ \times\ 10^{32}}=8.99\ \times\ 10^{-1}$$

$$\Pr\left(\mathrm{M}_{AASHTO}\middle|\mathrm{D}\right)=\frac{\Pr\left(\mathrm{D}\middle|\mathrm{M}_{AASHTO}\right)}{\sum_{i=1}^{4}\Pr\left(\mathrm{D}\middle|\mathrm{M}_i\right)}=\frac{2.712\ \times\ 10^{27}}{4.380\ \times\ 10^{32}}=6.19\ \times\ 10^{-6}$$

$$\Pr\left(\mathrm{M}_{CEB}\middle|\mathrm{D}\right)=\frac{\Pr\left(\mathrm{D}\middle|\mathrm{M}_{CEB}\right)}{\sum_{i=1}^{4}\Pr\left(\mathrm{D}\middle|\mathrm{M}_i\right)}=\frac{1.086\ \times\ 10^{27}}{4.380\ \times\ 10^{32}}=2.48\ \times\ 10^{-6}$$

$$\Pr\left(\mathrm{M}_{JSCE}\left|\mathrm{D}\right.\right)=\frac{\Pr\left(\mathrm{D}\left|\mathrm{M}_{JSCE}\right.\right)}{\sum_{i=1}^{4}\Pr\left(\mathrm{D}\left|\mathrm{M}_{i}\right.\right)}=\frac{4.406\times10^{31}}{4.380\times10^{32}}=1.01\times10^{-1}$$

The calculated posterior probabilities above indicate the degree of belief that each model is the best approximating model among the considered models given the measured creep strains. The calculated posterior probabilities imply that the ACI 209 creep-prediction model is most likely to give the closest predictions of unobserved creep strains among the models considered.

The predictions by the AASHTO and CEB-FIP models are positioned far away from the measured nine creep test data. The significantly low probabilities of the two models are due to the fact that the models fit the data very poorly. The performance of the models is situation-specific. The models that perform worse under a specific test condition might perform better under another condition. The derived result does not imply that the two models would show bad performance in any creep test. Model probability calculation is dependent on available test data with which model predictions are compared. The calculated model probabilities would be changed if more creep test data are measured.

3. Combination of Response Predictions from Multiple Models

Given that the probabilities of a model set are known, model-form uncertainty represented by the model probabilities can be propagated into the prediction of a system response using model combination techniques; model combination indicates the process for combining predictions by a set of models. Model combination aims to predict unknown responses more reliably than each model by incorporating model-form uncertainty that would not be captured if a model is only considered. Model combination is introduced in Section 3.1. Two model combination techniques called the adjustment factor approach and model averaging are described in Section 3.2 and 3.3, respectively. Those two techniques are demonstrated with the numerical problem of a nonlinear spring-mass system in the ends of the respective Sections.

3.1 Model Combination

3.1.1 Historical Perspective on Model Combination

The idea of combining multiple models can be traced back to 1963 when Barnard [92] first mentioned model combination in a paper studying airline passenger data. In 1965, Roberts [93] combined the probability distributions built based on two experts' opinions. In 1978, Leamer [94] offered the basic paradigm of Bayesian model averaging based on Bayesian inference and the idea of model averaging. In 1996, Zio and Apostolakis [33] combined model predictions weighted by model probabilities reflecting expert opinion using the adjustment factor approach.

3.1.2 Description of Model Combination

Model-form uncertainty associated with a set of models is propagated into the prediction of a system response by integrating all the predictions by the considered models into a single composite prediction. Model combination aims to predict unknown responses more reliably than each model in a set rather than better represent the physics of a real system or update prediction by each model given measured experimental data. Combination of response predictions by multiple models is carried out by averaging those predictions weighted by calculated model probabilities. This concept is the core of model combination [95]. Weight represents the effect that each model has on the composite prediction. As shown in Figure 3.1, the composite prediction of a system response is represented by a probability distribution. In general, combining multiple model predictions leads to an improvement in predictive accuracy [96].

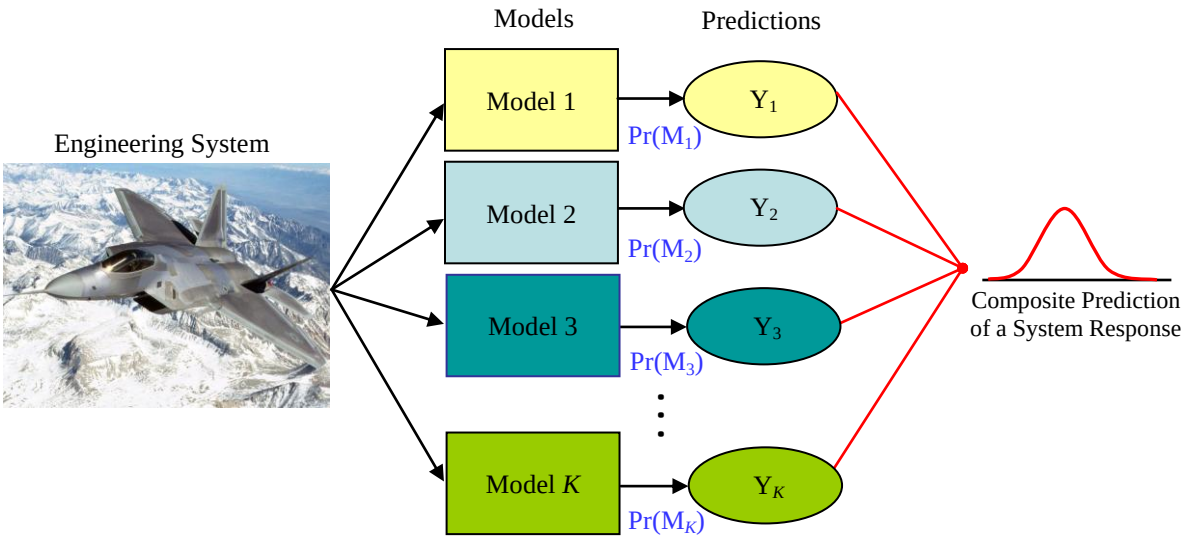

Figure 3.1 Illustrative concept of model averaging

Two model combination techniques are utilized for this research: the adjustment factor approach and model averaging. The application of the two model combination techniques is separated between the two distinct model groups. The adjustment factor approach supposes that the models to be combined are deterministic. Deterministic model indicates a type of models that have their input parameters uniquely determined and generates deterministic response predictions. On the other hand, model averaging can only deal with probabilistic models. Probabilistic model indicates the other type of models that involve uncertainty in its parameters and generates probabilistic response predictions generally represented by probability distributions. The adjustment factor approach adjusts the prediction of the model with the largest probability by an adjustment factor to account for model-form uncertainty. An adjustment factor is assessed by considering predictions by alternative models. The adjustment factor approach has the advantage of accommodating normal and log-normal distribution forms to represent model-form uncertainty in a deterministic model set. It is limited in its application in that a set of considered models must be deterministic. Model averaging can deal with model form uncertainty as well as other types of uncertainty in probabilistic prediction of a response by each model. Model averaging averages predictive distributions of a response estimated by a model set using model probabilities as weights. The advantage of model averaging is that any probabilistic model predictions can be combined as long as model predictions are represented by probability distributions. However, this technique cannot handle model-form uncertainty alone because model predictions are not allowed to take fixed values.

3.2 Adjustment Factor Approach

Mosleh and Apostolakis [97] suggest the adjustment factor approach to combine experts' estimates according to Bayes' theorem. The application of this approach was extended to the model-form uncertainty problem [33]. It has been applied to quantify model-form uncertainty for the problems of groundwater flow and contaminant transport [33], nuclear reactor safety [98], laser peening process [3], and wing flutter [99]. In this approach, model-form uncertainty is accounted for by an adjustment factor represented by a probability distribution. An adjustment factor can be evaluated by assuming the differences between the prediction by the model with the highest probability and those of alternate models to be normally or log-normally distributed. When quantifying an adjustment factor, model probabilities are assigned as weights to the models considered. A composite predictive distribution of a response is constructed by introducing the evaluated adjustment factor into the prediction by the model with the highest probability.

Depending on whether the assumption that the distribution representing model-form uncertainty in a response prediction is normal or log-normal, an additive or a multiplicative adjustment factor is used, respectively. An additive adjustment factor is added to the prediction by the model with the highest probability to construct a predictive distribution incorporating model-form uncertainty. Similarly, a multiplicative adjustment factor multiplies the prediction by the model with the highest probability to construct the predictive distribution.

3.2.1 Additive Adjustment Factor

When an additive adjustment factor is used, the prediction of a system response is represented by

$$y = y^* + E_a^* \tag{3.1}$$

where y^* represents the prediction of the unknown response by the model with the highest probability among a considered model set, E_a^* represents an additive adjustment factor, and y represents an adjusted prediction. An additive adjustment factor E_a^* is assumed to be a normal random variable as shown in Figure 3.2. Supposing that the predictions and probabilities of a set of models are known, the means and variances of both E_a^* and y are computed by

$$E\left(E_a^*\right) = \sum_{k=1}^{K} \Pr\left(\mathrm{M}_k\right)\left(y_k - y^*\right) \tag{3.2}$$

$$Var\left(E_a^*\right) = \sum_{k=1}^{K} \Pr\left(\mathrm{M}_k\right)\left(y_k - E\left(y\right)\right)^2 \tag{3.3}$$

$$E\left(y\right) = y^* + E\left(E_a^*\right) \tag{3.4}$$

$$Var\left(y\right) = Var\left(E_a^*\right) \tag{3.5}$$

where $E(\bullet)$ is mean of a variable, $Var(\bullet)$ is variance of a variable, y_k represents the prediction of the response by model M_k, $\Pr(\mathrm{M}_k)$ is the probability of M_k, and K is the number of considered models. As shown in Eqs. (3.2) and (3.3), the mean and variance of E_a^* are the averaged mean and variance of the differences between the prediction by the model with the highest probability and those by alternate models, using model probabilities as weights. The adjusted prediction y is also normally distributed. The mean of y is the sum of the prediction by the model with the highest probability and the mean

of E_a^*, as shown in Eq. (3.4). The variance of y is the same as that of E_a^*, as shown in Eq. (3.5).

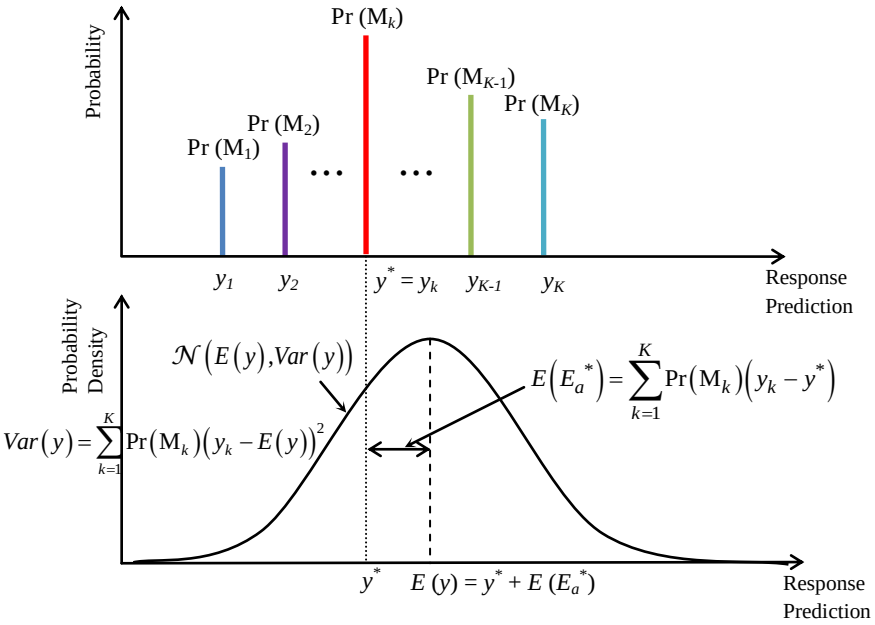

Figure 3.2 Additive adjustment factor approach

3.2.2 Multiplicative Adjustment Factor

When a multiplicative adjustment factor is used, the prediction of a response is represented by

$$y = y^* \times E_m^* \tag{3.6}$$

where E_m^* represents a multiplicative adjustment factor. A multiplicative adjustment factor E_m^* is assumed to be a log-normal random variable. The means and variances of the logarithms of both E_m^* and adjusted prediction y are computed by

$$E\left(\ln E_m^*\right) = \sum_{k=1}^{K} \Pr\left(M_k\right)\left(\ln y_k - \ln y^*\right) \tag{3.7}$$

$$Var\left(\ln E_m^*\right) = \sum_{k=1}^{K} \Pr\left(M_k\right)\left(\ln y_k - E\left(\ln y\right)\right)^2 \tag{3.8}$$

$$E\left(\ln y\right) = \ln y^* + E\left(\ln E_m^*\right) \tag{3.9}$$

$$Var\left(\ln y\right) = Var\left(\ln E_m^*\right) \tag{3.10}$$

where $E(\ln \bullet)$ is the mean of the logarithm of a variable, and $Var(\ln \bullet)$ is the variance of the logarithm of a variable. Adjusted prediction y is also log-normally distributed. The logarithm of y is normally distributed as shown in Figure 3.3. The means and variances of both E_m^* and y can be calculated with the means and variances of $\ln E_m^*$ and $\ln y$, according to the property of lognormal variable as expressed by

$$E\left(E_m^*\right) = \exp\left(E\left(\ln E_m^*\right) + \text{var}\left(\ln E_m^*\right)/2\right) \tag{3.11}$$

$$Var\left(E_m^*\right) = \left(\exp\left(Var\left(\ln E_m^*\right)\right) - 1\right)\exp\left(2E\left(\ln E_m^*\right) + Var\left(\ln E_m^*\right)\right) \tag{3.12}$$

$$E\left(y\right) = \exp\left(E\left(\ln y\right) + \text{var}\left(\ln y\right)/2\right) \tag{3.13}$$

$$Var\left(y\right) = \left(\exp\left(Var\left(\ln y\right)\right) - 1\right)\exp\left(2E\left(\ln y\right) + Var\left(\ln y\right)\right) = \left(y^*\right)^2 Var(E_m^*) \tag{3.14}$$

The bigger the absolute value of the mean of an adjustment factor is, the more the adjusted prediction is shifted from the prediction by the model with the highest probability. The bigger the variance of an adjustment factor is, the larger the degree of model-form uncertainty in prediction (the degree of uncertainty in the response prediction that results from model-form uncertainty).

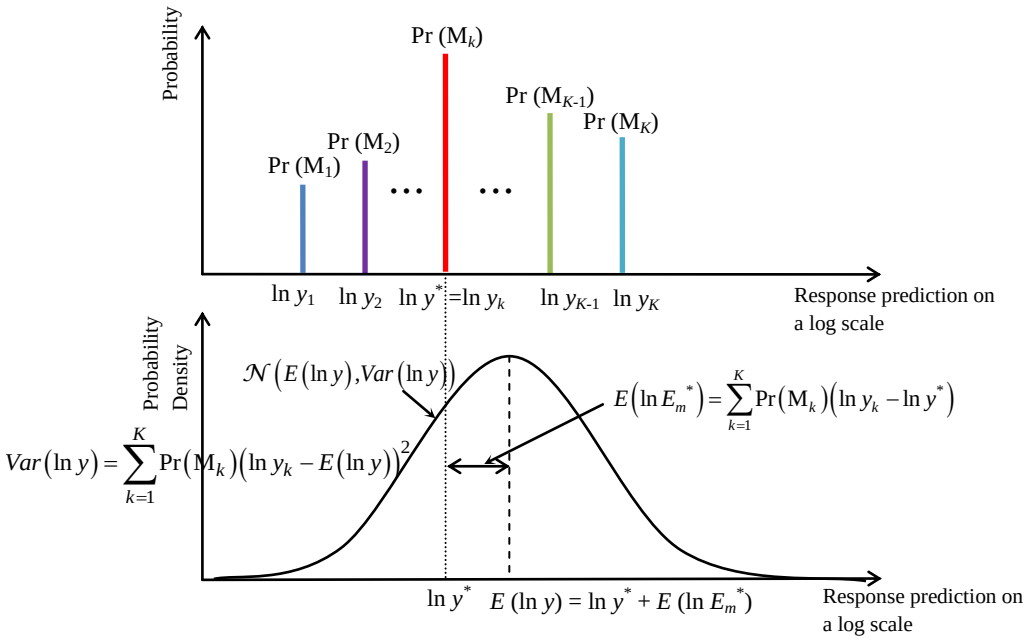

Figure 3.3 Multiplicative adjustment factor approach

Although both the adjustment factors can be used to quantify model-form uncertainty in response prediction, the problem may arise of deciding which of the two factors represents model-form uncertainty with higher fidelity. There is no quantitative instruction presented to address this problem, but it is reasoned that the use of a multiplicative adjustment factor would be more appropriate if weighted model predictions are significantly asymmetric.

3.2.3 Demonstration of the Adjustment Factor Approach

A nonlinear spring-mass system is used to numerically demonstrate the adjustment factor approach.

① Description of a Nonlinear Spring-Mass System

The free vibration of a single-degree-of-freedom system into which a spring introduces nonlinearity is described by the governing equation,

$$\mu\ddot{u} + h(u) = 0 \tag{3.15}$$

where μ is a mass, and spring force $h(u)$ is a nonlinear function of displacement u. Depending on the functions introduced to describe the relation between spring force and displacement, different models are generated to represent the nonlinear spring-mass system. Suppose that there are three types of nonlinear spring force functions suggested for this problem. They are

$$h_1(u) = \varepsilon u^{1/3} \tag{3.16}$$

$$h_2(u) = au + bu^3 \tag{3.17}$$

$$h_3(u) = cu + \frac{du}{\sqrt{1+u^2}} \tag{3.18}$$

The three force-displacement functions are graphically represented in Figure 3.4, given the values of constants ($\varepsilon = 0.65\ N/cm^{1/3}$, $a = 1\ N/cm$, $b = -0.35\ N/cm^3$, $c = 1\ N/cm$, and $d = -0.5\ N$). A nonlinear spring is described as the stiffest by Eq. (3.16) (Model 1) and described as the most flexible by Eq. (3.18) (Model 3).

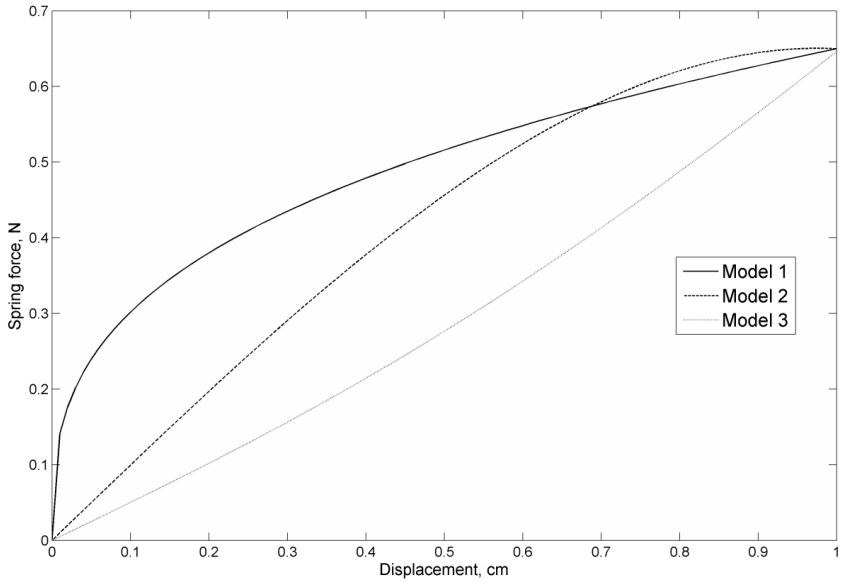

Figure 3.4 Three force-displacement functions to represent nonlinearity in the spring of a spring-mass system

Given the mass and initial conditions (μ = 1 *kg*, $u(0)$ = 1 *cm*, and $du/dt(0)$ = 0 *cm*/*sec*), the fundamental natural frequency of a nonlinear spring-mass system can be predicted by the three mathematical models, which put the force-displacement functions shown in Eqs. (3.16) - (3.18) into the governing equation shown in Eq. (3.15). The natural frequency predictions by the three mathematical models can be calculated by [100]

$$\omega = 1.070451\varepsilon^{1/2}u(0)^{-1/3} \tag{3.19}$$

$$\omega = \sqrt{a + \frac{3}{4}bu(0)^2} \tag{3.20}$$

$$\omega = \sqrt{\frac{\int_0^{\pi/2}\left\{c\cos^2 t + \frac{d\cos^2 t}{\sqrt{1+u(0)^2\cos^2 t}}\right\}dt}{\int_0^{\pi/2}\sin^2 t dt}} \tag{3.21}$$

The predicted natural frequencies by the three models are shown in Table 3.1. Model 1 predicts the largest frequency (0.863 *rad*/*sec*) among the models considered. Model 3 predicts the smallest frequency (0.808 *rad*/*sec*). Model-form uncertainty is involved in the model predictions due to ignorance about which of the three model predictions is the closest to the true natural frequency.

Table 3.1 Predictions and probabilities of three models for a spring-mass system

	Natural Frequency (rad/sec)	Model Probability
Model 1	0.863	0.3
Model 2	0.859	0.5
Model 3	0.808	0.2

② Quantification of Model Probability and Application of Two Adjustment Factor Approaches

Using both the additive and multiplicative adjustment factors, the adjustment factor approach is utilized to quantify the model-form uncertainty involved in the model predictions of the natural frequency. Model probabilities are assumed for this problem (Table 3.1) because there is no information available to evaluate them, and this numerical problem just aims to demonstrate the adjustment factor approach.

Model 2 is identified as the best model because it has the highest model probability (0.5) among the considered models. The prediction by the best model (Model 2), which would only be considered if model-form uncertainty was ignored, is adjusted by two adjustment factors to incorporate model-form uncertainty. Using an additive adjustment factor, the mean and standard deviation of the adjusted prediction of the natural frequency are

calculated using Eqs. (3.2) - (3.5). Using a multiplicative adjustment factor, the mean and standard deviation of the adjusted prediction are calculated using Eqs. (3.11) - (3.14). The mean and standard deviation of the adjusted prediction of the natural frequency is shown for each adjustment factor case in Table 3.2. The prediction by the best model is decreased for both the adjustment factor cases because the model (Model 3) making a smaller prediction than the best model has more effects on the adjustment of the best model prediction than the model making a lager prediction (Model 1). The prediction by the best model (0.859 *rad*/*sec*) is decreased by the amount of 0.0090 *rad*/*sec* for the additive adjustment factor case. The best model prediction is decreased by the amount of 0.0145 *rad*/*sec* for the multiplicative adjustment factor case. The standard deviation of adjusted prediction for the additive adjustment factor case (0.0208 *rad*/*sec*) is little different from the standard deviation for the multiplicative adjustment factor case (0.0240 *rad*/*sec*). The standard deviation indicates the degree of dispersion in the model predictions. The standard deviation also reflects the degree of model-form uncertainty resulting from consideration of the two alternate models.

Table 3.2 Mean and standard deviation of adjusted prediction for two adjustment factor cases

	Mean of adjusted prediction (rad/sec)	Standard deviation of adjusted prediction (rad/sec)
Additive adjustment factor	0.8500	0.0208
Multiplicative adjustment factor	0.8445	0.0240

A normal and a lognormal distribution are shown in Figure 3.5, which represents the adjusted predictions of the natural frequency for the additive and multiplicative adjustment factor cases, respectively. Both distributions of the natural frequency are

almost identical because the weighted predictions of the three models are almost symmetrical. So, for this problem, which of the two adjustment factors is used to represent the model-form uncertainty in the prediction of the natural frequency is of little concern. However, if the results of using the two adjustment factors show a significant difference, it would be important to decide which of the two represents the reality with higher confidence. It would be reasonable to select one of the two factors after considering the number of considered models and the symmetry of weighted model predictions.

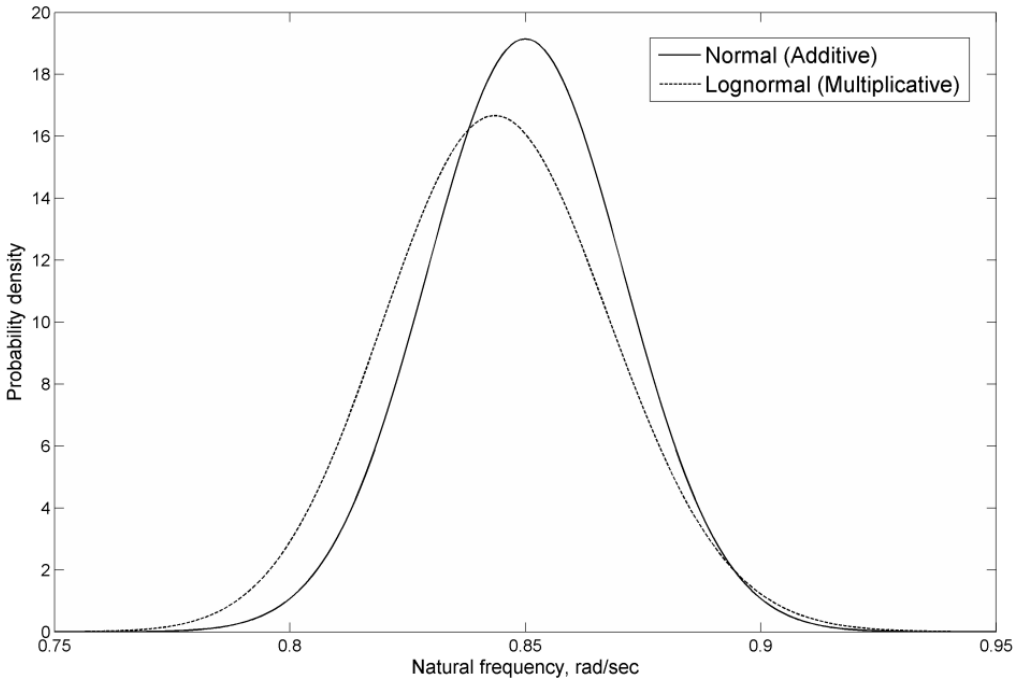

Figure 3.5 PDFs of fundamental natural frequency for additive and multiplicative adjustment factor cases

③ *Update of Model Probability and Adjusted Prediction*

Although model probabilities are simply assumed for this problem, they may also be evaluated based on experts' opinions [3, 33, and 101]. Suppose that the model

probabilities shown in Table 3.1 were quantified by a group of experts. When presented with the distributions of adjusted predictions shown in Figure 3.5, experts might feel the need to modify the model probabilities. By assuming the experts would alter the model probabilities into new model probabilities (e.g. Pr (M_1) = 0.3, Pr (M_2) = 0.4, and Pr (M_3) = 0.3), a new analysis would be executed to update the predictive distributions of the natural frequency using the modified model probabilities. The modification of model probabilities by experts might be iterated until the experts regard the predictive distributions reflecting their opinions about the models as full and appropriate characterizations of model-form uncertainty.

3.3 Model Averaging

Model averaging [9, 22, and 84] is the most common technique used to integrate multi-model predictions of a response, given each model prediction represented by a probability distribution.

3.3.1 Integration of Multiple Predictive Distributions

The integration of predictive distributions of a response by different models is represented by

$$g\left(y|\mathrm{D}\right)=\sum_{k=1}^{K}\Pr\left(\mathrm{M}_k|\mathrm{D}\right)g\left(y|\mathrm{M}_k,\mathrm{D}\right) \tag{3.22}$$

where y is a system response to be predicted, D is an observed experimental data set, and M_1, …, M_K are the models considered. g (• | D) and Pr (• | D), referred to as posterior probability distribution and posterior probability of •, are a conditional probability distribution and a conditional probability of • given experimental data D, respectively.

$g(y|\mathrm{M}_k, \mathrm{D})$ is the posterior predictive distribution of response y given experimental data D under model M_k. $g(y|\mathrm{M}_k, \mathrm{D})$ represents the uncertainty involved in the prediction of response y made by model M_k. $\Pr(\mathrm{M}_k|\mathrm{D})$ is the posterior probability of model M_k given experimental data D. Given no experimental data, D in Eq. (3.22) drops out.

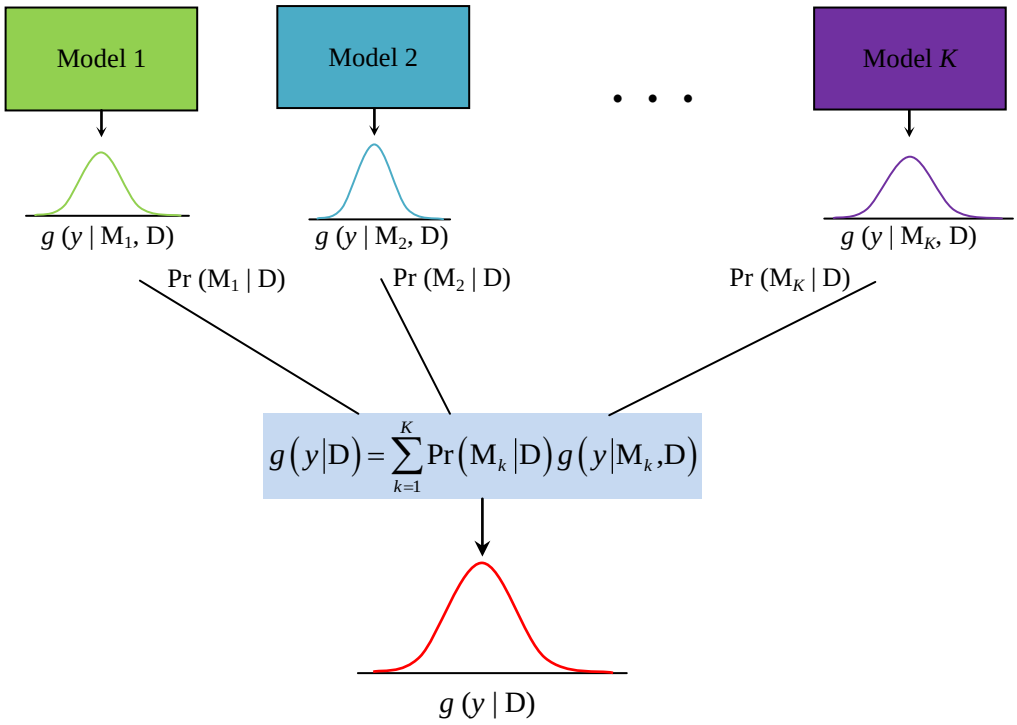

Figure 3.6 Integration of predictive distributions

If posterior predictive distribution $g(y|\mathrm{M}_k, \mathrm{D})$ estimated by model M_k has mean $E(y|\mathrm{M}_k, \mathrm{D})$ and variance $Var(y|\mathrm{M}_k, \mathrm{D})$, then the mean and variance of composite predictive distribution $g(y|\mathrm{D})$ are calculated by [9]

$$E(y|\mathrm{D}) = \sum_{k=1}^{K} \Pr(\mathrm{M}_k|\mathrm{D})\, E(y|\mathrm{M}_k, \mathrm{D}) \tag{3.23}$$

$$Var(y|\mathrm{D}) = \sum_{k=1}^{K} \Pr(\mathrm{M}_k|\mathrm{D})\, Var(y|\mathrm{M}_k,\mathrm{D}) + \sum_{k=1}^{K} \Pr(\mathrm{M}_k|\mathrm{D})\left(E(y|\mathrm{M}_k,\mathrm{D}) - E(y|\mathrm{D})\right)^2 \tag{3.24}$$

As shown in Eq. (3.23), the mean of $g(y|\mathrm{D})$ is the average of means of predictive distributions by the considered model set, using model probabilities as weights. The variance of $g(y|\mathrm{D})$ is decomposed into the sum of two terms. In Eq. (3.24), the first term, called within-model variance, represents the average degree of uncertainty in each model prediction of response y. The second term, called between-model variance, represents the degree of uncertainty in prediction of response y resulting from model-form uncertainty.

3.3.2 Demonstration of Model Averaging

Model averaging is numerically demonstrated using the problem of a nonlinear spring-mass system in Section 3.2.3. However, the mass and the initial displacement of the system are considered to be random variables.

① *Natural Frequency Predictions by Three Mathematical Models Involving Random Parameters*

As shown in Section 3.2.3, the fundamental natural frequency of a spring-mass system can be predicted by the three mathematical models using Eqs. (3.19) - (3.21). In this Section, the initial velocity of the system is the same as the velocity ($du/dt\,(0) = 0$) in Section 3.2.3, while the mass and initial displacement of it are considered as independent random variables, each of which is assumed to be normally distributed. The means and standard deviations of the mass and the initial displacement are shown in Table 3.3.

Table 3.3 Means and standard deviations of two independent normal variables; the mass and initial displacement of a spring-mass system

	Mean	Standard deviation
Mass	1 *kg*	0.1 *kg*
Initial displacement	1 *cm*	0.2 *cm*

Uncertainty in the mass and initial displacement of the spring-mass system leads to parametric uncertainty in prediction of the natural frequency by each model. To construct predictive distribution of the natural frequency of the system under each model, 100,000 random samples are drawn from the bivariate normal distribution constructed with the two uncorrelated random variables using Latin hypercube sampling. Figure 3.7 shows the kernel density estimates [102] for the predictive distributions of the natural frequency under the three models based on the 100,000 random samples. The means and standard deviations of the three predictive distributions are shown in Table 3.4. The mean of the natural frequency prediction by Model 1 (0.8747 rad/sec) is the largest among the three models since Model 1 describes the nonlinear spring of the system as the stiffest. The mean of the Model 3 prediction (0.7888 rad/sec) is the smallest since Model 3 describes the spring as the most flexible. The standard deviations of the Model 1 and Model 2 predictions of the natural frequency (7.77×10^{-2} rad/sec and 7.79×10^{-2} rad/sec, respectively) are little different from each other. The standard deviation of the Model 3 prediction (4.48×10^{-2} rad/sec) is considerably smaller compared to the standard deviations of Model 1 and Model 2.

Table 3.4 Model Probabilities and means and standard deviations of natural frequency predictions by three mathematical models and composite prediction for a spring-mass system

	Model Probability	Mean (rad/sec)	Standard Deviation (rad/sec)
Model 1	0.3	0.8747	7.77×10^{-2}
Model 2	0.5	0.8535	7.79×10^{-2}
Model 3	0.2	0.7888	4.48×10^{-2}
Composite	1.0	0.8469	$(5.25 \times 10^{-3} + 9.29 \times 10^{-4})^{1/2} = 7.86 \times 10^{-2}$

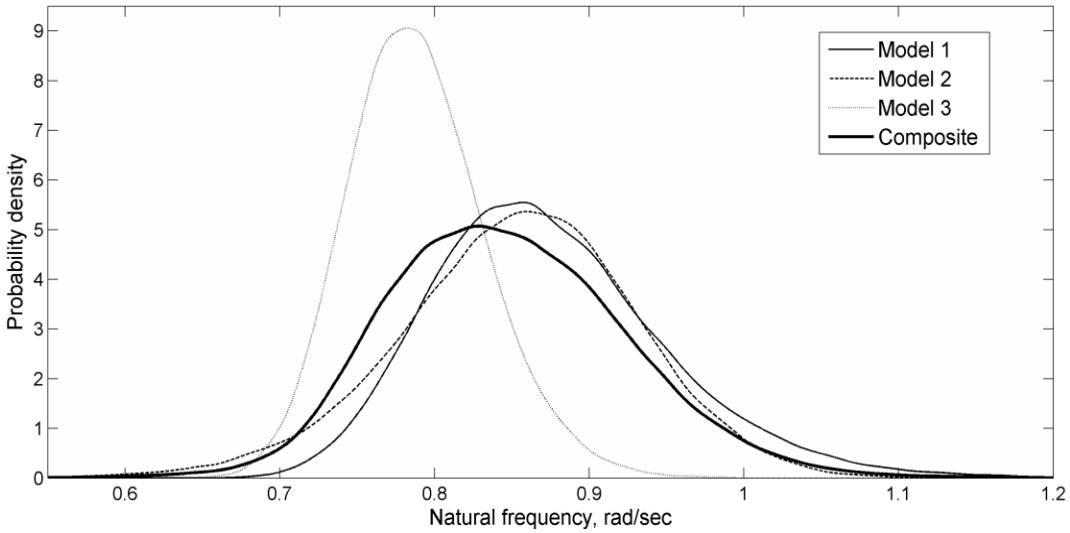

Figure 3.7 Predictive distributions of natural frequency estimated by three models together with composite predictive distribution

② *Integration of Predictive Distributions*

The probabilities of the three mathematical models must be quantified to weigh the predictive distributions under the three models. The same model probabilities as those in Section 3.2.3 are assigned to the three mathematical models.

Given the predictive distributions and probabilities of the three models, the probabilistic predictions of the natural frequency made by the considered models can be integrated into a composite predictive distribution using Eq. (3.22). The mean and standard deviation of the composite predictive distribution are calculated using Eqs. (3.23) and

(3.24) and are shown in Table 3.4. The mean of the composite predictive distribution is almost the same as the mean of the prediction by Model 2 because the weighted means of the three model predictions are almost symmetrical around the mean of Model 2 prediction. The standard deviation of the composite distribution (7.86×10^{-2} rad/sec) is the square root of the sum of the within-model variance (5.25×10^{-3} rad^2/sec^2), which represents the average degree of parametric uncertainty in each model prediction—and the between-model variance (9.29×10^{-4} rad^2/sec^2)—which represents the degree of uncertainty in the composite prediction resulting from model-form uncertainty. Although the standard deviation of the composite distribution is larger than standard deviation of predictive distribution estimated by any model in the considered model set, the difference is insigificant. The dominance of the within-model variance over the between-model variance indicates that the parametric uncertainty associated with the three models is more significant than the model-form uncertainty.

4. Application of the Proposed Methodology to Large-scale Simulation for a Laser Peening Process

The proposed methodology is applied to quantify multiple types of uncertainty associated with the finite element simulation of a laser peening process, a time-dependent high impact process. In Section 4.2, model-form uncertainty alone is incorporated into the composite prediction of a residual stress field. In Section 4.3, both model-form and predictive uncertainty are incorporated into the composite prediction. Finally, three different types of uncertainty (model-form, parametric, and predictive uncertainty) are incorporated into the composite prediction in Section 4.4.

4.1 Problem Description

Laser Peening (LP) is an advanced surface enhancement technique that has been shown to increase the fatigue life of metallic components. LP has also been shown to increase the corrosion and fretting properties of metals. During the LP process, laser energy is converted into shock waves at the surface that induce compressive residual stresses. Fatigue life is improved as the induced compressive residual stresses inhibit the formation of cracks. A detailed description of the LP process is found in the literature [103].

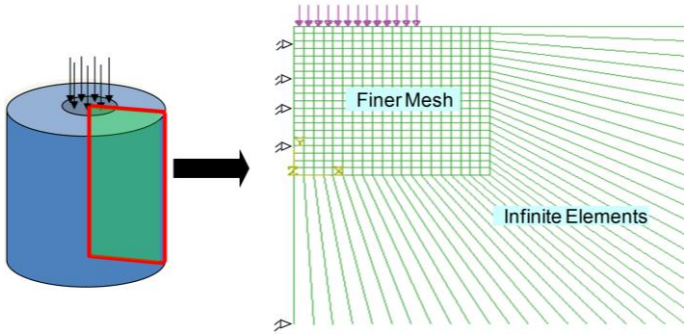

Figure 4.1 Representative axi-symmetric FE mesh for LP simulation model

In simulating the LP process [104-107], accurate description of material behavior is a challenging task because of the high strain rates experienced by the material. During the LP process, the strain rates experienced by a material can reach as high as 10^6/s. In such high strain-rate processes, different material models are available to describe the elastic-plastic behavior. For this problem, three material models are considered to describe the unknown material behavior: the Johnson-Cook (JC) model, the Zerilli-Armstrong (ZA) model, and the Khan-Huang-Liang (KHL) model [108, 109]. The JC, the ZA, and the KHL material models result in three different finite element (FE) models to predict the residual stress field induced by the LP process; the three FE models will be called the JC-based FE model, the ZA-based FE model, and the KHL-based FE model, respectively. The simulation requires an extensive computer effort due to the modeling of material behavior under high pressure shock waves with time marching numerical procedures. A schematic illustration of the LP FE model is shown in Figure 4.1.

The FE models to be considered in Section 4.2 and 4.3 do not account for parametric uncertainty. In Section 4.3, unknown error associated with prediction by each FE model in addition to model-form uncertainty is incorporated into the composite prediction. Each

FE model in Section 4.4 accounts for parametric uncertainty in the peak value of a pressure pulse as well as model-form and predictive uncertainty.

4.2 Case Incorporating Only Model-Form Uncertainty

4.2.1 Quantification of Model-Form Uncertainty in a Deterministic FE Model Set

The peak value of a pressure pulse inducing a residual stress field is assumed to be known as 5.5 GPa. The simulation results of the three FE models based on three different material theories are shown along with experimental data [110] in Figure 4.2. Basing a prediction of residual stress on a single model can cause unreliable results because it is beyond our capability to know which of the three FE models makes a prediction closest to the true residual stress field not yet observed. The significant differences between the three simulation results shown in Figure 4.2 imply that model-form uncertainty in the prediction of the residual stress field might be considerable. The experimental data measured at ten points are used as information to estimate the probabilities of the three FE models.

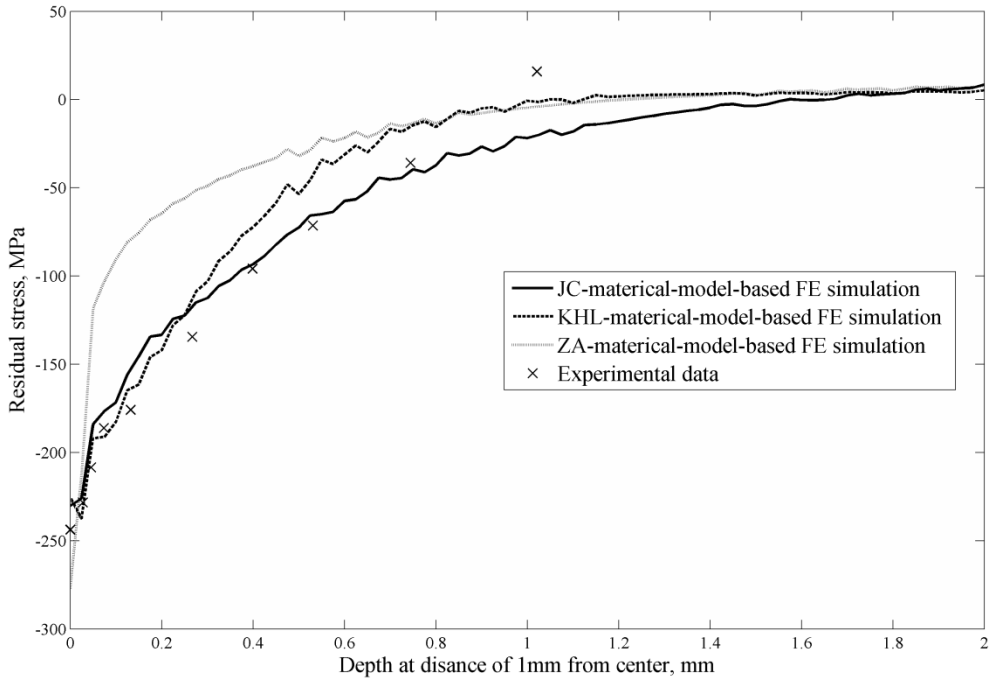

Figure 4.2 Residual stress comparison between the predictions of three FE models and experimental data for axi-symmetric LP component

The prior probabilities of the three FE models are assumed to be uniform as shown in Table 4.1 because of the unavailability of information to quantify them. The evaluation of model likelihoods is required to update the prior model probabilities into the posterior model probabilities using Bayes' theorem as shown in Eq. (2.30). The observed experimental data and model outcomes shown in Figure 4.2 are used to evaluate the likelihoods of the considered three models. The differences between the experimental data and the model outcomes are measured and are considered as a randomly sampled data set from independent and identical normal distributions. The variance of the measured differences (the errors involved in predictions of the experimental data by each FE model) is calculated using Eq. (2.20) and is shown in Table 4.1. The likelihoods of the experimental data for the three models are calculated using Eq. (2.21) and are shown in Table 4.1.

Table 4.1 Variance of errors involved in model predictions of experimental data and likelihood of each FE model

Model	Variance of errors (MPa^2)	Model Likelihood
JC-based FE model	2.795×10^{2}	4.034×10^{-19}
KHL-based FE model	3.113×10^{2}	2.354×10^{-19}
ZA-based FE model	3.631×10^{3}	1.090×10^{-24}

Table 4.2 shows the calculated posterior probabilities of the considered FE models. As shown in Eq. (2.28), equal prior model probabilities cancel out in the calculation of posterior model probabilities. So, the posterior probability of a model is the ratio of likelihood for the model to the sum of likelihoods for all the three models. A posterior model probability indicates the measure of how well a FE model is supported by the experimental data relative to the other FE models. The posterior probability of the ZA-based FE model (1.706×10^{-6}) is significantly smaller than those of the JC-based and the KHL-based FE models (6.318×10^{-1} and 3.682×10^{-1}, respectively) because the first FE model is poorly supported by the experimental data compared to the last two FE models. This implies that the ZA-based FE model has considerably less chance of being the best model than the other FE models. It can be inferred from this fact that the JC and the KHL material models are much more effective in the simulation of the LP component than the ZA material model. The JC-based FE model is identified as the best model because it has the highest probability among the models considered. However, uncertainty exists in the identification of the best model because there is a possibility that the other FE models, especially the KHL-based FE model, might be the best model if additional experimental data are observed.

Table 4.2 Prior and posterior probabilities of three FE models

Model	Prior Model Probability	Posterior Model Probability
JC-based FE model	3.333×10^{-1}	6.318×10^{-1}
KHL-based FE model	3.333×10^{-1}	3.682×10^{-1}
ZA-based FE model	3.333×10^{-1}	1.706×10^{-6}

4.2.2 Combination of Model Predictions Using the Adjustment Factor Approach

Using an additive adjustment factor, the adjustment factor approach is implemented to quantify the model-form uncertainty in the prediction of a residual stress. The reason for utilizing only an additive adjustment factor is that a multiplicative adjustment factor cannot deal with the negative numbers shown in some of the residual stresses. Using an additive adjustment factor, mean and variance of the adjusted prediction of a residual stress can be calculated by Eqs. (3.2) - (3.5).

The mean of the adjusted prediction of the residual stress field is shown in Figure 4.3. The mean of the adjusted prediction is the sum of the prediction by the best model (the JC-based FE model) to the mean of an additive adjustment factor, which accounts for the effects of the alternate FE models. The mean of an adjustment factor indicates the extent to which the weighted predictions of the alternate FE models are asymmetrical around the prediction by the best model. The mean of the adjusted prediction indicates the most likely estimate of residual stress at each depth because predictive distribution of residual stress at every depth is assumed to be normal. The variance of the adjusted prediction indicates the degree of disagreement about the prediction of the residual stress field

among the considered FE models. It also reflects the degree of model-form uncertainty in the prediction of the residual stress field.

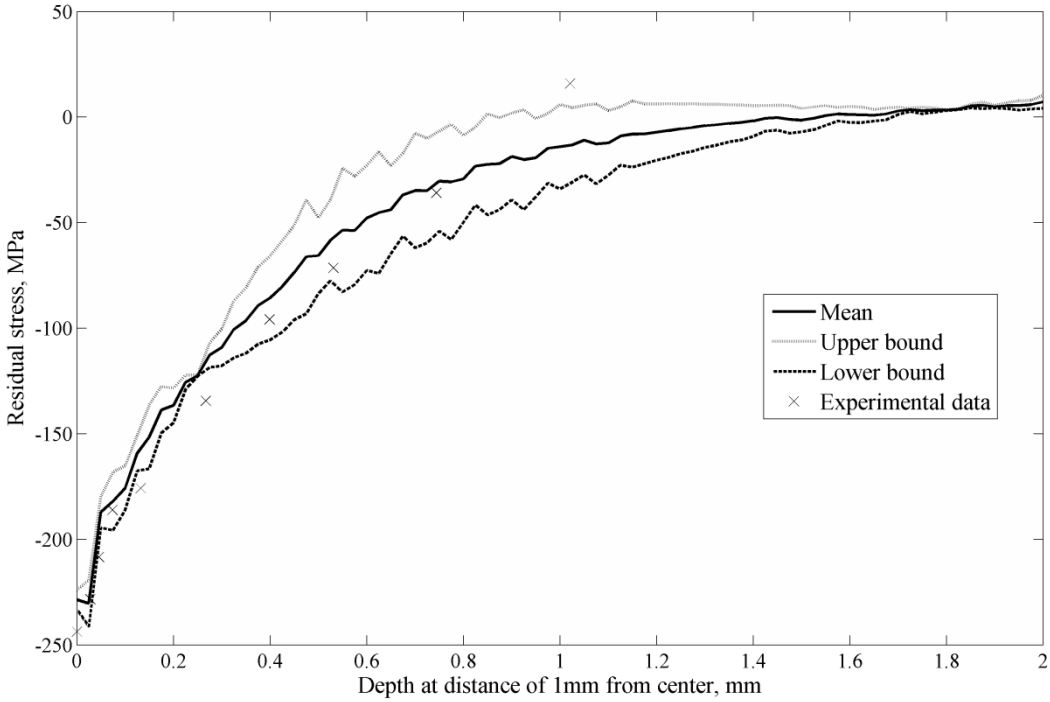

Figure 4.3 Mean of adjusted prediction incorporating model-form uncertainty alone and a 95% confidence band of predicted residual stress field

4.2.3 Establishment of a Confidence Band

In addition to the most likely estimate of a true residual stress at every depth represented as the mean of the adjusted prediction, an interval estimate of the residual stress must be made to indicate the reliability of model prediction. For this problem, a 95% confidence interval for a predicted residual stress is established at every depth in the considered LP component. A 95% confidence interval represents the interval that is expected to include the residual stress to be observed with a probability of 0.95. Because the adjusted prediction of a residual stress is assumed to be normal, the end points of a 95%

confidence interval are calculated at each depth using mean and variance of the adjusted prediction by

$$\left[E(y) - 1.96\sqrt{Var(y)}, E(y) + 1.96\sqrt{Var(y)} \right] \tag{4.1}$$

where $E(y)$ is the mean of the adjusted prediction of residual stress y, and $Var(y)$ is the variance of it. By connecting the upper end points at all the depths, an upper bound curve is drawn. Similarly, a lower bound curve is drawn by connecting the lower end points. A 95% confidence band bounded by the upper and lower curves shown in Figure 4.3 represents a collection of 95% confidence intervals. The confidence band is dominated by the differences between the predictions by the JC-based FE model and those by the KHL-based FE model because the probability of the ZA-based FE model is considerably smaller compared to those of the former two FE models. The width of the 95% confidence band is considerable in the region from the surface to around 0.2 mm in depth and between around 0.3 mm and around 1.3 mm in depth because the JC-based and the KHL-based FE models show significant differences in predictions of residual stresses in that region. This means that the degree of model-form uncertainty in that region is significant since the width of the confidence band reflects the degree of model-form uncertainty.

As mentioned above, a 95% confidence band is the band that is estimated to include the system responses to be observed with 95% probability. However, this statement would be feasible only if the correct model exists in the considered model set. It is not believed that the established confidence band encloses the true residual stresses with 95% probability because the considered FE models do not truly reflect the considered engineering system.

This fact explains why half of the observed experimental data are positioned outside the computed confidence band. The confidence band is too narrow because it incorporates only model-form uncertainty. To make a confidence band more reliable, unknown errors associated with model predictions need to be also incorporated into composite predictions.

4.2.4 Summary

The proposed methodology to evaluate model likelihood for each model by probabilistically comparing model predictions with experimental data is demonstrated with the deterministic FE simulation of a laser peening process. Model-form uncertainty resulting from the creation of different FE models is quantified by computing model likelihoods given the measured residual stresses. The additive adjustment factor approach is implemented to propagate the quantified model-form uncertainty into the composite prediction of a residual stress field. The adjusted prediction of the residual stress field is not conditional on a single FE model; the variance in the prediction that would be missing if the other FE models in the model set were disregarded is incorporated into the composite prediction of the residual stress field. The model-form uncertainty involved in the FE simulation due to the use of different material models proves to be significant in some regions. Half of the measured residual stresses are not held within the established confidence band. The reason for this is attributed to the fact that the errors of model predictions are not accounted for when combining multi-model predictions although they are considerably large. The combination of model predictions involving unknown errors is implemented using model averaging in the following Section.

4.3 Case Incorporating Both Model-Form and Predictive Uncertainty

4.3.1 Combination of Model Predictions Involving Predictive Uncertainty

Parametric uncertainty is not associated with any of the considered FE models as in Section 4.2. However, multi-model combination is performed using model predictions involving unknown errors unlike in Section 4.2. Model averaging is utilized to combine model predictions because model predictions are represented by probability distributions.

Supposing that model probabilities and multi-model predictions involving unknown errors are given, the integration of model predictions is represented by Eq. (3.22):

$$g\left(y|\mathrm{D}\right)=\sum_{k=1}^{K}\Pr\left(\mathrm{M}_k|\mathrm{D}\right)g\left(y|\mathrm{M}_k,\mathrm{D}\right)$$

In this problem, y is a residual stress to be predicted, and D is the set of the measured residual stresses. Predictive distribution $g\ (y \mid \mathrm{M}_k, \mathrm{D})$ under model M_k represents the prediction of residual stress y by FE model M_k involving an unknown error. $g\ (y \mid \mathrm{M}_k, \mathrm{D})$ is normally distributed because the unknown prediction error involved is assumed to be a normal variable as shown in Eq. (2.15). The mean of $g\ (y \mid \mathrm{M}_k, \mathrm{D})$ is the deterministic prediction of residual stress y by model M_k. The deterministic prediction of a residual stress at each depth is already obtained from each FE model in Section 4.2. The variance of $g\ (y \mid \mathrm{M}_k, \mathrm{D})$ indicates the variance of the error involved in prediction of y by M_k. The variance of $g\ (y \mid \mathrm{M}_k, \mathrm{D})$ and posterior model probability $\Pr\ (\mathrm{M}_k \mid \mathrm{D})$ are already calculated in Section 4.2 as shown in Table 4.1 and Table 4.2, respectively.

Because predictive distribution $g\,(y \mid \mathrm{M}_k, \mathrm{D})$ under each model M_k is normal, the composite predictive distribution $g\,(y \mid \mathrm{D})$ is also normal because a linear combination of normal random variables is also normally distributed. Using Eqs. (3.23) and (3.24), the composite predictive distribution that incorporates both model-form and predictive uncertainty is expressed by

$$g\left(y|\mathrm{D}\right) = \mathcal{N}\left(\sum_{k=1}^{K}\Pr\left(\mathrm{M}_k|\mathrm{D}\right) f_k, \sum_{k=1}^{K}\Pr\left(\mathrm{M}_k|\mathrm{D}\right)\sigma_k{}^2 + \sum_{k=1}^{K}\Pr\left(\mathrm{M}_k|\mathrm{D}\right)\left(f_k - E\left(y|\mathrm{D}\right)\right)^2\right) \quad (4.2)$$

f_k denotes the prediction of residual stress y made by deterministic FE model M_k and is shown in Fig. 4.2. $\sigma_k{}^2$ denotes the variance of predictive distribution $g\,(y \mid \mathrm{M}_k, \mathrm{D})$. The variance of $g\,(y \mid \mathrm{D})$ is decomposed into the sum of two terms as shown in Eq. (4.2). The first term represents the average degree of predictive uncertainty associated with each model. The second term represents the degree of uncertainty in response prediction resulting from model-form uncertainty.

As shown in Table 4.3, the calculated variance of the errors involved in the predictions by the KHL-based FE model (3.113×10^2) is larger than it involved in the predictions by the JC-based FE model (2.795×10^2). However, as shown in the last column of Table 4.3, because the probability of the JC-based FE model is much larger than that of the KHL-based FE model, the JC-based FE model has a larger effect on the variance of the composite prediction of an unknown residual stress.

Table 4.3 Posterior model probabilities and variances of errors associated with predictions by three FE models

Model	Pr (M_k | D)	σ_k^2 (MPa^2)	Pr (M_k | D) × σ_k^2 (MPa^2)
JC-based FE model	6.318×10^{-1}	2.795×10^{2}	1.766×10^{2}
KHL-based FE model	3.682×10^{-1}	3.113×10^{2}	1.146×10^{2}
ZA-based FE model	1.706×10^{-6}	3.631×10^{3}	6.193×10^{-3}
Sum	1.0		2.912×10^{2}

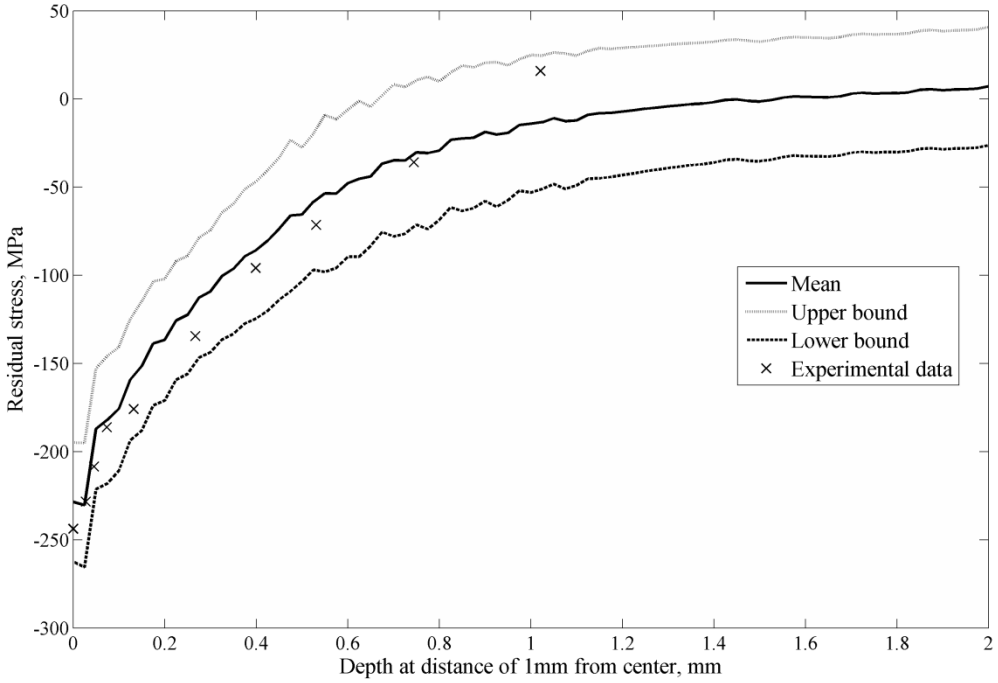

Figure 4.4 The mean of composite prediction incorporating uncertainty in both model form and prediction error and a 95% confidence band of the predicted residual stress field

Fig. 4.4 shows the mean of the composite prediction of the residual stress field, which is exactly the same as the mean in Fig 4.3. The standard deviation of composite prediction of a residual stress at each depth calculated by Eq. (4.2), which represents the degree of both types of uncertainty, is plotted on the scale of depth in Fig. 4.5 along with the standard deviation calculated by Eq. (3.3) in Section 4.2.2, which only represents the degree of model-form uncertainty. The degree of model-form uncertainty in the composite prediction is mainly subject to the differences between the predictions by the

JC-based FE model and those by the KHL-based FE model, as discussed in Section 4.2.3. The degree of model-form uncertainty in the composite prediction is larger than the average degree of predictive uncertainty associated with each model in the region between around 0.4 mm and around 1.0 mm in depth. On the other hand, the average degree of predictive uncertainty in each FE model prevails over the model-form uncertainty in the regions from the surface to around 0.4 mm and below around 1.0 mm in depth.

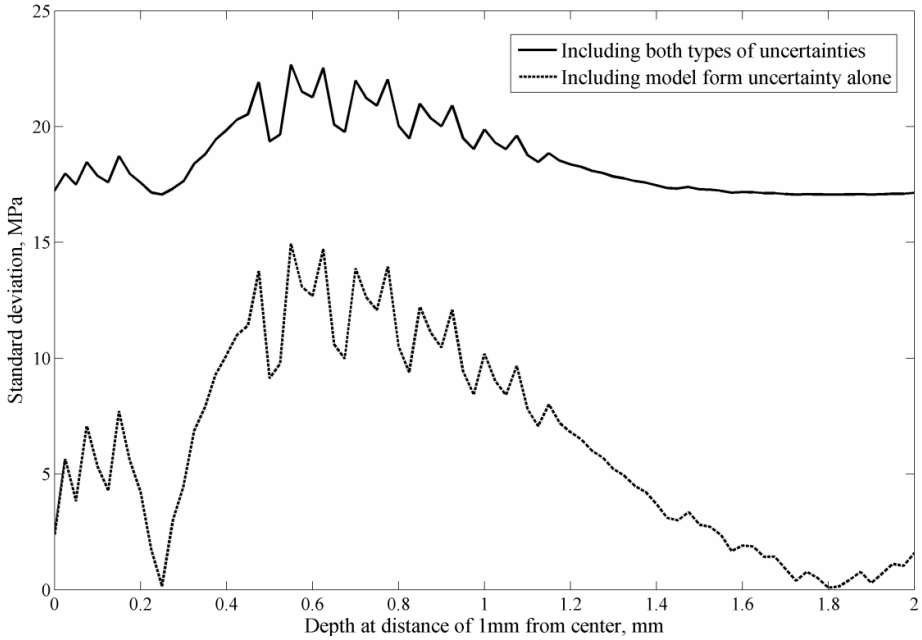

Figure 4.5 Comparison of standard deviations between the case involving model-form uncertainty alone and the case involving predictive uncertainty as well as model-form uncertainty

4.3.2 Establishment of a Confidence Band

Because composite prediction $g(y \mid D)$ of residual stress y at each depth is normal, the end points of a 95% confidence interval of predicted residual stress at each depth are calculated by

$$\left[E\left(y|\mathrm{D}\right) - 1.96\sqrt{\sum_{k=1}^{K}\Pr\left(M_k|\mathrm{D}\right)\sigma_k^{\,2} + \sum_{k=1}^{K}\Pr\left(M_k|\mathrm{D}\right)\left(f_k - E\left(y|\mathrm{D}\right)\right)^2}\,,\right.$$
$$\left. E\left(y|\mathrm{D}\right) + 1.96\sqrt{\sum_{k=1}^{K}\Pr\left(M_k|\mathrm{D}\right)\sigma_k^{\,2} + \sum_{k=1}^{K}\Pr\left(M_k|\mathrm{D}\right)\left(f_k - E\left(y|\mathrm{D}\right)\right)^2}\right] \tag{4.3}$$

Because the i.i.d. assumption is involved in deriving composite prediction $g(y|\mathrm{D})$, Eq. (4.3) would be effective in addressing the problems where the assumption is valid. An upper and a lower bound curve are drawn by connecting the upper and the lower end points at all the depths, respectively. Figure 4.4 shows a 95% confidence band bounded by the upper and lower curves which incorporates both model-form and predictive uncertainty. All the observed experimental data are shown to be within the established confidence band. This states that incorporating predictive uncertainty as well as model-form uncertainty into the composite prediction gives significantly more reliable predictions of residual stresses not yet observed.

4.3.3 Summary

Using the model averaging technique, both model-form and predictive uncertainty are incorporated into the composite prediction of a residual stress at each depth. The composite prediction is normal because the error involved in a residual stress prediction by each FE model is assumed to be normally distributed. The mean of the composite prediction is the average of the deterministic predictions by the considered FE models weighted by the calculated posterior model probabilities. Both the between-model and the within-model variances prove to be significant. By incorporating predictive uncertainty as well as model-form uncertainty into the composite predictions, all the measured residual stresses are found within the established 95% confidence band. To demonstrate

the applicability of the proposed methodology to probabilistic simulation models, parametric uncertainty is accounted for by each FE model in the next Section.

4.4 Case Incorporating Three Types of Uncertainty

4.4.1 Quantification of Model-Form Uncertainty in a Probabilistic FE Model Set

The peak value of a pressure pulse induced by a laser shot is considered to be a random input parameter. The parametric uncertainty in the peak pressure value is represented by a normal distribution with the mean of 5.5 GPa and the standard deviation of 0.275 GPa. To quantify uncertainty in prediction of the residual stress field by each model, 800 random samples are drawn from the normal distribution representing the uncertainty in the peak pressure value. Even if a comparatively small number of random data are sampled due to a high computational cost, a set of 800 sampled data (FE simulations) proves to be sufficient for representing the parametric uncertainty with acceptable accuracy after a convergence study.

The prediction of a residual stress at any depth by a FE model involves an unknown error as well as the parametric uncertainty arising from the randomness in the peak pressure pulse. The means of the predictions of the residual stress field by the three considered FE models are shown with the measured experimental data in Fig. 4.6. Given each of the 800 samples randomly drawn from the distribution for the peak pressure, the variance of unknown prediction error associated with each FE model is computed using the differences measured between the observed data and the predictions of the data made by

each model based on each random sample by Eq. (2.19). Using Eq. (2.24), the quantified unknown error is incorporated into the prediction of a residual stress made by each model. The likelihoods of the considered three FE models given the observed experimental data are computed using the number of the observed data and the calculated variances of unknown prediction errors as shown in Eq. (2.29). The calculated posterior probabilities of the three FE models are shown in Table 4.4 together with the prior model probabilities and model likelihoods. Small differences are observed between the posterior probabilities of the three FE models with parametric uncertainty in Table 4.4 and those of the three FE models without parametric uncertainty in Table 4.2.

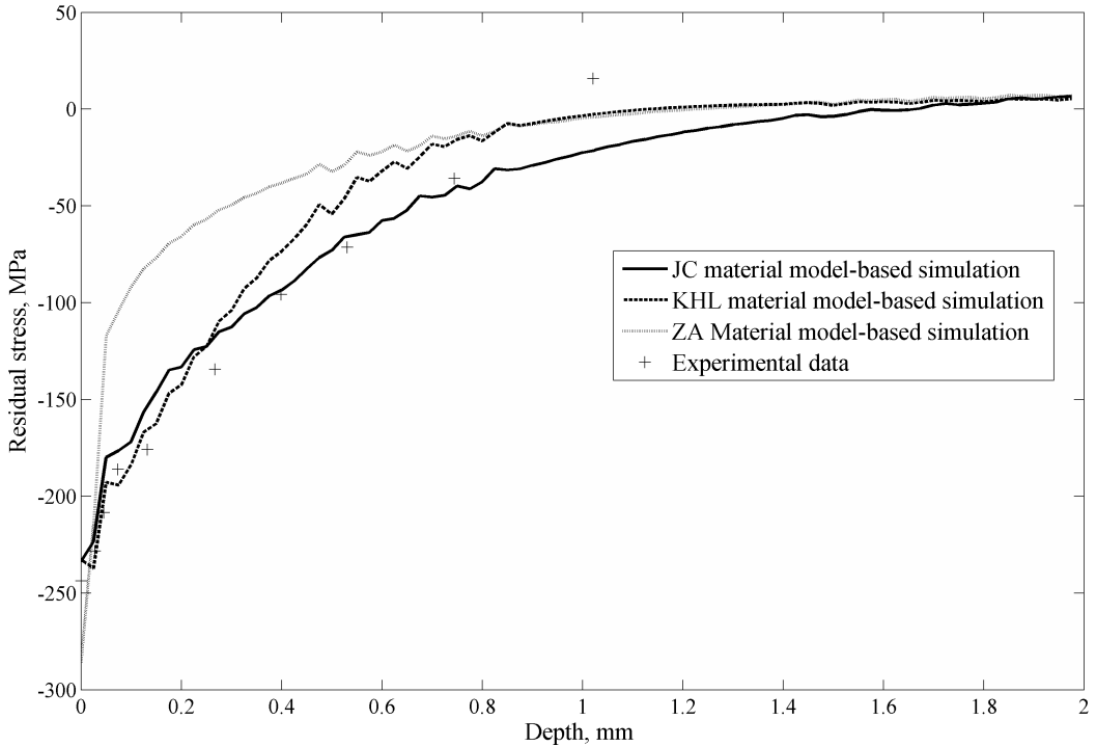

Figure 4.6 Residual stress comparisons between experimental data and means of the predictions by three FE models

Table 4.4 Prior probabilities, likelihoods, and posterior probabilities of three probabilistic FE models

Model	Prior Model Probability	Model likelihood	Posterior Model Probability
JC-based FE model	3.333×10^{-1}	4.305×10^{-19}	8.075×10^{-1}
KHL-based FE model	3.333×10^{-1}	1.026×10^{-19}	1.925×10^{-1}
ZA-based FE model	3.333×10^{-1}	8.450×10^{-25}	1.585×10^{-6}

4.4.2 Combination of Model Predictions Involving both Parametric and Predictive Uncertainty

Using model averaging, the predictions of a residual stress at any depth by the three FE models involving both parametric and predictive uncertainty are combined into a single composite prediction. The composite predictive distribution of a residual stress incorporates the uncertainties arising from the uncertainty associated with the use of the three different FE models, the randomness in the peak pressure value, and the randomness in the errors involved in the predictions of the residual stress by the considered FE models. The mean and variance of the composite prediction of a residual stress are calculated using Eqs. (3.23) and (3.24).

Figure 4.7 shows the composite predictive distribution of the residual stress on the surface at 1 mm distance from the center of the LP component and the predictive distribution of the stress estimated by each FE model. The mean and standard deviation of the composite prediction of the residual stress are shown in Table 4.5 along with the mean and standard deviation of prediction of the stress by each FE model.

Table 4.5 Mean and standard deviation of predictions by three FE models and the composite prediction of the residual stress on the surface at 1mm distance from center

Model	Mean, MPa	Standard deviation, MPa
JC-based FE model	-233.732	29.586
KHL-based FE model	-232.719	66.308
ZA-based FE model	-285.596	96.769
Composite	-233.537	39.413

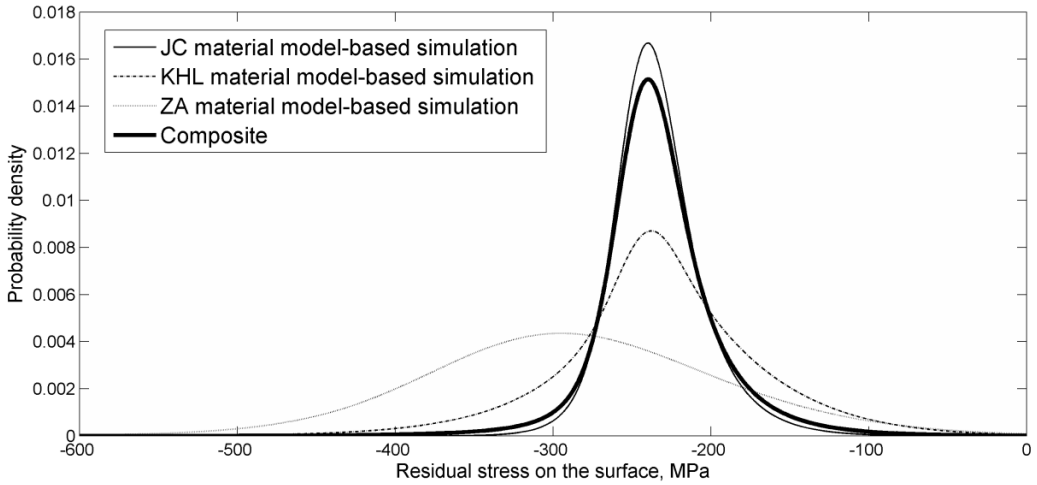

Figure 4.7 Composite predictive distribution of the residual stress on the surface along with predictive distributions estimated by three FE models

The mean of the composite prediction (-233.54 MPa) is little different from the mean of the JC-based FE model prediction (-233.73 MPa) because the effect of the JC-based FE model prediction on the mean of the composite prediction is significant due to the comparatively large value of the probability of the JC-based FE model. The standard deviation of the composite prediction (39.41 MPa) is larger than the standard deviation of the JC-based FE model prediction (29.59 MPa) mainly due to the considerably large standard deviation of the KHL-based FE model prediction (66.31 MPa). The standard deviation of the composite prediction indicates the total degree of uncertainty in the

prediction of the residual stress due to model-form, parametric, and predictive uncertainty. Figure 4.8 shows the mean of the composite prediction of the residual stress field that indicates the expected value of the true residual stress at every depth.

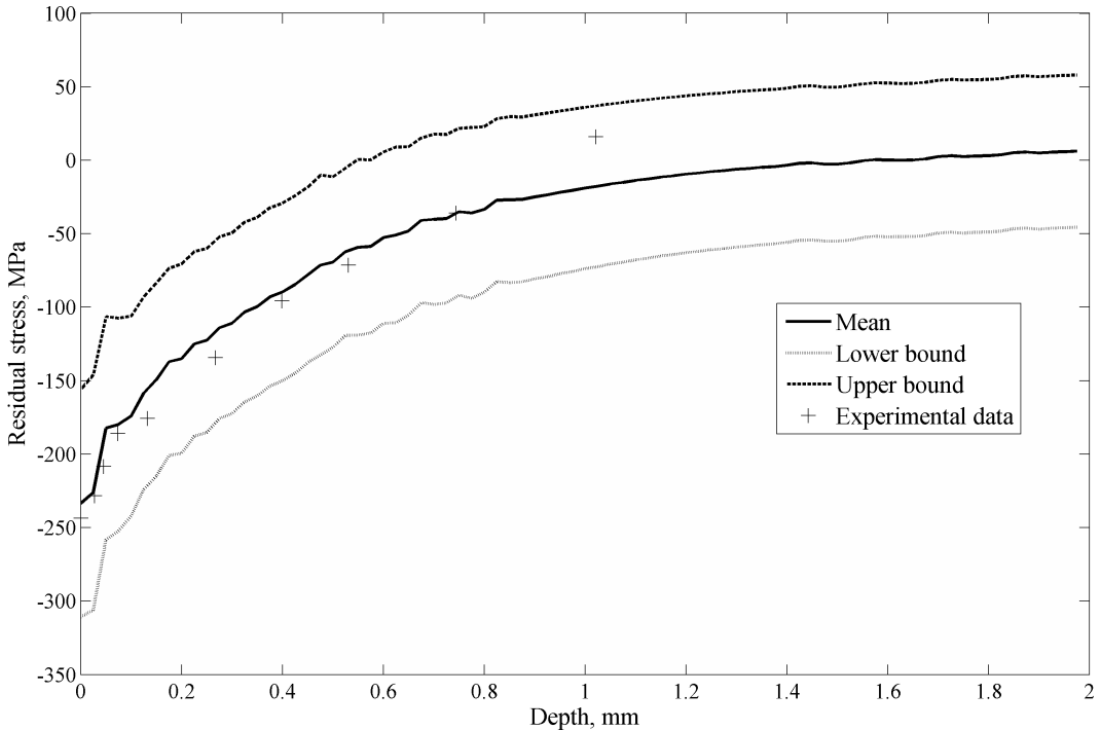

Figure 4.8 Mean of composite prediction and 95% confidence band of residual stress field

4.4.3 Establishment of a Confidence Band

In addition to the expected value of the true residual stress at every depth represented by the mean of the composite prediction, an interval estimate of the true stress is made to indicate the reliability of the composite prediction. A 95% confidence interval for a residual stress at every depth is established by choosing an interval where the probability of being below the interval is the same as the probability of being above it [29]. By connecting the upper and lower end points at all the depths, an upper and a lower bound curve are drawn in Fig. 4.8, respectively. The width of the 95% confidence band may be

thought of as the measure of the degree of uncertainty in the composite prediction of the residual stress field due to the three types of uncertainty. As shown in Fig. 4.8, all the observed experimental data are included within the established confidence band. Therefore, residual stresses not yet observed are expected with a high degree of reliability to fall within the established confidence band.

4.4.4 Summary

The proposed methodology to evaluate model likelihood using the measured differences between observed experimental data and model predictions of the data involving both parametric and predictive uncertainty is demonstrated with the probabilistic FE simulation of the axisymmetric laser peened component. Using the model averaging technique, the predictions by the three probabilistic FE models that involve both parametric and predictive uncertainty are integrated into the composite prediction of the residual stress field. Because the composite prediction accounts for multiple types of uncertainty (model-form, parametric, and predictive uncertainty), it is believed to be highly reliable.

4.5 Summary

To demonstrate the proposed methodology in an organized way, three different cases are addressed in Section 4. The composite prediction that only accounts for model-form uncertainty is shown to have too small variance to capture all the observed residual stresses. A more reliable prediction of the residual stress field is made by incorporating predictive uncertainty as well as model-form uncertainty; all the measured residual

stresses are held within the computed 95% confidence band. By accounting for the randomness in the peak value of a pressure pulse, it proves that the proposed methodology can also address the problem of quantifying model-form, parametric and predictive uncertainty associated with large-scale engineering simulation.

5. Quantification of Model-Form Uncertainty Using Expert Evidence

The methodology proposed in Chapter 2—which quantifies model-form uncertainty using Bayesian probability theory—involves the constraint that probability should be assigned to each member of a model set. Because of the constraint put on assigning model probability, probability theory is not suitable for representing model-form uncertainty depending on human knowledge systems; probability theory cannot effectively deal with epistemic uncertainty deriving from impreciseness inherently present in subjective knowledge as stated in Section 1.3.2. A methodology is developed to quantify model-form and parametric uncertainty using expert evidence under evidence theory which deals with imprecise human knowledge more realistically than probability theory.

Model-form uncertainty is quantified on a model set using expert evidence, and distinct pieces of evidence are aggregated using the Dempster's rule of combination in Section 5.2. Predictions by a model set are combined using the disjunctive rule of combination in Section 5.3. Then, the process for implementing the proposed methodology is numerically demonstrated with three mathematical models for a nonlinear spring mass system in Section 5.4. Finally, the problem of simulating a laser peening process depending on different material model theories is solved to examine the applicability of the proposed approach to large-scale engineering problems in Section 5.5.

5.1 Introduction

The methodology presented in Chapter 2 requires the assignment of prior probability to each model using available information such as accumulated data and human expertise before observing experimental data. Zio and Apostolakis [33] investigated the formal process of eliciting and interpreting expert judgments to quantify prior model probability. It is believed that the well-organized framework developed by Zio and Apostolakis is very effective in evaluating prior model probability depending on the elicitation of expert judgments. However, we can hardly establish a mathematically explicit relation between available expert evidence and prior model probability because the quantification of prior model probability using a corpus of expert knowledge is subjective in nature. To avoid the difficulty of numerically specifying expert judgments, prior probability is usually given a uniform value over a given model set.

However, assigning a uniform probability value to each model means discarding all the meaningful information available prior to observing experimental data. Also, a uniform distribution of probability values over a model set cannot strictly express the state of total ignorance about the model set [111]. Because the state of total ignorance about a model set implies that there should be no preference in assigning probability to each possible subset of model(s), each sub-model-set should receive the same probability value. In probability theory, the same probability value cannot be given to each sub-model-set because a probability measure must follow the additivity axiom ($\Pr(\boldsymbol{M}_i \cup \boldsymbol{M}_j) = \Pr(\boldsymbol{M}_i) + \Pr(\boldsymbol{M}_j)$, $\boldsymbol{M}_i$ and $\boldsymbol{M}_j$: two disjoint sub-model-sets). For that reason, it is impossible that

$\Pr(\boldsymbol{M}_i) = \Pr(\boldsymbol{M}_j) = \Pr(\boldsymbol{M}_i \cup \boldsymbol{M}_j)$ for two sub-model-sets $\boldsymbol{M}_i$ and $\boldsymbol{M}_j$ with $\Pr(\boldsymbol{M}_i) \neq 0$ or $\Pr(\boldsymbol{M}_j) \neq 0$.

Evidence theory, which was initiated by Dempster [65] and further developed by Shafer [66], is a promising theory for effectively modeling imprecise human knowledge. In Evidence theory, degrees of belief (subjective probabilities) can be assigned to possibly overlapping subsets of propositions, as well as individual propositions because this theory is not subject to the additivity axiom. Evidence theory can effectively handle epistemic uncertainty which is due to limited data and knowledge. Distinct pieces of evidence can be easily combined unless a significant conflict arises between different sources of evidence.

Evidence theory has been successfully used to quantify parametric uncertainty involved in mathematical problems and large-scale engineering applications [67, 112, and 113]. Parametric uncertainty associated with a model is expressed depending on expert judgments, and then is propagated through the model to obtain the corresponding representation of the uncertainty in model predictions.

This Chapter presents a methodology developed to quantify model-form and parametric uncertainty using the mathematical structures of evidence theory. Model-form uncertainty associated with considering different models is numerically specified depending on expert knowledge systems. Then, using the disjunctive rule of combination, it is

attempted to combine the predictions of considered models which involve parametric uncertainty.

5.2 Representation of Model-Form Uncertainty by Belief Function

The quantification of model-form uncertainty within Bayesian probability theory involves a restriction that each member of a model set must be assigned a probability value. Because of the strict restriction on a model set, probability theory is not appropriate for representing model-form uncertainty using an expert knowledge system. The fundamental concepts of evidence theory are described in Section 5.2.1, and the quantification of model-form uncertainty within evidence theory is discussed in this Section 5.2.2.

5.2.1 Evidence Theory

① Belief Functions

In evidence theory, evidence is fundamentally represented by assigning basic belief masses to available propositions; the basic belief mass assigned to a proposition expresses the proportion of total belief supporting the proposition. Assignment of basic belief mass can be made in a universal set U of finite and mutually exclusive elementary propositions (also known as the frame of discernment). Basic Belief Assignment (BBA) is defined as the function that maps the elements of the power set 2^U of U to values in [0, 1]: m: $2^U \rightarrow$ [0, 1]. The power set 2^U consists of all possible subsets of U including an empty set Ø. A BBA must satisfy the requirement that $\sum m(A) = 1$ for all $A \in 2^U$, and

generally $m(\emptyset) = 0$. It should be noted that $m(A)$ for a subset A can never be distributed within A unless a new body of evidence is available. It means that a portion $m(A)$ of total belief only supports the proposition that the true state is in A and does not make a claim regarding any specific subset of A.

From a BBA, Belief and Plausibility functions (*Bel* and *Pl*) are defined to represent the lower and upper probability bounds of the relevant considered propositions. *Bel* and *Pl* are expressed by Eqs. (5.1) and (5.2), and they are related to each other by Eq. (5.3): [66]

$$Bel(A) = \sum_{B \subseteq A} m(B) \tag{5.1}$$

$$Pl(A) = \sum_{B \cap A \neq \emptyset} m(B) \tag{5.2}$$

$$Pl(A) = 1 - Bel(A^C) \tag{5.3}$$

The belief of a proposition is the sum of the belief masses assigned to all the propositions that completely support the first proposition. On the other hand, the plausibility of a proposition is the sum of the belief masses assigned to all the propositions that support that proposition completely or partially. It is believed that *Bel* and *Pl* are introduced due to the fact that the belief mass assigned to a set cannot be forcefully partitioned into subsets of it. The impreciseness in the human knowledge system is adequately expressed by defining the upper and the lower probability bounds on relevant propositions.

② Dempster's Rule of Combination

When two or more bodies of evidence from different sources, assumed to be independent, are available, the BBAs derived from the bodies of evidence can be combined using the

Dempster's rule of combination. This combination rule can be applied when multiple independent sources are all reliable. When BBAs m_1 and m_2 are generated from two independent evidential sources, the combination is calculated by [66, 114]

$$m_{1\cap 2}(A) = \frac{\sum_{B\cap C=A\neq\varnothing} m_1(B)m_2(C)}{1-K},\ K = \sum_{B\cap C=\varnothing} m_1(B)m_2(C) \tag{5.4}$$

where the denominator (the normalization factor) results in disregarding all the conflicting evidence existing between different sources. This rule considers only the evidential claims consistent between different sources. This fact results in a counterintuitive outcome when bodies of evidence from different sources show significant inconsistency or contradiction. A variety of combination rules have been suggested to address this problem [114]. In this research, it is implicitly supposed that little inconsistency is encountered between different evidential sources.

5.2.2 Quantification of Model-form Uncertainty under Evidence Theory

Consider that a BBA is induced on a finite model set $\mathcal{M} = \{M_1, M_2, \ldots, M_K\}$ from a body of evidence. $m(\boldsymbol{M})$ assigned to a sub-model-set $\boldsymbol{M} \subseteq \mathcal{M}$ expresses the proportion of total belief that supports the evidential claim that the correct model (or the best approximating model) is in the sub-model-set $\boldsymbol{M}$. By definition, it is possible that $m(\boldsymbol{M}_1) > m(\boldsymbol{M}_2)$ even for $\boldsymbol{M}_1 \subset \boldsymbol{M}_2$. The state of total ignorance, which is equivalent to the non-existence or unavailability of required evidence, can be perfectly expressed by assigning total belief to the universal set itself: $m(\mathcal{M}) = 1$, and $m(\boldsymbol{M}) = 0$ for any $\boldsymbol{M} \subsetneq \mathcal{M}$. $Bel(\boldsymbol{M})$ and $Pl(\boldsymbol{M})$ measure the minimum and the maximum degree of belief assigned to the proposition that the correct model is in a sub-model-set M. Three belief functions $m(\boldsymbol{M})$, $Bel(\boldsymbol{M})$ and

$Pl(\boldsymbol{M})$ convey the same information in different forms because $Bel(\boldsymbol{M})$ and $Pl(\boldsymbol{M})$ are directly derived from $m(\boldsymbol{M})$ as shown in Eqs. (5.1) and (5.2).

Suppose that two independent experts (or groups of experts) derive BBAs m_1 and m_2 on a model set $\mathcal{M}$ from their expertise and available evidence. Given that two different experts are assumed to be independent and equally reliable, m_1 and m_2 can be combined into a new BBA $m_{1\cap2}$ using Eq. (5.4). $m_{1\cap2}(\boldsymbol{M})$ for a sub-model-set $\boldsymbol{M} \subseteq \mathcal{M}$ expresses a normalized portion of total belief for the proposition that the correct model is in $\boldsymbol{M}$ supported by both the experts. If $m_2(\mathcal{M}) = 1$, $m_{1\cap2}$ is equal to m_1.

5.3 Combination of Response Predictions from Multiple Models

As discussed in Chapter 3, given two or more different models assigned their own probabilities, the predictions by the individual models are generally averaged using the probability values as weights. The model combination techniques are not suited for the problems of quantifying model-form uncertainty by assigning degrees of belief to subsets of a model set. The disjunctive rule of combination is successfully utilized to perform the process of combining the response predictions by given models which involve parametric uncertainty. The disjunctive rule of combination is described in Section 5.3.1, and this rule is applied to combine model predictions in Section 5.3.2.

5.3.1 The Disjunctive Rule of Combination

The disjunctive rule of combination [111, 115] aims to combine the BBAs from two independent evidence sources of which at least one is fully reliable. Consider that BBAs

m_1 and m_2 stem from two different evidence sources. The knowledge that one can only accept is that at least one of the two sources is reliable without knowing which one is reliable. Therefore, all that can be concluded is that the true state is in the disjunctive propositions supported by either m_1 or m_2. Mathematically, the disjunctive rule of combination is expressed by [111, 115]

$$m_{1\cup 2}(A) = \sum_{B\cup C=A} m_1(B)\, m_2(C) \tag{5.5}$$

The disjunctive rule of combination addresses the disjunctive case whereas the Dempster's rule of combination, which assumes that the BBAs to be combined are all derived from reliable evidence sources, fits the conjunctive case. Both rules of combination are based on the assumption that evidence sources to be combined are independent of each other. While the Dempster's rule of combination takes into consideration only conjunctive propositions asserted by both evidence sources, the disjunctive rule of combination does not reject any proposition supported by either evidence source. For that reason, all the propositions with nonzero belief masses are explicitly represented, and a normalization factor such as 1 - K in Eq. (5.4) is unnecessary in the disjunctive rule of combination.

Let Θ and $\mathcal{Y}$ denote two frames of discernment. Suppose that a BBA $m(y \mid \theta_i)$ can be established on $\mathcal{Y}$ given that an element θ_i in Θ is known to be true; $m(y \mid \theta_i)$ is called the conditional BBA of y given θ_i. The set of every possible BBA $m(y \mid \theta_i)$ on $\mathcal{Y}$ given $\theta_i \in \Theta$ represents all that one knows about $\mathcal{Y}$ at the present stage. The disjunctive rule of

combination makes it possible to construct a disjunctively combined BBA from two BBAs $m(y|\theta_i)$ and $m(y|\theta_j)$ when it is only known that the disjunction of θ_i and θ_j is true. Using Eq. (5.5), the calculation of the disjunctively combined BBA denoted by $m(y|\boldsymbol{\theta})$, $\{\theta_i, \theta_j\} \in \boldsymbol{\theta}$, is expressed by

$$m\left(y|\boldsymbol{\theta}\right) = \sum_{y_i \cup y_j = y} m\left(y_i|\theta_i\right) m\left(y_j|\theta_j\right) \tag{5.6}$$

Eq. (5.6) can be easily extended to any subset $\boldsymbol{\theta} \subseteq \Theta$ by applying it successively. The BBA, *Bel*, and *Pl* corresponding to the general case are succinctly represented by [111]

$$m\left(y|\boldsymbol{\theta}\right) = \sum_{\left(\cup_{i:\theta_i \in \boldsymbol{\theta}} y_i\right) = y} \prod_{i:\theta_i \in \boldsymbol{\theta}} m\left(y_i|\theta_i\right) \tag{5.7}$$

$$Bel\left(y|\boldsymbol{\theta}\right) = \prod_{\theta_i \in \boldsymbol{\theta}} Bel\left(y|\theta_i\right) \tag{5.8}$$

$$Pl\left(y|\boldsymbol{\theta}\right) = 1 - \prod_{\theta_i \in \boldsymbol{\theta}} \left(1 - Pl\left(y|\theta_i\right)\right) \tag{5.9}$$

The equations shown above provide the solution when no belief is assumed on Θ. Eqs. (5.7) – (5.9) can be extended to the case where there exists a BBA $m(\boldsymbol{\theta})$ on Θ. $m(y|\boldsymbol{\theta})$, $Bel(y|\boldsymbol{\theta})$, or $Pl(y|\boldsymbol{\theta})$ is combined with $m(\boldsymbol{\theta})$ to be [111, 116]

$$m\left(y\right) = \sum_{\boldsymbol{\theta} \subseteq \Theta} m\left(y|\boldsymbol{\theta}\right) m\left(\boldsymbol{\theta}\right) \tag{5.10}$$

$$Bel\left(y\right) = \sum_{\boldsymbol{\theta} \subseteq \Theta} Bel\left(y|\boldsymbol{\theta}\right) m\left(\boldsymbol{\theta}\right) \tag{5.11}$$

$$Pl\left(y\right) = \sum_{\boldsymbol{\theta} \subseteq \Theta} Pl\left(y|\boldsymbol{\theta}\right) m\left(\boldsymbol{\theta}\right) \tag{5.12}$$

$m(y)$, $Bel(y)$, or $Pl(y)$ is the unconditional belief function on $\mathcal{Y}$. Two distinct belief functions, $m(\theta)$, and $m(y \mid \theta)$, $Bel(y \mid \theta)$, or $Pl(y \mid \theta)$, are conjunctively combined because both are considered to be reliable.

5.3.2 Combination of Model Predictions Involving Parametric Uncertainty

Using the disjunctive rule of combination, a composite belief function on the prediction of an unknown response is now derived from the belief functions on the prediction that the individual members of a model set support. Let $\mathcal{X}$, $\mathcal{Y}$, and $\mathcal{M}$ be a frame of discernment of input parameters, a frame of discernment of response predictions, and a frame of discernment of considered models, respectively. Usually, input parameters of an engineering model are considered to involve parametric uncertainty. When uncertainty in a set of input parameters X within each model $\mathrm{M}_k \in \mathcal{M}$ is represented by a BBA $m(\mathrm{X} \mid \mathrm{M}_k)$ on $\mathcal{X}$, the corresponding uncertainty in the prediction of a response y is also represented by a BBA $m(y \mid \mathrm{M}_k)$ on $\mathcal{Y}$. The detailed descriptions of representing parametric uncertainty by a BBA, and propagating it into response prediction through a model are found in the literature [67, 113].

Given a set of belief functions on $\mathcal{Y}$ given $\mathrm{M}_k \in \mathcal{M}$, $k = 1, \ldots, \mathrm{K}$, ($\{m(y \mid \mathrm{M}_k)\}$, $\{Bel(y \mid \mathrm{M}_k)\}$, or $\{Pl(y \mid \mathrm{M}_k)\}$), the belief function $m(y \mid \boldsymbol{M})$, $Bel(y \mid \boldsymbol{M})$ or $Pl(y \mid \boldsymbol{M})$ associated with a sub-model-set $\boldsymbol{M} \subseteq \mathcal{M}$ can be obtained using Eqs. (5.7) – (5.9). With respect to $m(y \mid \boldsymbol{M})$, $Bel(y \mid \boldsymbol{M})$, or $Pl(y \mid \boldsymbol{M})$, it is supposed that a *priori* belief on the sub-model-set $\boldsymbol{M}$ is vacuous. Given a BBA $m(\boldsymbol{M})$ induced on $\mathcal{M}$ from available expert

evidence, an unconditional belief function $m(y)$, $Bel(y)$, or $Pl(y)$ can be calculated using Eqs. (5.10) – (5.12). $m(y)$, $Bel(y)$, or $Pl(y)$, which incorporates the expert evidence quantified on $\mathcal{M}$, reflects the relative effect of each sub-model-set $\boldsymbol{M} \subseteq \mathcal{M}$ on the prediction of unknown response y. To demonstrate the presented approach, a numerical problem and a large-scale engineering problem which involves both model-form and parametric uncertainty are addressed in the following two Sections.

5.4 A Nonlinear Spring-Mass System to Demonstrate the Proposed Approach

5.4.1 Predictions of the Natural Frequency by Three Mathematical Models

A single-degree-of-freedom spring-mass system with a nonlinear spring considered in Section 3.2.3 and Section 3.3.2—which is represented by $\mu\ddot{u} + h(u) = 0$—is also utilized to demonstrate the methodology presented in this Chapter. The mass and the initial velocity of the system are given as $\mu = 1$ kg, and $du/dt(0) = 0$ cm/s. The initial displacement $u(0)$ is regarded as a random input parameter. The parametric uncertainty in $u(0)$ is represented by a BBA $m(u_0)$ which is assumed to be defined by an expert (or a group of experts) (Fig. 5.1). The parametric uncertainty in $u(0)$ is propagated into the prediction of the natural frequency by each of the three models. The uncertainty in the prediction of the natural frequency is expressed by a BBA $m(\omega \,|\, \mathrm{M}_k)$ on the frame of discernment Ω of finite frequency intervals on the assumption that each model $\mathrm{M}_k \in \mathcal{M} = \{\mathrm{M}_1, \mathrm{M}_2, \mathrm{M}_3\}$ is known to be correct. Frequency prediction by each model monotonically varies depending on the initial displacement value $u(0)$. Therefore, the prediction intervals of the frequency given model M_k can be obtained by putting the end point

values of $u(0)$ (0.7 cm, 0.9 cm, 1.1 cm, and 1.2 cm) into each model M_k. Figure 5.1 shows the calculated endpoint values of prediction intervals from each model M_k along with the belief masses directly transferred from the masses given to the intervals for $u(0)$.

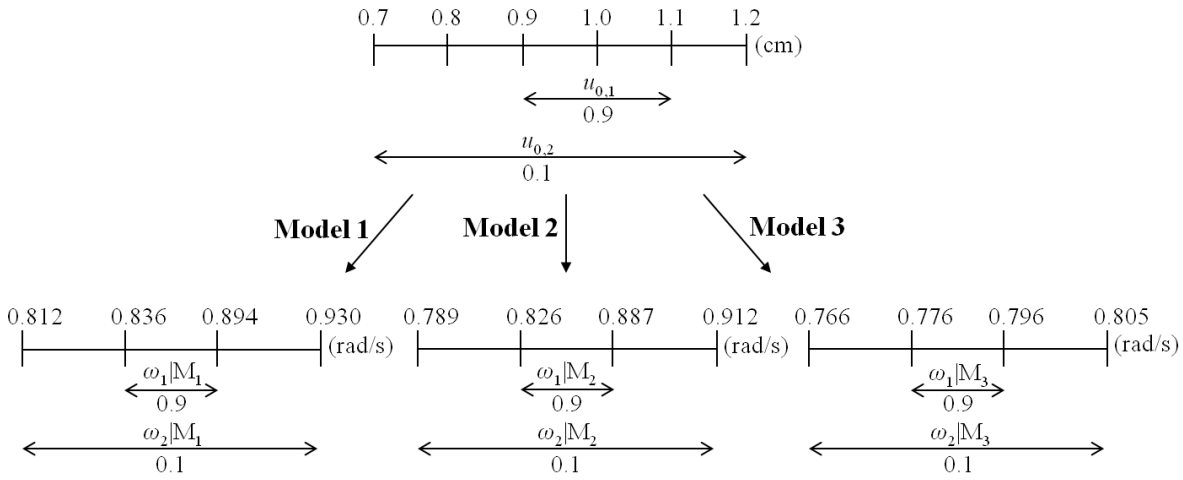

Figure 5.1 Parametric uncertainty in the initial displacement of a spring mass system and its propagation into predicted frequency through three mathematical models

5.4.2 Quantification of Model-Form Uncertainty in Prediction of the Natural Frequency

Three different cases (1. disregarding model-form uncertainty, 2. addressing the state of total ignorance, and 3. representing expert judgments) for which different BBAs (Table 5.1) are constructed on the set of the three models are addressed to demonstrate the presented methodology in a systematic manner.

Table 5.1 Basic belief masses on a set of three models for three cases (case 1: disregarding model form uncertainty, case 2: addressing the state of total ignorance, and case 3: representing expert judgments)

Subsets of a model set	Basic belief masses		
	case 1	case 2	case 3
$\{M_1\}$	1.0	–	0.3
$\{M_1, M_2\}$	–	–	0.6
$\{M_1, M_2, M_3\}$	–	1.0	0.1
$\sum$	1.0	1.0	1.0

① The Case of Disregarding Model-Form Uncertainty

It is assumed that model M_1 is known to be correct. Because the total belief of an analyzer is assigned to model M_1 as expressed by $m(M_1) = 1$, model-form uncertainty is not associated with the prediction of the natural frequency. The BBA $m(\omega)$ is equivalent to $m(\omega \mid M_1)$ since model M_1 is supposed to be correct. $m(\omega)$ in Table 5.1 represents the parametric uncertainty associated with the natural frequency prediction by M_1. The frequency prediction is expressed by the two intervals that the two intervals for $u(0)$ map to.

② The Case of Addressing The State of Total Ignorance

It is supposed that there exists no knowledge about the plausibility of the considered models. The total belief is assigned to the universal set of the three models as represented by $m(\mathcal{M}) = 1$. A BBA $m(\omega)$ is derived on Ω using the disjunctive rule of combination. Because the total belief is given to the considered model set, $m(\omega)$ is equal to $m(\omega \mid \mathcal{M})$. All the possible disjunctions of the prediction intervals from models M_1, M_2 and M_3 (Fig. 5.1) are $\{\omega_1 \mid M_1\} \cup \{\omega_1 \mid M_2\} \cup \{\omega_1 \mid M_3\}$, $\{\omega_1 \mid M_1\} \cup \{\omega_1 \mid M_2\} \cup \{\omega_2 \mid M_3\}$, $\{\omega_1 \mid M_1\} \cup \{\omega_2 \mid M_2\} \cup \{\omega_1 \mid M_3\}$, $\{\omega_1 \mid M_1\} \cup \{\omega_2 \mid M_2\} \cup \{\omega_2 \mid M_3\}$,

$\{\omega_2 | M_1\} \cup \{\omega_1 | M_2\} \cup \{\omega_1 | M_3\}$, $\{\omega_2 | M_1\} \cup \{\omega_1 | M_2\} \cup \{\omega_2 | M_3\}$, $\{\omega_2 | M_1\} \cup \{\omega_2 | M_2\} \cup \{\omega_1 | M_3\}$, and $\{\omega_2 | M_1\} \cup \{\omega_2 | M_2\} \cup \{\omega_2 | M_3\}$. The belief masses $m(\omega)$ assigned to those eight disjunctive intervals are calculated using Eq. (5.7) (Table 5.2).

Table 5.2 Basic belief masses of predicted frequency for three cases (case 1: disregarding model form uncertainty, case 2: addressing the state of total ignorance, and case 3: representing expert judgments)

Case 1: $m(\{M_1\})=1$		Case 2: $m(\{M_1, M_2, M_3\})=1$		Case 3: $m(\{M_1\})=0.3$, $m(\{M_1, M_2\})=0.6$, $m(\{M_1, M_2, M_3\})=0.1$	
ω (rad/s)	$m(\omega)$	ω (rad/s)	$m(\omega)$	ω (rad/s)	$m(\omega)$
[0.836, 0.894]	0.9	[0.776, 0.796]∪[0.826, 0.894]	0.729	[0.836, 0.894]	0.2700
[0.812, 0.930]	0.1	[0.766, 0.805]∪[0.826, 0.894]	0.081	[0.812, 0.930]	0.0300
∑	1.0	[0.776, 0.910]	0.081	[0.826, 0.894]	0.4860
		[0.766, 0.910]	0.009	[0.789, 0.910]	0.0540
		[0.776, 0.796]∪[0.812, 0.930]	0.081	[0.812, 0.930]	0.0540
		[0.766, 0.805]∪[0.812, 0.930]	0.009	[0.789, 0.930]	0.0060
		[0.776, 0.930]	0.009	[0.776, 0.796]∪[0.826, 0.894]	0.0729
		[0.766, 0.930]	0.001	[0.766, 0.805]∪[0.826, 0.894]	0.0081
		∑	1.0	[0.776, 0.910]	0.0081
				[0.766, 0.910]	0.0009
				[0.776, 0.796]∪[0.812, 0.930]	0.0081
				[0.766, 0.805]∪[0.812, 0.930]	0.0009
				[0.776, 0.930]	0.0009
				[0.766, 0.930]	0.0001
				∑	1.0

③ *The Case of Representing Expert Judgments*

A BBA is assumed to be derived from available expert evidence, and is represented by $m(\{M_1\}) = 0.3$, $m(\{M_1, M_2\}) = 0.6$, and $m(\{M_1, M_2, M_3\}) = 0.1$. Following the same procedure for attaining $m(\omega | \mathcal{M})$, $m(\omega | \{M_1, M_2\})$ is calculated with $m(\omega | M_1)$ and $m(\omega | M_2)$ to be $m([0.826 \text{ rad/s}, 0.894 \text{ rad/s}]) = 0.9 \times 0.9 = 0.81$, $m([0.789 \text{ rad/s}, 0.910 \text{ rad/s}]) = 0.9 \times 0.1 = 0.09$, $m([0.812 \text{ rad/s}, 0.930 \text{ rad/s}]) = 0.1 \times 0.9 = 0.09$, and

$m([0.789 \text{ rad/s}, 0.930 \text{ rad/s}]) = 0.1 \times 0.1 = 0.01$. Using Eq. (5.10), $m(\omega)$ in Table 5.2 is obtained by summing up the previously calculated $m(\omega \mid \{M_1\})$, $m(\omega \mid \{M_1, M_2\})$, and $m(\omega \mid \{M_1, M_2, M_3\})$ multiplied by $m(\{M_1\}) = 0.3$, $m(\{M_1, M_2\}) = 0.6$, and $m(\{M_1, M_2, M_3\}) = 0.1$. $m(\omega \mid \boldsymbol{M})$ induced on the assumption that the correct model is in a sub-model-set $\boldsymbol{M}$ is reduced proportionally with the value of $m(\boldsymbol{M})$. As shown in Table 5.2, more prediction intervals than the case of addressing the state of total ignorance are established because of taking account of two sub-model-sets $\{M_1\}$, $\{M_1, M_2\}$ in addition to $\{M_1, M_2, M_3\}$. The case of representing expert judgments accounts for uncertainty associated with both identifying the sub-model-set including the correct model among three sub-model-sets $\{M_1\}$, $\{M_1, M_2\}$ and $\{M_1, M_2, M_3\}$, and selecting the correct one within each of $\{M_1\}$, $\{M_1, M_2\}$, and $\{M_1, M_2, M_3\}$.

5.4.3 CBFs and CPFs to Illustrate Composite Response Predictions

Cumulative Belief Functions (CBFs) and Cumulative Plausibility Functions (CPFs) are built to summarize the information contained in the BBAs in Table 5.2. A CBF and the corresponding CPF are defined by [67, 113]

$$\mathrm{CBF}(\nu) = \mathrm{Bel}(y \le \nu), \ \ \nu \in (-\infty, +\infty) \tag{5.20}$$

$$\mathrm{CPF}(\nu) = \mathrm{Pl}(y \le \nu), \ \ \nu \in (-\infty, +\infty) \tag{5.21}$$

For this problem, y is the predicted frequency ω. The CBFs and the CPFs are easily computed for the three cases depending on the definitions of *Bel* and *Pl* represented by Eqs. (5.1) and (5.2). The CBFs and the CPFs can also be directly obtained using Eqs. (5.8), (5.9), (5.11), and (5.12) although the calculation procedures are not presented.

Figure 5.2 graphically represents the degree of belief and the degree of plausibility in the claim that the true natural frequency is in $(-\infty, v]$ with the varying value v.

The values of a CBF and the corresponding CPF for a given value v on the abscissa make a pair of the smallest and the largest probabilities for the set $\{\omega \leq v\}$. The difference between the CBF and CPF values for a value $v \in (-\infty, +\infty)$ indicates the degree of impreciseness in the frequency prediction which occurs due to representing the prediction with overlapping intervals. In the case of disregarding model-form uncertainty, the CBF and the CPF are separated within relatively narrow interval [0.812 rad/s, 0.930 rad/s] compared to the other cases. The vertical space between the CBF and the CPF in the case of addressing the state of total ignorance is considerably big in the interval [0.776 rad/s, 0.894 rad/s] owing to the wide prediction intervals to which relatively high degrees of belief are assigned. The degree of impreciseness in the case of representing expert judgments is smaller than it is in the case of addressing the state of total ignorance because the total belief is divided among three sub-model-sets $\{M_1\}$, $\{M_1, M_2\}$ and $\{M_1, M_2, M_3\}$.

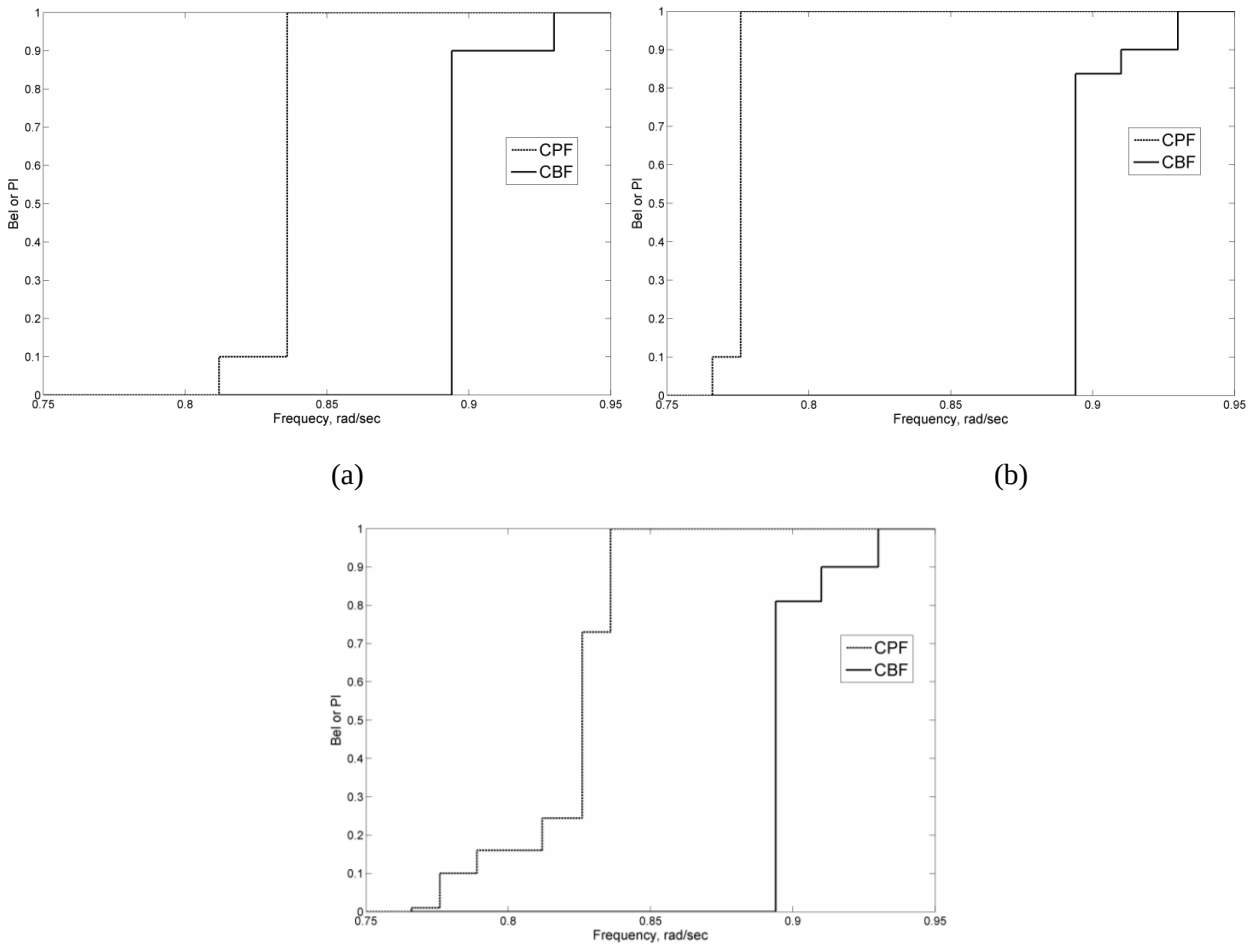

Figure 5.2 CBFs and CPFs of frequency prediction for three cases; (a) considering only Model 1, (b) addressing the state of total ignorance, and (c) representing expert judgments

5.5 Finite Element Simulation for a Laser Peening Process

The problem of simulating a laser peening process addressed in Chapter 4 is also utilized to illustrate the applicability of the proposed methodology to large-scale engineering problem.

5.5.1 Predictions of a Residual Stress Field by Three FE Models

The peak value of a pressure pulse induced by a laser shot which is set at 5.5 GPa is regarded as a random input parameter due to its natural variability of the equipment, and measurement techniques. Suppose that two experts independently provide BBAs to represent the uncertainty in the peak pressure value. The two sets of belief masses assigned to three intervals [5.2 GPa, 5.8 GPa], [4.9 GPa, 6.1 GPa], and [4.6 GPa, 6.4 GPa] are combined using the Dempster's rule of combination (Table 5.3). Interval [5.2 GPa, 5.8 GPa] has a larger belief mass value than it has before the two BBAs are combined because the other two intervals enclose it.

Table 5.3 Basic belief masses of peak pressure value given by two experts and their conjunctive combination

Peak pressure, GPa	Basic belief masses		
	Expert 1	Expert 2	Combined
[5.2, 5.8]	0.6	0.3	0.72
[4.9, 6.1]	0.3	0.5	0.26
[4.6, 6.4]	0.1	0.2	0.02
∑	1.0	1.0	1.00

The parametric uncertainty in the peak pressure is propagated into prediction of the residual stress field by each FE model. The residual stress field is simulated using as inputs only the endpoint values of the three intervals for the peak pressure because simulated outcomes monotonically vary depending on the peak pressure value. The belief masses assigned to the three intervals for the peak pressure are directly transmitted to three prediction intervals of a residual stress at each depth obtained from each FE model. The prediction intervals of the compressive residual stress on the surface from each of the three FE models are shown in Table 5.4 together with the transmitted belief masses. The

belief mass for a prediction interval from a FE model indicates the strength of belief that the true residual stress is in the interval supported by the FE model.

Table 5.4 The prediction intervals of compressive residual stress on the surface supported by the four subsets of three FE models, and the basic belief masses assigned to the intervals

Subsets of the FE models	$m(\boldsymbol{M})$	y, MPa	$m(y \mid \boldsymbol{M})$	$m(y) = m(\boldsymbol{M})m(y \mid \boldsymbol{M})$
{JC-based FE model}	0.713	[396.8, 590.8]	0.7200	0.5134
		[324.1, 689.6]	0.2600	0.1854
		[287.5, 787.3]	0.0200	0.0143
{KHL-based FE model}	0.055	[580.7, 700.7]	0.7200	0.0396
		[504.1, 748.5]	0.2600	0.0143
		[416.9, 842.0]	0.0200	0.0011
{JC-based FE model, KHL-based FE model}	0.220	[396.8, 700.7]	0.5184	0.1140
		[396.8, 748.5]	0.1872	0.0412
		[396.8, 842.0]	0.0144	0.0032
		[324.1, 700.7]	0.1872	0.0412
		[324.1, 748.5]	0.0676	0.0149
		[324.1, 842.0]	0.0052	0.0011
		[287.5, 787.3]	0.0144	0.0032
		[287.5, 787.3]	0.0052	0.0011
		[287.5, 842.0]	0.0004	0.0001
{ZA-based FE model}	0.012	[207.9, 358.0]	0.7200	0.0086
		[158.4, 441.1]	0.2600	0.0031
		[116.8, 518.7]	0.0200	0.0002
$\sum$	1.0			1.0

5.5.2 Quantification of Model Probability and Combination of Response Predictions

The model-form uncertainty in the three FE models is quantified also depending on expert knowledge systems. Suppose that two independent experts assign belief masses to subsets of the model set as shown in Table 5.5. The two BBAs induced on the model set are combined using the Dempster's rule of combination because the experts are assumed to be both reliable. The conjunctively combined BBA (Table 5.5) indicates the average

degree of belief as a compromise that the correct (or at least the best approximating) FE model is in each sub-model-set.

Table 5.5 Basic belief masses induced on a set of three FE models by two experts and their conjunctive combination

Subsets of the FE model set	Basic belief masses		
	Expert 1	Expert 2	Combined
{JC-based FE model}	0.6	0.25	0.713
{KHL-based FE model}	0.0	0.15	0.055
{JC-based FE model, KHL-based FE model}	0.3	0.5	0.220
{ZA-based FE model}	0.1	0.0	0.012
{JC-based FE model, KHL-based FE model, ZA-based FE model}	0.0	0.1	0.0
$\sum$	1.0	1.0	1.0

Because the subset of the JC-based and the ZA-based FE models is given a nonzero belief mass value, the prediction intervals from the two models must be combined using the disjunctive rule of combination. For the residual stress on the surface, each prediction interval supplied by the JC-based FE model is united with each one by the ZA-based FE model (Table 5.4). The belief masses given to any two intervals from each of the two models are multiplied, and then assigned to the union of the two intervals as in Eq. (5.6).

To incorporate the model-form uncertainty into the prediction of the residual stress field, the belief mass values of prediction intervals supported by a sub-model-set are adjusted proportionally with the belief mass value given to the sub-model-set using Eq. (5.10). For the residual stress on the surface, the calculated belief mass value $m(y)$ of each prediction interval (Table 5.4) represents the degree of belief in the proposition that the true stress value exists in each interval, which is obtained by considering the relative effects of the four subsets of the considered FE models.

A CBF and the corresponding CPF of residual stress prediction are established at each depth using Eqs. (5.17) and (5.18). For the residual stress on the surface, a CBF and the corresponding CPF are derived from the values of $m(y)$ in Table 5.4. The obtained CBF and CPF (Fig. 5.3) express the degree of belief and the degree of plausibility that the true residual stress will be found at a value less than or equal to $v \in (-\infty, +\infty)$. The significant differences between the vertical values of the two curves within the horizontal interval [396.8 MPa, 590.8 MPa] are mostly due to the assignment of the relatively high value (0.5134) of belief mass to that interval. The ZA-based FE model has much less effect on the stress prediction as expected from the significantly low value (0.012) of belief mass given to that FE model.

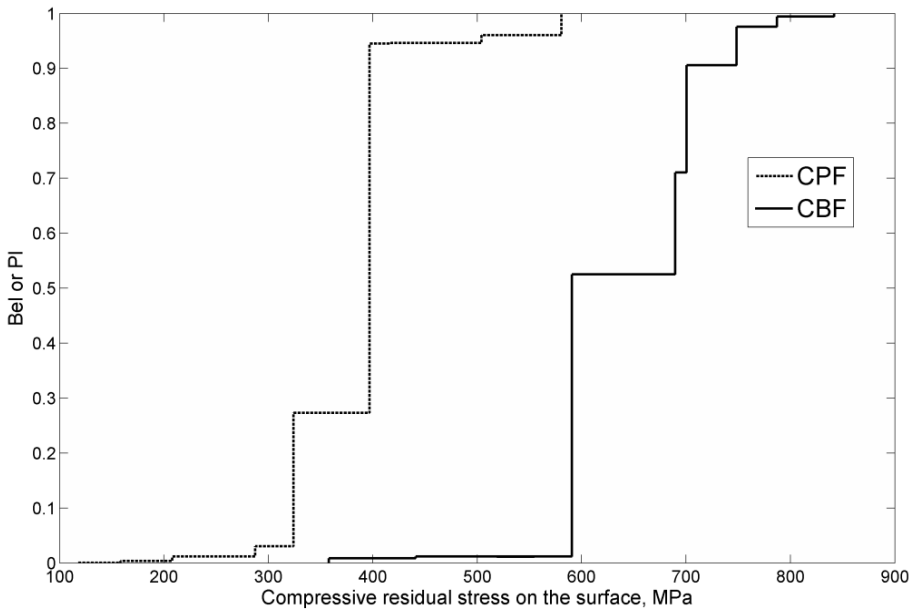

Figure 5.3 CBF and CPF of the predicted compressive residual stress on the surface

5.6 Summary

A mathematical framework is devised to quantify both model-form and parametric uncertainty in response prediction under evidence theory. The constraint that probability theory demands regarding assigning model probability is loosen to effectively represent imprecise expert judgments. The disjunctive rule of combination is effectively utilized to combine predictions from individual models comprising a subset of a model set. Because response predictions are made depending on a model set, the model-to-model variance is incorporated into the composite predictions.

The proposed methodology is demonstrated using the numerical problem of a nonlinear spring-mass system which involves the three cases for assigning model probability. When degrees of belief are distributed among the subsets of the considered models depending on expert judgments, the impreciseness associated with the frequency prediction are moderated due to the increase in the amount of information. Finally, the applicability of the approach to the large-scale physics-based simulations is investigated with the engineering problem of a laser peening process. Because the end points of intervals for the peak pressure map to the min/max values of residual stress predictions, the simulation cost taken to derive the BBAs on the stress predictions are shown to be tolerable.

6. Summary

Model-form uncertainty arises from creating a set of different simulation models to analyze an engineering system. Given observed experimental data, model likelihood must be evaluated to quantify model-form uncertainty. A methodology is developed to evaluate model likelihood using the measured differences between observed experimental data and model predictions of the data in Chapter 2. A formulation that assumes the measured differences to be a data set randomly sampled from independent and identical normal distributions is utilized to describe the probabilistic relationship between experimental data and model predictions. Although the formulation does not accommodate a correlated error structure, it makes the evaluation of model likelihood easy to implement.

Model-form uncertainty represented by discrete model probabilities leads to the corresponding uncertainty in the prediction of a system response represented by a probability distribution. Chapter 3 describes the adjustment factor approach and model averaging used to propagate model-form uncertainty in a given model set into the composite prediction of a system response. The adjustment factor approach is utilized to incorporate only model-form uncertainty into the composite prediction, while model averaging is utilized to incorporate parametric and predictive uncertainty as well as model-form uncertainty. Because the prediction of a response is not conditional on a specific model in a model set, the variance in the prediction that would be missing if the

other models in the considered model set were disregarded is incorporated into the composite prediction of a response.

The proposed methodology is applied to the FE simulation of a laser peening process in Chapter 4. To effectively demonstrate the proposed methodology, three different cases are addressed; incorporating model-form uncertainty alone in Section 4.2, incorporating model-form and predictive uncertainty in Section 4.3, and incorporating model-form, parametric and predictive uncertainty in Section 4.4. Model-form uncertainty is quantified by computing model probability using limited experimental data on residual stresses and the predictions of the data by a set of deterministic or probabilistic FE models. The adjustment factor approach is utilized to combine multi-model predictions for the case of accounting for only model-form uncertainty, while model averaging is utilized for the cases of accounting for parametric and predictive uncertainty in addition to model-form uncertainty. It shows that the composite prediction of the residual stress field is highly reliable when parametric and predictive uncertainty as well as model-form uncertainty is accounted for. Given observed experimental data, the proposed methodology can be applied to any problem of model-form uncertainty quantification regardless of the type (deterministic or probabilistic) of considered simulation models and the numbers of experimental data and simulation models.

Although the methodology developed in Chapter 2 systematically deals with model-form uncertainty from a Bayesian point of view given observed experimental data, it does not furnish a mathematical framework to effectively quantify model-form uncertainty using

prior information such as expert opinion and partial engineering knowledge mainly due to the existence of impreciseness inherent in mathematical expression of human knowledge. A methodology is developed in Chapter 5 to quantify both model-form and parametric uncertainty using expert evidence under evidence theory. The proposed methodology is founded on the idea that model-form uncertainty can be mathematically expressed by constructing belief functions on subsets of a model set. Using the disjunctive rule of combination, response predictions by multiple models are integrated to generate a composite prediction. The proposed methodology is numerically demonstrated with the nonlinear spring-mass system problem. Finally, the methodology is applied to the finite element simulation of the laser peening process to examine its applicability to large-scale engineering problems.

7. Future Works

In this research, the error term introduced to account for the inaccuracy of prediction by each model is succinctly stated as described in Section 2.3.2; it is assumed that the effects of model discrepancy and experimental error on the difference measured between observed and predicted response can be adequately represented by a single probability distribution. It is told that the measured difference results from two error sources; one is the model discrepancy due to the imperfectness of a constructed model, unsatisfactory numerical implementation and any inaccurate input parameters, and the other is the experimental error occurring in measuring data. The assumption of not discerning between the model discrepancy and the experimental error may be an oversimplification especially if model predictions are significantly biased against experimental data due to the effect of model discrepancy rather than due to the effect of experimental error. In that case, it is requested to distinguish the causes of prediction error before quantifying model-form uncertainty.

Although each observed experimental data is considered as a fixed value (e.g. 10 kg) in the current research, a measurement of experimental data is usually represented in the form of error bar (e.g. 10 ± 0.2 kg). Error bar is a graphical expression of the variability of measured data and used to indicate the uncertainty in a reported measurement. Error bar can be used as a measure of how accurate a measurement is (or how far the measured value is from the true (error free) value). Error bar often represents one standard deviation of uncertainty, one standard error, or a certain confidence interval (e.g. a 95%

interval). The mean and standard deviation of experimental data are known in any representation of error bar. Usually, it is assumed that the experimental error is an independent normal variable. In that case, the mean of the normal distribution representing the uncertainty involved in measuring an experimental data is the middle value of a given error bar (10 kg in the above-mentioned example), and the standard deviation of the distribution is the half size of the error bar (0.2 kg in the same example) if it represents one standard deviation of the uncertainty.

If each experimental data is given as an error bar rather than a single constant value, the model likelihood computation should be modified to take account of the information that the error bar contains about the experimental error. As described in Chapter 2.3.2, the prediction of unknown response y by each model M_k is represented by deterministic prediction f_k of y directly obtained from model M_k to which unknown error ε_k is added; $y = f_k + \varepsilon_k$, $\varepsilon_k \sim \mathcal{N}(0, \sigma_k^2)$. Given a single experimental data d_n, the likelihood function of σ_k for model M_k is $\Pr\left(d_n \middle| M_k, \sigma_k\right) = \mathcal{N}\left(d_n; f_{k_n}, \sigma_k^2\right) = \frac{1}{\sqrt{2\pi\sigma_k^2}} \exp\left(-\frac{\left(d_n - f_{k_n}\right)^2}{2\sigma_k^2}\right)$

where f_{k_n} is the deterministic prediction of data d_n by M_k. In the current research, observed experimental data d_n is considered to be a fixed value. In the future research, d_n will be regarded as a normal variable of which the mean and standard deviation are determined from the error bar representation of d_n.

Table 7.1 Construction of the likelihood function of σ_k in the cases when experimental error is independently accounted for or not

Experimental data given as fixed values	Experimental data represented by error bars
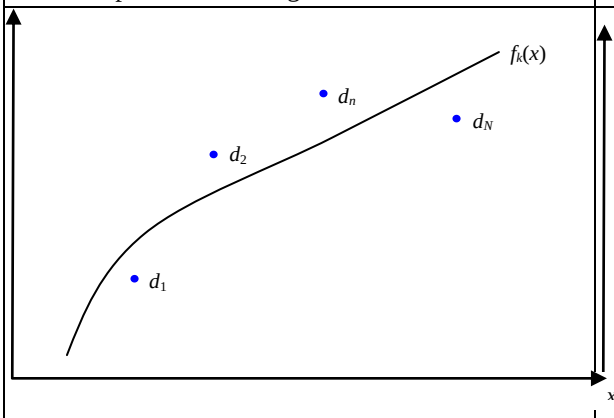	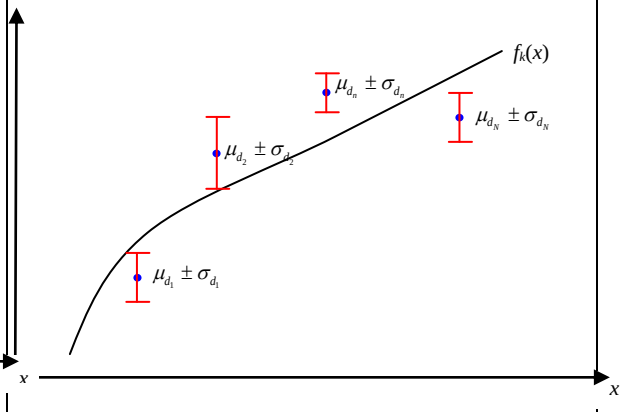
Deterministic model predictions and fixed experimental data	Deterministic model predictions and experimental data represented by error bars
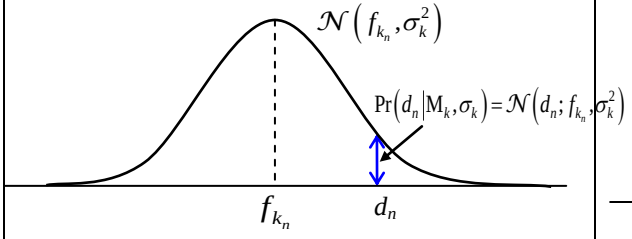	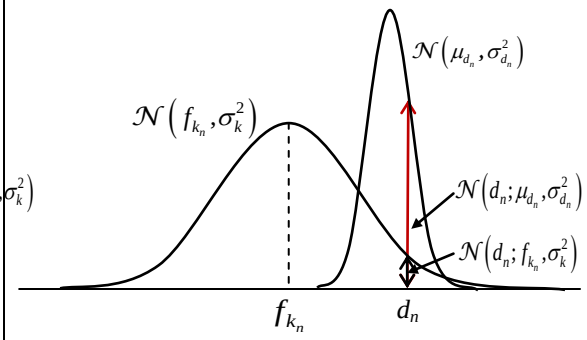
Probabilistic distribution of model prediction and a fixed experimental data d_n	Probabilistic distribution of model prediction and a normally distributed experimental data d_n
$\Pr\left(d_n\middle\|\mathrm{M}_k,\sigma_k\right)$ $=\mathcal{N}\left(d_n;f_{k_n},\sigma_k^2\right)$	$\Pr\left(d_n\middle\|\mathrm{M}_k,\sigma_k\right)$ $=\int_{d_n}\mathcal{N}\left(d_n;f_{k_n},\sigma_k^2\right)\mathcal{N}\left(d_n;\mu_{d_n},\sigma_{d_n}^2\right)dd_n$

Suppose that the mean and standard deviation of normal variable d_n are known to be μ_{d_n} and σ_{d_n}, respectively; $d_n \sim \mathcal{N}\left(\mu_{d_n},\sigma_{d_n}^2\right)$. We have two random variables denoted by d_n and σ_k. Random variable d_n needs to be marginalized out (or discarded) to obtain likelihood function $\Pr\left(d_n\middle|\mathrm{M}_k,\sigma_k\right)$ of σ_k for model M_k. To do so, the probability density $\mathcal{N}\left(d_n;f_{k_n},\sigma_k^2\right)$ given a particular value of d_n is averaged over the probability

distribution $\mathcal{N}\left(\mu_{d_n}, \sigma_{d_n}^2\right)$ of all values of d_n; $\Pr\left(d_n \middle| \mathrm{M}_k, \sigma_k\right)$= $\int_{d_n} \mathcal{N}\left(d_n; f_{k_n}, \sigma_k^2\right) \mathcal{N}\left(d_n; \mu_{d_n}, \sigma_{d_n}^2\right) dd_n$. In other words, two probability density functions $\mathcal{N}\left(f_{k_n}, \sigma_k^2\right)$ and $\mathcal{N}\left(\mu_{d_n}, \sigma_{d_n}^2\right)$ are multiplied and then integrated over all the possible values of experimental data d_n. In Table 7.1, $\mathcal{N}\left(f_{k_n}, \sigma_k^2\right)$ and $\mathcal{N}\left(\mu_{d_n}, \sigma_{d_n}^2\right)$ are graphically represented to illustrate the meaning of them; $\mathcal{N}\left(f_{k_n}, \sigma_k^2\right)$ represents the uncertainty in each model M_k's prediction of y given a specific value of experimental data d_n while $\mathcal{N}\left(\mu_{d_n}, \sigma_{d_n}^2\right)$ represents the uncertainty in the measurement of experimental data d_n. It is worthy of noting that $\Pr\left(d_n \middle| \mathrm{M}_k, \sigma_k\right)$ is a function of σ_k because the only unknown parameter is σ_k. If an observed set of experimental data $\mathrm{D} = \{d_1, d_2, \ldots, d_N\}$ is available and the data are assumed to be mutually independent, the likelihood function of σ_k is represented by

$$\Pr\left(\mathrm{D} \middle| \mathrm{M}_k, \sigma_k\right) = \prod_{n=1}^{N} \Pr\left(d_n \middle| \mathrm{M}_k, \sigma_k\right) = \prod_{n=1}^{N} \int_{d_n} \mathcal{N}\left(d_n; f_{k_n}, \sigma_k^2\right) \mathcal{N}\left(d_n; \mu_{d_n}, \sigma_{d_n}^2\right) dd_n \,.$$

Model likelihood $\Pr(\mathrm{D} \mid \mathrm{M}_k)$ is expressed by marginal likelihood integral $\Pr\left(\mathrm{D} \middle| \mathrm{M}_k\right) = \int \Pr\left(\mathrm{D} \middle| \mathrm{M}_k, \sigma_k\right) g\left(\sigma_k \middle| \mathrm{M}_k\right) d\sigma_k$ where $g(\sigma_k \mid \mathrm{M}_k)$ is the prior distribution of σ_k conditional on M_k. The model likelihood integral will not be able to be handled in an analytical way. A sampling technique such as MCMC could be implemented to numerically solve the integral. Alternatively, the MLE can be used to make the best point estimate of unknown parameter σ_k. The maximum likelihood estimator of σ_k can be

obtained by taking the derivative of the logarithm of $\Pr\left(\mathrm{D}\middle|\mathrm{M}_k,\sigma_k\right)$ shown above with respect to σ_k and setting it equal to zero.

Furthermore, a research needs to be made to simultaneously carry out not only model combination but also model validation and model update while differentiating the causes of prediction error.

References

[1] Burnham K. P., and Anderson, D. R., *Model Selection and Multi-model Inference: A Practical Information-theoretic Approach*, 2nd ed, Springer- Verlag, New York, NY, 2002

[2] Ching, J., Lin, H. D., and Yen, M. T., "Model Selection Issue in Calibrating Reliability-nased Resistance Factors Based on Geotechnical In-situ Test Data," Structural Safety, Vol. 31, No. 5, 2009, pp. 420-431

[3] Park, I., Amarchinta, H. K., and Grandhi, R. V., "A Bayesian Approach for Quantification of Model Uncertainty," Reliability Engineering & System Safety, Vol. 95, No. 7, 2010, pp. 777-785

[4] Apostolakis, G., "A Commentary on Model Uncertainty," Proceedings of Workshop on Model Uncertainty: Its Characterization and Quantification, Annapolis, Maryland, 1993

[5] Bunge, M., *Foundations of Physics*, Springer-Verlag, New York, 1967

[6] Vamos, T., "Epistemic Background Problems of Uncertainty," First International Symposium on Uncertainty Modeling and Analysis, College Park, Maryland, 1990, pp. 96-100

[7] Akaike, H., "A New Look at the Statistical Model Identification," IEEE Transactions on Automatic Control, Vol. 19, No. 6, 1974, pp. 716-723

[8] Schwarz, G., "Estimating the Dimension of a Model," The Annals of Statistics, Vol. 6, No. 2, 1978, pp. 461-464

[9] Draper, D., "Assessment and Propagation of Model Uncertainty," Journal of the Royal Statistical Society series B, Vol. 57, No. 1, 1995, pp. 45-97

[10] Raftery, A. E. "Approximate Bayes Factors and Accounting for Model Uncertainty in Generalized Linear Models," Biometrika, Vol. 83, No. 2, 1996, pp. 251-266

[11] Draper, D., "Model Uncertainty in Stochastic and Deterministic Systems," Proceedings of the 12th International Workshop on Statistical Modeling, Biel/Bienne, Switzerland, 1997, pp. 43-59

[12] Neath, A. A., and Cavanaugh, J. E., "Regression and Time Series Model Selection Using Variants of the Schwarz Information Criterion," Communications in Statistics-Theory and Methods, Vol. 26, No.3, 1997, pp. 559-580

[13] Yang, Y., "Regression with Multiple Candidate Models: Selecting or Mixing?," Statistica Sinica, Vol. 13, 2003, pp. 783-809

[14] Mallows, C. L., "Some Comments on Cp," Technometrics, Vol. 15, No. 4, 1973, pp. 661-675

[15] Daniel, C., and Wood, F. S., *Fitting Equations to Data: Computer Analysis of Multifactor Data,* 2nd ed., John Wiley & Sons, New York, 1980

[16] Stone, M., "Cross-validatory Choice and Assessment of Statistical Predictions," Journal of the Royal Statistical Society. Series B (Methodological), Vol. 36, No. 2, 1974, pp. 111-147

[17] Picard, R. R., and Cook, R. D., "Cross-validation of Regression Models," Journal of the American Statistical Association, Vol. 79, No. 387, 1984, pp. 575-583

[18] Rissanen, J., "Modeling by the Shortest Data Description," Automatica, Vol. 14, No. 5, 1978, pp. 465-471

[19] Claeskens, G., and Hjort, N. L., "The Focused Information Criterion," Journal of the American Statistical Association, Vol. 98, No. 464, 2003, pp. 900-916

[20] Leamer, E. E., *Specification Searches: Ad Hoc Inference with Nonexperimental Data*, John Wiley & Sons, New York, 1978

[21] Raftery, A. E., Madigan, D., and Hoeting, J. A., "Bayesian Model Averaging for Linear Regression Models," Journal of the American Statistical Association, Vol. 92, No. 437, 1997, pp. 179-191

[22] Hoeting, J. A., Madigan, D., Raftery, A. E., and Volinsky, C. T., "Bayesian Model Averaging: A Tutorial," Statistical Science, Vol. 14, No. 4, 1999, pp. 382-401

[23] Madigan, D., and York, J., "Bayesian Graphical Models for Discrete Data," International Statistical Review, Vol. 63, No. 2, 1995, pp. 215-232

[24] Gilks, W. R., Richardson, S., and Spiegelhalter, D. J., *Markov Chain Monte Carlo in Practice*, Chapman & Hall, London, 1996

[25] Green, P. J., "Reversible Jump Markov Chain Monte Carlo Computation and Bayesian Model Determination," Biometrika, Vol. 82, No. 4, 1995, pp. 711-732

[26] Raftery, A. E., "Bayesian Model Selection in Social Research," Sociological Methodology, Vol. 25, 1995, pp. 111-163

[27] Buckland, S. T., Burnham, K. P., and Augustin, N. H., "Model Selection: An Integral Part of Inference," Biometrics, Vol. 53, No. 2, 1997, pp. 603-618

[28] Augustin, N. H., Sauerbrei, W., and Schumacher, M., "The Practical Utility of Incorporating Model Selection Uncertainty into Prognostic Models for Survival Data," Statistical Modelling, Vol. 5, No. 2, 2005, pp. 95-118

[29] Hansen, B. E., "Least Squares Model Averaging," Econometrica, Vol. 75, No. 4, 2007, pp. 1175-1189

[30] Wolpert, D., "Stacked Generalization," Neural Networks, Vol. 5, No. 2, 1992, pp. 241-259

[31] LeBlanc, M., and Tibshirani, R., "Combining Estimates in Regression and Classification," Journal of the American Statistical Association, Vol. 91, No. 436, 1996, pp. 1641-1650

[32] Claeskens, G., and Hjort, N. L., "Minimizing Average Risk in Regression Models," Econometric Theory, Vol. 24, No. 2, 2008, pp. 493-527

[33] Zio, E., and Apostolakis, G., "Two Methods for the Structured Assessment of Model Uncertainty by Experts in Performance Assessments of Radioactive Waste Repositories," Reliability Engineering & System Safety, Vol. 54, No. 2-3, 1996, pp. 225-241

[34] Alvin, K. F., Oberkampf, W. L., Diegert, K. V., and Rutherford, B. M., "Uncertainty Quantification in Computational Structural Dynamics: A New Paradigm for Model Validation," Proceedings of the 16th International Modal Analysis Conference, Santa Barbara, CA, 1998, pp. 1191-1198

[35] Zhang, R., and Mahadevan, S., "Model Uncertainty and Bayesian Updating in Reliability-based Inspection," Structural Safety, Vol. 22, No. 2, 2000, pp. 145-160

[36] Zouaoui, F., and Wilson, J. R., "Accounting for Input Model and Parameter Uncertainty in Simulation," Proceedings of the 2001 Winter Simulation Conference, Arlington, VA, 2001, pp. 290-299

[37] McFarland, J. M., and Bichon, B. J., "Bayesian Model Averaging for Reliability Analysis with Probability Distribution Model Form Uncertainty," 50th AIAA/ASME/ASCE/AHS/ASC Structures, Structural Dynamics and Materials Conference, AIAA 2009-2231, Palm Springs, CA, 2009

[38] Lee, S. H., and Chen, W., "A Comparative Study of Uncertainty Propagation Methods for Black-box-type Problems," Structural and Multidisciplinary Optimization, Vol. 37, No. 3, 2009, pp.239-253

[39] Metropolis, N., and Ulam, S., "The Monte Carlo Method," Journal of the American Statistical Association, Vol. 44, No. 247, 1949, pp. 335-341

[40] Rubinstein, R. Y., and Kroese, D. P., *Simulation and the Monte Carlo Method*, 2nd ed., John Wiley & Sons, New York, 2007

[41] Srinivasan, R., *Importance sampling - Applications in Communications and Detection*, Springer-Verlag, New York, 2002

[42] Engelund, S., and Rackwitz, R., "A Benchmark Study on Importance Sampling Techniques in Structural Reliability," Structural safety, Vol. 12, No. 4, 1993, pp. 255-276

[43] McKay, M. D., Beckman, R. J., and Conover, W. J., "A Comparison of Three Methods for Selecting Values of Input Variables in the Analysis of Output from a Computer Code," *Technometrics*, Vol. 21, No. 2, 1979, pp. 239-245

[44] Helton, J. C., and Davis, F. J., "Latin Hypercube Sampling and the Propagation of Uncertainty in Analyses of Complex Systems," Reliability Engineering & System Safety, Vol. 81, No. 1, 2003, pp. 23-69

[45] Christensen, P., and Baker, M. J., *Structural Reliability Theory and Its Applications*, Springer-Verlag, New York, 1982

[46] Connell, L. D., "An Analysis of Perturbation Based Methods for the Treatment of Parameter Uncertainty in Numerical Groundwater Models," Transport in Porous Media, Vol. 21, No. 3, 1995, pp. 225-240

[47] Rahman, S., and Rao, B. N., "A Perturbation Method for Stochastic Meshless Analysis in Elastostatics," International Journal for Numerical Methods in Engineering, Vol. 50, No. 8, 2001, pp. 1969-1991

[48] Yamazaki, F., Shinozuka, M., and Dasgupta, G., "Neumann Expansion for Stochastic Finite Element Analysis," Journal of Engineering Mechanics, Vol. 114, No. 8, 1988, pp. 1335-1354

[49] Adomian, G., and Malakian, K., "Inversion of Stochastic Partial Differential Operators: The Linear Case," Journal of Mathematical Analysis and Applications, Vol. 77, No. 2, 1980, pp. 505-512

[50] Hasofer, A. M., and Lind, N. C., "Exact and Invariant Second-moment Code Format," Journal of the Engineering Mechanics Division, Vol. 100, No. 1, 1974, pp. 111-121

[51] Choi, S.-K., Grandhi, R.V., and Canfield, R. A., *Reliability-based Structural Design*, Springer, London, 2006

[52] Fiessler, B., Rackwitz, R., and Neumann, H., "Quadratic Limit States in Structural Reliability," Journal of the Engineering Mechanics Division. Vol. 105, No. 4, 1979, pp. 661-676

[53] Ghanem, R. G., and Spanos, P. D., *Stochastic Finite Elements: A Spectral Approach*, Springer-Verlag, New York, 1991

[54] Choi, S.-K., Grandhi, R.V., and Canfield, R. A., "Structural Reliability under Non-Gaussian Stochastic Behavior," Computers & Structures, Vol. 82, No. 13-14, 2004, pp. 1113-1121

[55] Isukapalli, S. S., Roy, A., and Georgopoulos, P. G., "Stochastic Response Surface Methods (SRSMs) for Uncertainty Propagation: Application to Environmental and Biological Systems," Risk Analysis, Vol. 18, No. 3, 1998, pp. 351-363

[56] Evans, D. H., "An Application of Numerical Integration Techniques to Statistical Tolerancing," Technometrics, Vol. 9, No. 3, 1967, pp. 441-456

[57] Rahman, S., and Xu, H., "A Univariate Dimension-reduction Method for Multi-Dimensional Integration in Stochastic Mechanics," Probabilistic Engineering Mechanics, Vol. 19, No. 4, 2004, pp. 393-408

[58] Youn, B. D., Xi, Z., Wells, L. J., and Wang, P. "Enhanced Dimension Reduction (eDR) Method for Sensitivity-free Uncertainty Quantification," Proceedings of 11th AIAA/ISSMO multidisciplinary analysis and optimization conference, Portsmouth, VA, 2006

[59] Zadeh, L. A., "Fuzzy Sets," Information and Control, Vol. 8, No. 3, 1965, pp. 338-353

[60] Zimmermann, H. J., *Fuzzy Set Theory—And Its Applications*, 3rd ed., Kluwer Academic Publishers, Norwell, MA, 1996

[61] Möller, B., Graf, W., and Beer, M., "Safety Assessment of Structures in View of Fuzzy Randomness," Computers & Structures, Vol. 81, No. 15, 2003, pp. 1567-1582

[62] Zadeh, L. A., "Fuzzy Sets as a Basis for a Theory of Possibility," Fuzzy Sets and Systems, Vol. 1, No. 1, 1978, pp. 3-28

[63] Dubois, D., and Prade, H., "Possibility Theory, Probability Theory and Multiple-Valued Logics: A Clarification," Annals of Mathematics and Artificial Intelligence, Vol. 32, No. 1-4, 2001, pp. 35-66

[64] Penmetsa, R. C., and Grandhi, R.V., "Uncertainty Propagation Using Possibility Theory and Function Approximations," Mechanics Based Design of Structures and Machines, Vol. 31, No. 2, 2003, pp. 257-279

[65] Dempster, A. P., "A Generalization of Bayesian Inference," Journal of the Royal Statistical Society. Series B (Methodological), Vol. 30, No. 2, 1968, pp. 205–247

[66] Shafer, G., *A Mathematical Theory of Evidence*, Princeton University Press, Princeton, NJ, 1976

[67] Bae, H.-R., Grandhi, R.V., and Canfield, R. A., "Epistemic Uncertainty Quantification Techniques Including Evidence Theory for Large-Scale Structures," Computers & Structures, Vol. 82, No. 13-14, 2004, pp. 1101-1112

[68] Romero, V. J., "Validated Model? Not So Fast. The Need for Model "Conditioning" As an Essential Addendum to Model Validation," 48th AIAA/ASME/ASCE/AHS/ASC Structures, Structural Dynamics and Materials Conference, Honolulu, HI, April 2007

[69] Bates, D. M., and Watts, D. G., *Nonlinear Regression Analysis and Its Application*, Wiley, New York, 1988

[70] Trucano, T. G., Swilera, L. P., Igusab, T., Oberkampf, W. L., and Pilch, M., "Calibration, Validation, and Sensitivity Analysis: What's What," Reliability Engineering & System Safety, Vol. 91, No. 10-11, 2006, pp. 1331-1357

[71] Kennedy, M. C., and O'Hagan, A., "Bayesian Calibration of Computer Models," Journal of the Royal Statistical Society. Series *B*, Vol. 63, No. 3, 2001, pp. 425-464

[72] Bayarri, M. J., Berger, J. O., Paulo, R., Sacks, J., Cafeo, J. A., Cavendish, J., Lin, C. H., and Tu, J., "A Framework for Validation of Computer Models," Technometrics, Vol. 49, No. 2, 2007, pp. 138-154

[73] Higdon, D., Kennedy, M., Cavendish, J., Cafeo, J., and Ryne, R. D., "Combining Field Observations and Simulations for Calibration and Prediction," SIAM Journal on Scientific Computing, Vol. 26, No. 2, 2004, pp. 448-466

[74] Xiong, Y., Chen, W., Tsui, K. L., and Apley, D. W. , "A Better Understanding of Model Updating Strategies in Validating Engineering Models," Journal of Computer Methods in Applied Mechanics and Engineering, Vol. 198, No. 15-16, 2009, pp. 1327-1337

[75] Liu, F., Bayarri, M. J., Berger, J., Paulo, R., and Sacks, J., "A Bayesian Analysis of the Thermal Challenge Problem," Computer Methods in Applied Mechanics and Engineering, Vol. 197, No. 29-32, 2008, pp. 2457-2466

[76] Link, W. A., and Barker, R. J., "Model Weights and the Foundations of Multimodel Inference," Ecology, Vol. 87, No. 10, 2006, pp. 2626-2635

[77] Burnham, K. P., and Anderson, D. R., "Multi-model Inference: Understanding AIC and BIC Model Selection," Sociological Methods and Research, Vol. 33, No. 2, 2004, pp. 261-304

[78] Gelman, A., Carlin, J., Stern, H., and Rubin, D., *Bayesian Data Analysis*, Chapman and Hall, London, 1995

[79] Bolstad, W., *Introduction to Bayesian Statistics*, John Wiley & Sons, New York, 2004

[80] D'Agostini, G., *Bayesian Reasoning in Data Analysis: A Critical Introduction*, World Scientific Publishing, Singapore, 2003

[81] Fisher, R. A., "On the Mathematical Foundations of Theoretical Statistics," Philosophical Transactions of the Royal Society of London. Series A, Vol. 222, 1922, pp. 309-368

[82] McFarland, J. M., Mahadevan, S., Swiler, L., and Giunta, A., "Bayesian Calibration of the QASPR Simulation," 48th AIAA/ASME/ASCE/AHS/ASC Structures, Structural Dynamics and Materials Conference, Honolulu, HI, April 2007

[83] McFarland, J. M., *Uncertainty Analysis for Computer Simulations through Validation and Calibration*, PhD Dissertation, Vanderbilt University, Nashville, TN, 2008

[84] Park, I., and Grandhi, R. V., "Quantifying Multiple Types of Uncertainty in Physics-Based Simulation Using Bayesian Model Averaging," AIAA Journal, Vol. 49, No. 5, 2011, pp. 1038-1045

[85] Kalos, M. H., and Whitlock, P. A., *Monte Carlo Methods*, John Wiley & Sons, New York, 1986

[86] Ronchetti, E., and Staudte, R. G., "A Robust Version of Mallows's Cp," Journal of the American Statistical Association, Vol. 89, No. 426, 1994, pp. 550-559

[87] ACI Committee 209, *ACI 209R-92: Prediction of Creep, Shrinkage, and Temperature Effects in Concrete Structures* (Reapproved 1997), Farmington Hills, Michigan: American Concrete Institute, 1997

[88] AASHTO, *AASHTO LRFD Bridge Design Specifications: Customary U.S. Units*, 3rd ed, Washington D.C.: American Association of State Highway and Transportation Officials (AASHTO), 2007

[89] CEB, *Creep and Shrinkage, In CEB-FIP Model Code 1990*, Lausanne, Switzerland: Comite Euro-International du Beton (CEB), 1990

[90] Sakata, K., and Shimomura, T., "Recent Progress in Research on and Code Evaluation of Concrete Creep and Shrinkage in Japan," Journal of Advanced Concrete Technology, Vol. 2, No. 2, 2004, pp.133-140

[91] Kavanaugh, B., *Creep Behavior of Self-Consolidating Concrete*, MS Thesis, Auburn University, Alabama, 2008

[92] Barnard, G. A., "New Methods of Quality Control," Journal of the Royal Statistical Society series A, Vol. 126, 1963, pp. 255-258

[93] Roberts, H. V., "Probabilistic Prediction," Journal of the American Statistical Association, Vol. 60, No. 309, 1965, pp. 50–62

[94] Leamer, E. E., *Specification Searches: Ad Hoc Inference with Nonexperimental Data*, John Wiley & Sons, New York, 1978

[95] Gibbons, J. M., Cox, G. M., Wood, A. T. A., Craigon, J., Ramsden, S. J., Tarsitano, D., and Crout, N. M. J., "Applying Bayesian Model Averaging to Mechanistic

Models: An Example and Comparison of Methods," Environmental Modelling and Software, Vol. 23, No. 8, 2008, pp. 973 -985

[96] Clemen, R. T., "Combining Forecasts: A Review and Annotated Bibliography," International Journal of Forecasting, Vol. 5, No. 4, 1989, pp. 559-583

[97] Mosleh, A., and Apostolakis, G., "The Assessment of Probability Distributions from Expert Opinions with an Application to Seismic Fragility Curves," Risk Analysis, Vol. 6, No. 4, 1986, pp. 447-461

[98] Reinert, J. M., and Apostolakis, G. E., "Including Model Uncertainty in Risk-informed Decision Making," Annals of Nuclear Energy, Vol. 33, No.4, 2006, pp. 354-69

[99] Riley, M. E., and Grandhi, R. V., "Quantification of Model-form and Predictive Uncertainty for Multi-Physics Simulation," Computers & Structures, Vol. 89, No. 11-12, 2011, pp. 1206-1213

[100] He, J. H., "Variational Approach for Nonlinear Oscillators," Chaos Solitons and Fractals, Vol. 34, No. 5, 2007, pp. 1430-9

[101] Riley, M. E., Grandhi, R. V., and Kolonay, R. "Quantification of Modeling Uncertainty in Aeroelastic Analyses," AIAA Journal of Aircraft, Vol. 48, No. 3, 2011, pp. 866-873

[102] Silverman, B. W., *Density Estimation for Statistics and Data Analysis*, Chapman and Hall, New York, 1986

[103] Ding, K., and Ye, L., *Laser Shock Peening Performance and Process Simulation*, Woodhead Publishing Limited, Cambridge, England, 2006

[104] Singh, G., and Grandhi, R. V., "Mixed-variable Optimization Strategy Employing Multifidelity Simulation and Surrogate Models," AIAA Journal, Vol. 48, No. 1, 2010, pp. 215-223

[105] Singh, G., Grandhi, R. V., and Stargel, D. S., "Modified Particle Swarm Optimization for a Multimodal Mixed-Variable Laser Peening Process," Structural and Multidisciplinary Optimization, Vol. 42, No. 5, 2010, pp. 769-782

[106] Singh, G., Grandhi, R. V., and Stargel, D. S., "Modeling and Parameter Design of a Laser Shock Peening Process," International Journal for Computational Methods in Engineering Science and Mechanics, Taylor and Francis, Philadelphia, Pennsylvania, In Print

[107] Spradlin, T. J., Grandhi, R. V., and Langer, K., "Experimental Validation of Simulated Fatigue Life Estimates in Laser-Peened Aluminum," International Journal of Structural Integrity, Vol. 2, No. 1, 2011, pp. 74-86

[108] Amarchinta, H. K., Grandhi, R. V., Langer, K., and Stargel, D. S., "Material Model Validation for Laser Shock Peening Process Simulation," Modelling and Simulation in Materials Science and Engineering, Vol. 17, No.1, 2009, paper id. 015010

[109] Amarchinta, H. K., Grandhi, R. V., Clauer, A. H., Langer, K., and Stargel, D., "Simulation of Residual Stress Induced by a Laser Peening Process through Inverse Optimization of Material Models," Journal of Materials Processing Technology, Vol. 210, No. 14, 2010, pp. 1997-2006

[110] Nam, T., *Finite Element Analysis of Residual Stress Field Induced by Laser Shock Peening*, PhD Dissertation, The Ohio State University, Columbus, Ohio, 2002

[111] Smets, P., "Belief Functions: The Disjunctive Rule of Combination and the Generalized Bayesian Theorem," International Journal of Approximate Reasoning, Vol. 9, No. 1, 1993, pp. 1-35

[112] Toussi, S., and Yao, J. T. P., "Assessment of Structural Damage Using the Theory of Evidence," Structural Safety, Vol. 1, No. 2, 1982, pp. 107-121

[113] Helton, J. C., Oberkampf, W. L., and Johnson, J. D., "Competing Failure Risk Analysis Using Evidence Theory," Risk Analysis, Vol. 25, No. 4, 2005, pp. 973-995

[114] Sentz, K., and Ferson, S., *Combination of Evidence in Dempster–Shafer Theory*, SAND 2002-0835 Report, Sandia National Laboratories, Albuquerque, New Mexico, 2002

[115] Dubois, D., and Prade, H., "A Set-Theoretic View on Belief Functions: Logical Operations and Approximations by Fuzzy Sets," International Journal of General Systems, Vol. 12, No. 3, 1986, pp. 193-226

[116] Dubois, D., and Prade, H., "On the Unicity of Dempster Rule of Combination," International Journal of Intelligent Systems, Vol. 1, No. 2, 1986, pp. 133-142